

**SENSITIVITY ANALYSIS OF WING
AEROELASTIC RESPONSES**

by

Jason Cherian Issac

Dissertation submitted to the Faculty of the
Virginia Polytechnic Institute and State University
in partial fulfillment of the requirements for the degree of

DOCTOR OF PHILOSOPHY

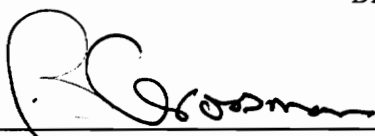
in

Aerospace and Ocean Engineering

APPROVED:



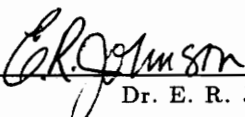
Dr. Rakesh K. Kapania, Chairman



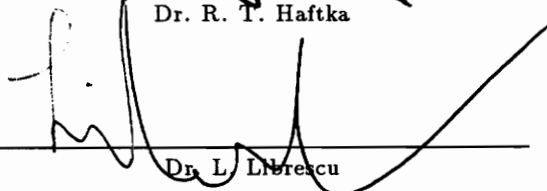
Dr. B. Grossman



Dr. R. T. Haftka



Dr. E. R. Johnson



Dr. L. Librescu

November, 1995

Blacksburg, Virginia

c.2

LD
5655
V856
1995
I873
c.2

SENSITIVITY ANALYSIS OF WING AEROELASTIC RESPONSES

by

Jason Cherian Issac

Dr. Rakesh K. Kapania, Chairman

Aerospace and Ocean Engineering

(ABSTRACT)

Design for prevention of aeroelastic instability (that is, the critical speeds leading to aeroelastic instability lie outside the operating range) is an integral part of the wing design process. Availability of the sensitivity derivatives of the various critical speeds with respect to shape parameters of the wing could be very useful to a designer in the initial design phase, when several design changes are made and the shape of the final configuration is not yet frozen. These derivatives are also indispensable for a gradient-based optimization with aeroelastic constraints.

In this study, flutter characteristic of a typical section in subsonic compressible flow is examined using a state-space unsteady aerodynamic representation. The sensitivity of the flutter speed of the typical section with respect to its mass and stiffness parameters, namely, mass ratio, static unbalance, radius of gyration, bending frequency and torsional frequency is calculated analytically. A strip-theory formulation is newly developed to represent the unsteady aerodynamic forces on a wing. This is coupled with an equivalent plate structural model based on a Rayleigh-Ritz formulation and the aeroelastic equations are solved as an eigenvalue problem to determine the critical speed of the wing. The sensitivity

of divergence and flutter speeds to shape parameters, namely, aspect ratio, area, taper ratio and sweep angle are computed analytically. The aeroelastic equations are also integrated with respect to time using the Wilson- θ method at different values of freestream speed, to observe the aeroelastic phenomena in real time.

Flutter analysis of the wing is also carried out using a lifting-surface subsonic kernel function aerodynamic theory (FAST) and an equivalent plate structural model. The flutter speed is obtained using a $V-g$ type of solution. The novel method of automatic differentiation using ADIFOR is implemented to generate exact derivatives of the flutter speed with respect to shape and modal parameters of the wing.

Finite element modeling of the wing is done using NASTRAN so that wing structures made of spars and ribs and top and bottom wing skins could be analyzed. The free vibration modes of the wing obtained from NASTRAN are input into FAST to compute the flutter speed. The derivatives of flutter speed with respect to shape parameters are computed using a combination of central difference scheme and ADIFOR and the sensitivity to modal parameters is calculated using ADIFOR.

An equivalent plate model which incorporates first-order shear deformation theory is then examined so it can be used to model thick wings, where shear deformations are important. The sensitivity of natural frequencies to changes in shape parameters is obtained using ADIFOR. A simple optimization effort is made towards obtaining a minimum weight design of the wing, subject to flutter constraints, lift requirement constraints for level flight and side constraints on the planform parameters of the wing using the IMSL subroutine NCONG, which uses successive quadratic programming.

ACKNOWLEDGEMENTS

I would like to express my sincere gratitude to my advisor, Dr. Rakesh Kapania for guiding me in my research work and giving me encouragement and support through the completion of my degree. I would like to thank the members of my committee, Dr. Bernard Grossman, Dr. Raphael Haftka, Dr. Eric Johnson and Dr. Liviu Librescu for reading my dissertation and giving me valuable suggestions and Dr. Efstratios Nikolaidis for serving on my examining committee.

Many individuals have helped me during my research. I would like to express my sincere thanks to Dr. Jean-Francois Barthelemy and Dr. Robert Bennett for the fruitful discussions I have had with them during my brief stay at NASA Langley. Thanks are also due to Laura Scott, Kathy Young and other colleagues at NASA Langley for their help and creating a good working atmosphere for pursuing my research.

This research was part of the work done in a project sponsored by NASA Langley Research Center under Grant NAG-1-1411. This support is gratefully acknowledged.

I would like to acknowledge the support of all my friends, especially, Satish Haryadi, Andrew Lovejoy, Tom Stoumbos, Himakar Borra, Abraham Thomas, Somnath Nagendra, Pradeep Sensharma and Anthony Stoxstell for helping me through the good and bad times during the period of my study.

I would like to extend my deep gratitude to my parents, Saramma Cherian and P.C. Cherian and my brothers, Enson and Monson, for encouraging me to pursue my studies and supporting my decisions.

TABLE OF CONTENTS

ABSTRACT	ii
ACKNOWLEDGEMENTS	iv
LIST OF TABLES	viii
LIST OF FIGURES	ix
1. Introduction	1
<i>1.1 Background</i>	1
<i>1.2 Literature Review</i>	3
<i>1.2.1 Aeroelastic Analysis</i>	3
<i>1.2.2 Sensitivity Analysis</i>	5
<i>1.2.3 Multidisciplinary Optimization</i>	7
<i>1.3 Objectives</i>	9
2. Sensitivity of Aeroelastic Response of a Typical Section	11
<i>2.1 Overview</i>	11
<i>2.2 Aerodynamic Model</i>	13
<i>2.3 Aeroelastic Model</i>	14
<i>2.4 Sensitivity Equations</i>	16
<i>2.5 Aeroelastic Analysis</i>	18
<i>2.5.1 Eigenvalue Solution of the Aeroelastic Equations</i>	19
<i>2.5.2 Time Integration of the Aeroelastic Equations</i>	19
<i>2.6 Sensitivity Results</i>	21
3. Sensitivity of Aeroelastic Response of a Wing Using	
Time Domain Approach	33
<i>3.1 Overview</i>	33

3.2	<i>Structural Model for the Wing</i>	34
3.3	<i>Aeroelastic Model for the Wing</i>	36
3.4	<i>Numerical Examples</i>	40
3.4.1	<i>Eigenvalue Solution of the Aeroelastic Equations</i>	40
3.4.2	<i>Time Integration of the Aeroelastic Equations</i>	40
3.5	<i>Sensitivity Results</i>	42
4.	Sensitivity of Aeroelastic Response of a Wing Using	
	Frequency Domain Approach	65
4.1	<i>Overview</i>	65
4.2	<i>Aeroelastic Model</i>	66
4.3	<i>Sensitivity Analysis Using Automatic Differentiation</i>	68
4.3.1	<i>Automatic Differentiation</i>	68
4.3.2	<i>Sensitivity to Shape Parameters</i>	68
4.3.3	<i>Sensitivity to Modal Parameters</i>	69
5.	Finite Element Wing Modeling Using NASTRAN for	
	Aeroelastic Sensitivity Calculations	80
5.1	<i>Overview</i>	80
5.2	<i>NASTRAN Elements Used in this Study</i>	81
5.2.1	<i>CQUAD4 Shell Element</i>	81
5.2.2	<i>CTRIA3 Shell Element</i>	81
5.2.3	<i>CBAR Beam Element</i>	82
5.2.4	<i>CSHEAR Shear Panel Element</i>	82
5.3	<i>Numerical Examples</i>	83
5.3.1	<i>Finite Element Box-beam Model Using NASTRAN</i>	83
5.3.2	<i>Static and Dynamic Analysis of a Swept Wing</i>	84
5.4	<i>Sensitivity of flutter speed</i>	86

5.4.1	<i>Airfoil Coordinates for the Wing</i>	87
5.4.2	<i>Free Vibration Modes of the Wing</i>	88
5.4.3	<i>Sensitivity to Shape and Modal Parameters</i>	89
6.	Shape Sensitivity for Optimization with Aeroelastic	
	Constraints	109
6.1	<i>Overview</i>	109
6.2	<i>Structural Model</i>	109
6.3	<i>Effect of Transverse Shear on Vibration and Aeroelastic</i>	
	<i>Characteristics</i>	111
6.3.1	<i>Effect of Transverse Shear on Natural Frequency</i>	112
6.3.2	<i>Shape Sensitivity Results</i>	112
6.3.3	<i>Effect of Transverse Shear on Flutter Speed</i>	113
6.4	<i>Optimization With Aeroelastic Constraints</i>	114
6.4.1	<i>Formulation of the Optimization Problem</i>	114
6.4.2	<i>Method of Solution</i>	115
6.4.3	<i>Optimization Results</i>	117
7.	Concluding Remarks	130
	REFERENCES	134
	APPENDIX A	142
	APPENDIX B	147
	VITA	148

LIST OF TABLES

2.1	Sensitivity of flutter speed with respect to various parameters at $M=0.85$ (Logarithmic derivatives)	32
3.1	Comparison of natural frequencies of an unswept wing (Area= 0.02318 m^2 , AR= 4.0132 , TR= 1.0) for different laminate sequences	64
3.2	Comparison of flutter speed of an unswept wing (Area= 0.02318 m^2 , AR= 4.0132 , TR= 1.0) in subsonic flow	64
4.1	Sum of the absolute values of the logarithmic derivatives (Parameter P_i for each mode i)	79
5.1	Natural frequencies of the AGARD Swept Wing Model	108
6.1	Comparison of natural frequencies predicted by the two theories for the 6-ply, 12-ply and 18-ply laminates	128
6.2	Comparison of natural frequencies predicted by the two theories for the 24-ply and 36-ply laminates	128
6.3	Optimization results for the minimum weight wing design	129
6.4	Optimization results for the minimum weight wing design (Composite objective function)	129

LIST OF FIGURES

2.1	Two degree of freedom airfoil	22
2.2	Variation of damping ratio, ζ with nondimensional speed, $V/b\omega_\theta$	23
2.3	Variation of nondimensional speed, $V/b\omega_\theta$ with ratio of frequencies, ω_h/ω_θ	24
2.4	Plunge displacement vs time	25
2.5	Pitch displacement vs time	26
2.6	Flutter speed vs Mass ratio ($M=0.85$)	27
2.7	Flutter speed vs Static unbalance ($M=0.85$)	28
2.8	Flutter speed vs Radius of gyration ($M=0.85$)	29
2.9	Flutter speed vs Bending frequency ($M=0.85$)	30
2.10	Flutter speed vs Torsional frequency ($M=0.85$)	31
3.1	Original and transformed coordinate systems	45
3.2	Wing section used	46
3.3	Displacement vs time at $V=66.24$ m/s ($AR=10$, $Area=20m^2$, $TR=0.5$, $Sweep=5^\circ$)	47
3.4	Displacement vs time at $V=70.00$ m/s ($AR=10$, $Area=20m^2$, $TR=0.5$, $Sweep=5^\circ$)	48
3.5	Displacement vs time at $V=92.64$ m/s ($AR=10$, $Area=20m^2$, $TR=0.5$, $Sweep=20^\circ$)	49
3.6	Displacement vs time at $V=95.90$ m/s ($AR=10$, $Area=20m^2$, $TR=0.5$, $Sweep=20^\circ$)	50
3.7	Displacement vs time at $V=90.00$ m/s ($AR=10$, $Area=20m^2$, $TR=0.5$, $Sweep=30^\circ$)	51

3.8	Displacement vs time at $V=98.87$ m/s (AR=10, Area=20m ² , TR=0.5, Sweep=30°)	52
3.9	Displacement vs time at $V=100.00$ m/s (AR=10, Area=20m ² , TR=0.5, Sweep=30°)	53
3.10	Flutter speed from strip-theory (state-space aerodynamics) compared to lifting-surface theory (FAST) (M=0.7, Area=20m ² , TR=0.5, Sweep=0°)	54
3.11	Critical speed vs sweep angle	55
3.12	Divergence speed vs aspect ratio (M=0.7) (AR=10, Area=20m ² , TR=0.5, Sweep=0°)	56
3.13	Divergence speed vs area (M=0.7) (AR=10, Area=20m ² , TR=0.5, Sweep=0°)	57
3.14	Divergence speed vs taper ratio (M=0.7) (AR=10, Area=20m ² , TR=0.5, Sweep=0°)	58
3.15	Divergence speed vs sweep angle (M=0.7) (AR=10, Area=20m ² , TR=0.5, Sweep=0°)	59
3.16	Flutter speed vs aspect ratio (M=0.7) (AR=10, Area=20m ² , TR=0.5, Sweep=15°)	60
3.17	Flutter speed vs area (M=0.7) (AR=10, Area=20m ² , TR=0.5, Sweep=15°)	61
3.18	Flutter speed vs taper ratio (M=0.7) (AR=10, Area=20m ² , TR=0.5, Sweep=15°)	62
3.19	Flutter speed vs sweep angle (M=0.7) (AR=10, Area=20m ² , TR=0.5, Sweep=15°)	63
4.1	Flutter speed vs aspect ratio (M=0.6) from FAST (AR=10, Area=20m ² , TR=0.5, Sweep=30°)	72
4.2	Flutter speed vs area (M=0.6) from FAST (AR=10, Area=20m ² , TR=0.5, Sweep=30°)	73
4.3	Flutter speed vs taper ratio (M=0.6) from FAST	

	(AR=10, Area=20m ² , TR=0.5, Sweep=30°)	74
4.4	Flutter speed vs sweep angle (M=0.6) from FAST (AR=10, Area=20m ² , TR=0.5, Sweep=30°)	75
4.5	Flutter speed sensitivity to natural frequency (M=0.6) (AR=10, Area=20m ² , TR=0.5, Sweep=30°)	76
4.6	Flutter speed sensitivity to generalized mass (M=0.6) (AR=10, Area=20m ² , TR=0.5, Sweep=30°)	77
4.7	Flutter speed sensitivity to generalized aerodynamic forces (GAF) (M=0.6) (AR=10, Area=20m ² , TR=0.5, Sweep=30°)	78
5.1	CQUAD4 shell element	91
5.2	CTRIA3 shell element	91
5.3	CBAR beam element	92
5.4a	CSHEAR element coordinate system	92
5.4b	CSHEAR element forces	92
5.5	Cantilevered box-beam	93
5.6	Static deflection of the box-beam for two load cases	94
5.7	Planform dimensions and cross-section properties of the wing	95
5.8	Finite element discretization of the AGARD swept back wing model	96
5.9	Deflection of front and rear spar for a tip load of 1 lb. at the rear spar	97
5.10	Airfoil generated by transformation from a circle	98
5.11	Finite element discretization of the wing	99
5.12	Mode shapes of the wing	100
5.13	Flutter speed vs aspect ratio (M=0.6) (AR=3.33, Area=7.5m ² , TR=0.5, Sweep=15°)	101

5.14 Flutter speed vs area ($M=0.6$)
 ($AR=3.33$, $Area=7.5m^2$, $TR=0.5$, $Sweep=15^\circ$) 102

5.15 Flutter speed vs taper ratio ($M=0.6$)
 ($AR=3.33$, $Area=7.5m^2$, $TR=0.5$, $Sweep=15^\circ$) 103

5.16 Flutter speed vs sweep angle ($M=0.6$)
 ($AR=3.33$, $Area=7.5m^2$, $TR=0.5$, $Sweep=15^\circ$) 104

5.17 Flutter speed sensitivity to natural frequency ($M=0.6$)
 ($AR=3.33$, $Area=7.5m^2$, $TR=0.5$, $Sweep=15^\circ$) 105

5.18 Flutter speed sensitivity to generalized mass ($M=0.6$)
 ($AR=3.33$, $Area=7.5m^2$, $TR=0.5$, $Sweep=15^\circ$) 106

5.19 Flutter speed sensitivity to generalized aerodynamic forces (GAF) ($M=0.6$)
 ($AR=3.33$, $Area=7.5m^2$, $TR=0.5$, $Sweep=15^\circ$) 107

6.1 First three natural frequencies vs aspect ratio for a thick plate
 ($AR=3.111$, $Area=0.040645m^2$, $TR=0.5$, $Sweep=15^\circ$) 120

6.2 First three natural frequencies vs area for a thick plate
 ($AR=3.111$, $Area=0.040645m^2$, $TR=0.5$, $Sweep=15^\circ$) 121

6.3 First three natural frequencies vs taper ratio for a thick plate
 ($AR=3.111$, $Area=0.040645m^2$, $TR=0.5$, $Sweep=15^\circ$) 122

6.4 First three natural frequencies vs sweep angle for a thick plate
 ($AR=3.111$, $Area=0.040645m^2$, $TR=0.5$, $Sweep=15^\circ$) 123

6.5 Effect of transverse shear on flutter
 [Flutter speed vs aspect ratio ($M=0.6$)]
 ($Area=20m^2$, $TR=0.5$, $Sweep=30^\circ$) 124

6.6 Effect of transverse shear on flutter
 [Flutter speed vs area ($M=0.6$)]
 ($AR=10$, $TR=0.5$, $Sweep=30^\circ$) 125

6.7 Effect of transverse shear on flutter
 [Flutter speed vs taper ratio ($M=0.6$)]
 ($AR=10$, $Area=20m^2$, $Sweep=30^\circ$) 126

6.8 Effect of transverse shear on flutter
 [Flutter speed vs sweep angle ($M=0.6$)]
 ($AR=10$, $Area=20m^2$, $TR=0.5$) 127

CHAPTER 1

INTRODUCTION

1.1 BACKGROUND

Since aircraft structures are flexible and they deform under the aerodynamic loads encountered during flight, studies on structure-fluid interactions and the response of the aircraft structure under these conditions are very important. The interaction between the elastic forces and the aerodynamic forces on a flexible structure in motion alters its vibration characteristics. In an aircraft structure, for example, the lift forces and moments on the wing are modified by the elastic deformation of the structure and the new airloads, in turn, produce a new deformation pattern. The aerodynamic forces causing the deformation are proportional to the square of the velocity, whereas the elastic restoring forces are proportional to the stiffness of the structure. Therefore, at speeds above the critical speeds, when the aerodynamic forces exceed the elastic restoring forces or when the structure undergoes oscillations of increasing amplitude forced by the oscillatory unsteady airloads, aeroelastic instabilities [1–3] like divergence and flutter occur.

In a multidisciplinary design environment, the problems involving interactions between two or more disciplines have to be addressed. Design for aeroelastic stability of an aircraft is an integral part of the wing design process. It is imperative during aircraft design that the critical speeds leading to instability lie outside the operating range of the aircraft. The structural and aerodynamic characteristics of a wing are functions of its shape and hence the aeroelastic response is

sensitive to changes in shape parameters. Sensitivity analysis is an important tool which yields information about the dependence of the aeroelastic instability on the design parameters of the wing.

Sensitivity derivatives of the aeroelastic response of a wing with respect to its shape parameters are very useful for preliminary design purposes. In conceptual and preliminary design, shape variations of the airplane should be considered, before the shape of the configuration is frozen. The generalized unsteady aerodynamic forces need to be updated with changes in wing planform and have to be evaluated at several values of reduced frequencies before an aeroelastic analysis can be performed. However, if the sensitivity derivatives are computed at the baseline configuration, it gives a linear approximation to the aeroelastic response curve and can be used for small changes in the shape design parameters from the baseline, without having to perform a reanalysis at the new configuration.

Sensitivity derivatives are also of great importance in multidisciplinary design optimization. It is very beneficial in regards to time and cost, when an integrated multidisciplinary design and synthesis approach is followed, where all the relevant disciplines are considered simultaneously [4–6]. The systems that are decomposable into top-down hierarchy of engineering disciplines and subsystems may be optimized by multilevel procedure made up of suboptimizations performed concurrently at each level of the hierarchy and linked by optimum sensitivity derivative information [7]. In a gradient-based optimization with aeroelastic constraints, the sensitivity derivatives of the aeroelastic response of a wing will comprise the local sensitivity information at the subsystem level.

The sensitivity derivatives of a system can be found using either analytical or finite difference methods. Analytical sensitivity analysis has found increased interest in engineering design as it eliminates uncertainty in the choice of step size needed in the finite difference method. The step size if too large leads to truncation errors and if too small leads to ill-conditioning.

1.2 LITERATURE REVIEW

1.2.1 AEROELASTIC ANALYSIS

The various methods that are used for aeroelastic analysis of a typical section or a wing differ in the prediction of aerodynamic loads. For many years, aeroelastic analysis has been performed using linearized aerodynamic and structural theories [8–12]. To generate sensitivity derivatives for use in preliminary design or an optimization routine, reasonably quick and accurate methods for aeroelastic analysis are desired. The lift and moment predictions on an airfoil undergoing harmonic motion have been obtained by Theodorsen [13]. Several CFD methods which are used to determine the transonic flowfield around two dimensional airfoils are listed by Ballhaus and Bridgeman [14] and used in [15–17].

In recent years, considerable effort has been made to integrate the aerodynamic, structural and control aspects of the design of an aircraft. Livne *et al* [18] comment that for integrated multidisciplinary wing synthesis, where design for aeroservoelastic stability is an objective, it is required to represent the aeroelastic equations of motion in Linear Time Invariant (LTI) state-space form. The unsteady aerodynamic loads on the wing can be represented in a state-space form,

thereby adding only a small number of states to the mathematical model of the aeroservoelastic system.

The unsteady aerodynamic loads on a typical section in response to an arbitrary forcing can be represented through the use of indicial (step) response functions [19]. The indicial response method is a fundamental approach to the problem, and affords considerable insight into the physical aspects of unsteady airfoil flow. One main advantage of the approach is that when the indicial response to a particular forcing mode is known, e.g., that due to angle of attack or pitch rate, the cumulative response to an arbitrary forcing can be obtained in the time-domain by means of Duhamel superposition. Indicial response for an incompressible flow was obtained theoretically by Wagner [20]. Jones [21] used a two-pole exponential approximation to the Wagner function. Venkatesan and Friedmann [22] have given a three-pole indicial response function that can express the Theodorsen's function over the entire reduced frequency range.

Leishman and Nguyen [23] have represented the aerodynamic indicial response functions for compressible flow by upto three-pole approximations, the response consisting of two parts, one due to non-circulatory loading and the other due to circulatory loading. This has advantages over the CFD-based methods in the sense that the CFD methods are in general computationally very expensive. The state equations describing the unsteady aerodynamic response can be obtained by direct application of Laplace transforms to these indicial response functions [24,25]. State-space representation of aerodynamic characteristics of an aircraft at high angles of attack considering flow separation and flow with vortex breakdown has been presented by Goman and Khrabrov [26].

Aerodynamic methods based on strip-theory formulations [27,28] and advanced codes such as XTRAN3S [29] and CAP-TSD [30], which use the transonic small disturbance equation are currently being used for aeroelastic analysis. Linear lifting-surface theories such as the Doublet Lattice method [31,32] and Kernel function methods [33,34] give adequate prediction of aerodynamic loads required for aeroelastic analysis in the subsonic and supersonic regimes.

1.2.2 SENSITIVITY ANALYSIS

Sensitivity analysis is becoming an important design tool in engineering design applications. It was first recognized as a useful tool for assessing the effects of changing parameters in mathematical models of control systems. The gradient based mathematical programming method used in optimal control and structural optimization furthered the development of sensitivity derivatives, because sensitivity derivatives are used in search directions to find optimum solution [35]. Sensitivity analysis has also become a versatile design tool, rather than just an instrument of optimization programs [36]. Sobieski [37] discusses in detail about the System Design Derivatives which help in understanding the effect a particular design variable would have on the desired performance of the system, if it were perturbed by a small percentage from its original value.

Adelman and Haftka [36] have shown that structural sensitivity analysis has been available for over two decades. Rudisill and Bhatia [38] developed expressions for the analytical derivatives of the eigenvalues, reduced frequency and flutter speed with respect to structural parameters for use in minimizing the total mass. Murthy

and Haftka [39] have presented a survey of methods for calculating sensitivity of general eigenproblems. Eigenvalue and eigenvector derivatives for general matrices are discussed and various approximation methods for eigenvalues are proposed and evaluated by Murthy [40]. Pedersen and Seyranian [41] examined the change in flutter load as a function of change in stiffness, mass, boundary conditions or load distribution. They performed sensitivity analysis without resorting to any new eigenvalue analysis. The solution to the main and an adjoint problem provide all the necessary information for evaluating sensitivities. Their paper mainly focused on column and beam critical load distributions.

Hawk and Bristow [42] developed aerodynamic sensitivity analysis capabilities in subcritical compressible flow. They first analyzed a baseline configuration, and then calculated a matrix containing partial derivatives of the potential at each control point with respect to each known geometric parameter by applying a first order expansion to the baseline configuration. The matrix of partial derivatives is used in each iteration cycle to analyze the perturbed geometry. However, this analysis only handles chordwise perturbation distributions, such as changes in camber, thickness and twist. Another approach has been presented by Yates [43] that considers general geometric variations, including planform, and subsonic, sonic and supersonic unsteady, nonplanar lifting-surface theory.

Recently, Livne *et al* [44] applied an equivalent plate structural modeling, which includes transverse shear, to an HSCT wing. Simple polynomials were used for Ritz functions and depth and thickness distributions. The derivatives of the stiffness and mass matrices were obtained analytically with respect to the shape

variables of the wing. Livne [45] observed that as higher order polynomials are used for better modeling of the structure, the more sensitive is the finite difference derivative to the step-size used and in some cases, it is impossible to obtain any valuable information by finite differences.

Barthelemy and Bergen [46] explored the analytical shape sensitivity derivatives of the wing's aeroelastic characteristics, such as section lift, angle of attack, rolling moment, induced drag and divergence dynamic pressure, for subsonic sub-critical flow, with respect to geometric parameters. Results showed the characteristics nonlinearity to be small enough to be well approximated by sensitivity based linear approximations. These approximations are valid within a range that is useful to designers in the initial design phase.

Kapania [47] has obtained sensitivity derivatives of the flutter speed of a two dimensional airfoil in incompressible flow with respect to the mass and stiffness parameters. Kapania, Bergen and Barthelemy [28] have obtained the shape sensitivity derivatives of the flutter response of a laminated wing in incompressible flow. In this work, Yates' modified strip analysis [48] was used for the aerodynamic model in conjunction with Giles' equivalent plate analysis [49,50] for the structural model.

1.2.3 MULTIDISCIPLINARY OPTIMIZATION

Research carried out on structural design optimization under various static and dynamic behavior constraints including flutter and static aeroelastic constraints has been presented in [51–65]. Rudisill and Bhatia [38] used projected

gradient search to arrive at a relative optimum design of the structure for a specified minimum flutter velocity. Further, they made use of second derivatives of the flutter velocity with respect to structural design parameters to reduce design cycles [66]. Haftka [67] has written a survey paper on application of structural optimization techniques to problems of design under aeroelastic constraints. Haftka and Yates [68] adopted a method of avoiding repetition of calculations which do not depend on the structural sizes, when repeated flutter calculations have to be made. Haftka and Prasad [69] resorted to computing vibration modes only periodically. For intermediate calculations, old modes were used as generalized coordinates to calculate approximate new modes, thus mostly avoiding the expensive direct vibration modes calculation.

Sensitivity derivatives are of great importance in integrated multidisciplinary design optimization of aircrafts. More attention is directed towards multidisciplinary structural/aerodynamic synthesis of wings [70-72]. Karpel [73] used a gradient-based constrained optimization on a composite active-flexible wing to achieve aircraft performance requirements and sufficient flutter and control stability margins with a minimum weight penalty and without violating the design constraints. The sensitivity derivatives of the flutter dynamic pressure, control stability margins and control effectiveness with respect to structural and control design variables were obtained analytically.

Hajela *et al* [74] applied Sobieski's Global Sensitivity Equations (GSE) in an aircraft synthesis problem where the constraints involved the coupled disciplines of structures, aerodynamics and flight mechanics. The coupled system was represented by smaller subsystems and the total behavior sensitivities were determined

by applying the GSE method. Barthelemy *et al* [75] discuss a multidisciplinary design optimization method applied to a supersonic transport wing. Aerodynamic and structural disciplines are integrated for a minimum weight design under static aeroelastic constraints. The authors point out that as the number of dependent variables in each discipline becomes large, the calculation of the finite difference derivatives contributes substantially to the total optimization cost.

1.3 OBJECTIVES

The primary objective of this research is to calculate sensitivity derivatives of aeroelastic responses at the critical condition (i.e., flutter and divergence) of a wing for use in preliminary design or a multidisciplinary optimization with aeroelastic constraints. Though advanced finite element structural models and computational fluid dynamics (CFD) models can be adopted for a detailed analysis, simpler structural and aerodynamic models are desired for aeroelastic analysis at the preliminary stages of design. Both equivalent plate and finite element models are used in this study for structural modeling and strip-theory and lifting-surface theory are used for the unsteady aerodynamics. Since analytic expressions exist for computing the derivatives of the eigenvalues of a general matrix, if the aeroelastic stability problem is solved as an eigenvalue problem, then sensitivities of the critical speeds with respect to various wing parameters must be computed analytically whenever possible so that finite difference methods do not have to be resorted to. With this objective in mind, the sensitivity derivatives of the critical speeds have been calculated analytically as well as using automatic differentiation.

In Chapter 2, the onset of aeroelastic instability of a typical section in subsonic compressible flow is determined using a state-space unsteady aerodynamics representation. The sensitivity of flutter speed with respect to the mass and stiffness parameters are calculated analytically. A strip-theory aerodynamic formulation based on this state-space model is coupled with an equivalent plate structural model to determine the critical speed of a wing in Chapter 3. The sensitivity of divergence and flutter speeds to shape parameters, namely, aspect ratio, area, taper ratio and sweep angle are computed analytically. The aeroelastic equations are also integrated with respect to time using the Wilson- θ method. Flutter analysis is carried out using a lifting-surface aerodynamic theory in Chapter 4, and the sensitivity of flutter speed to shape and modal parameters is computed using automatic differentiation (ADIFOR). Finite element modeling of wings is resorted to in Chapter 5 for structural modeling to generate the free vibration mode shapes required for aeroelastic analysis. The derivatives of flutter speed with respect to shape parameters are computed using a combination of central difference scheme and ADIFOR and the sensitivity to modal parameters are calculated using ADIFOR. An equivalent plate model incorporating first-order shear deformation theory is used in Chapter 6 for structural modeling and the natural frequencies and flutter speeds obtained using the first-order shear deformation theory are compared with those obtained using the classical laminated plate theory. The sensitivity of natural frequencies to changes in shape parameters is obtained using ADIFOR. In order to demonstrate the use of shape sensitivities, an optimization problem of minimum weight design of a wing subject to flutter constraints is also presented.

CHAPTER 2

SENSITIVITY OF AEROELASTIC RESPONSE OF A TYPICAL SECTION

2.1 OVERVIEW

In recent years, considerable effort has been made to integrate the aerodynamic, structural and control aspects of the design of an aircraft. Since the control and the structural dynamic behaviors can easily be expressed in the state-space form (i.e., in terms of a set of first order ordinary differential equations in time), it is desirable that the unsteady aerodynamic airloads be also expressed in the same form.

The state-space approach has the advantage that any system of differential equations can be represented by a set of first order ordinary differential equations of the form

$$\dot{\mathbf{x}} = \mathbf{Ax} + \mathbf{Bu}$$

with the output equations given by

$$\mathbf{y} = \mathbf{Cx} + \mathbf{Du} \tag{2.1}$$

where \mathbf{x} are the aerodynamic state variables, \mathbf{u} are the system inputs and \mathbf{y} are the system outputs. If the unsteady aerodynamic behavior can be represented by state equations, then they can be easily coupled to the structural equations of motion and the resulting system can be examined for aeroelastic stability.

The unsteady aerodynamic loads on a typical section in response to an arbitrary forcing can be represented through the use of indicial (step) response functions. By definition, an indicial function is the response to a disturbance that is applied instantaneously at time zero and held constant thereafter, i.e., a disturbance given by a step function. A main advantage of the approach is that when the indicial response to a particular forcing mode is known, (e.g., that due to angle of attack or pitch rate) the cumulative response to an arbitrary forcing function can be obtained in the time-domain by means of Duhamel superposition. For incompressible flow, the indicial lift response was first derived by Wagner [20] and is known exactly in terms of Bessel functions. However, since it is impractical in several applications to repetitively evaluate the Bessel functions, the Wagner function is usually approximated using sum of exponential functions. For example, Jones [21] used a two-pole exponential approximation to the Wagner function [20] given by

$$\phi(S) = 1 - 0.165\exp(-0.0455S) - 0.335\exp(-0.3S) \quad (2.2)$$

where $S = 2Vt/c$, V is the freestream velocity, t is the time and c is the chord. The state equations describing the unsteady aerodynamic response can then be obtained by the application of Laplace transforms to these indicial functions. The resulting state equations are

$$\begin{Bmatrix} \dot{x}_1 \\ \dot{x}_2 \end{Bmatrix} = \begin{bmatrix} 0 & 1 \\ -0.01375(\frac{2V}{c})^2 & -0.3455(\frac{2V}{c}) \end{bmatrix} \begin{Bmatrix} x_1 \\ x_2 \end{Bmatrix} + \begin{Bmatrix} 0 \\ 1 \end{Bmatrix} \alpha_{3/4}(t) \quad (2.3)$$

with the output equation given by

$$C_N(t) = 2\pi[0.006825(\frac{2V}{c})^2 \quad 0.10805(\frac{2V}{c})] \begin{Bmatrix} x_1 \\ x_2 \end{Bmatrix} + 0.5\alpha_{3/4}(t) \quad (2.4)$$

where C_N is the normal force coefficient and $\alpha_{3/4}(t)$ is the quasisteady angle of attack at 3/4 chord.

2.2 AERODYNAMIC MODEL

In this analysis, the state-space representation given by Leishman and Nguyen [23] has been used to represent the compressible unsteady aerodynamics. They have represented the aerodynamic indicial response functions for compressible flow by up to three-pole approximations, the response consisting of two parts, one due to non-circulatory loading and the other due to circulatory loading. The indicial normal force and quarter chord pitching moment responses for a typical section to a step change in angle of attack α and a step change in pitch rate q can be written as [23]

$$\begin{aligned}
 \frac{C_N(S)}{\alpha} &= \frac{4}{M} \phi_{\alpha}^I(S, M) + C_{N_{\alpha}}(M) \phi_{\alpha}^C(S, M) \\
 \frac{C_M(S)}{\alpha} &= -\frac{1}{M} \phi_{\alpha M}^I(S, M) + C_{N_{\alpha}}(M) \phi_{\alpha}^C(S, M)(0.25 - x_{ac}(M)) \\
 \frac{C_N(S)}{q} &= \frac{1}{M} \phi_q^I(S, M) + \frac{C_{N_{\alpha}}(M)}{2} \phi_q^C(S, M) \\
 \frac{C_M(S)}{q} &= -\frac{7}{12M} \phi_{qM}^I(S, M) - \frac{C_{N_{\alpha}}(M)}{16} \phi_{qM}^C(S, M)
 \end{aligned} \tag{2.5}$$

where $\phi_{\alpha}^C, \phi_{\alpha}^I, \phi_{\alpha M}^I, \phi_q^C, \phi_q^I, \phi_{qM}^C, \phi_{qM}^I$ are exponential functions of S and M . Here, M is the Mach number, $q = \dot{\alpha}c/V$ is the pitch rate, C_N is the normal force coefficient, C_M is the pitching moment coefficient about the quarter chord and $C_{N_{\alpha}}$ is the normal force curve slope. The superscripts C and I refer to circulatory and non-circulatory components of the indicial response functions. Note that $\frac{2\pi}{\beta}$ (where $\beta = \sqrt{1 - M^2}$ is the compressibility factor) in [23] has been replaced by

$C_{N_\alpha}(M)$, so that experimental values of C_{N_α} obtained as functions of Mach number can be used.

The aerodynamic state equations have been shown by Leishman and Nguyen [23] to be given by

$$\dot{\mathbf{x}} = \mathbf{A}\mathbf{x} + \mathbf{B}\begin{Bmatrix} \alpha \\ q \end{Bmatrix} \quad (2.6)$$

where

$$\mathbf{A} = \text{diag}[a_{11} \ a_{22} \ a_{33} \ a_{44} \ a_{55} \ a_{66} \ a_{77} \ a_{88}]$$

$$\mathbf{B} = \begin{bmatrix} 1 & 1 & 1 & 0 & 1 & 1 & 0 & 0 \\ 0.5 & 0.5 & 0 & 1 & 0 & 0 & 1 & 1 \end{bmatrix}^T$$

The output equations are given by

$$\begin{Bmatrix} C_N \\ C_M \end{Bmatrix} = \mathbf{C}\mathbf{x} + \mathbf{D}\begin{Bmatrix} \alpha \\ q \end{Bmatrix} \quad (2.7)$$

where

$$\mathbf{C} = \begin{bmatrix} c_{11} & c_{12} & c_{13} & c_{14} & 0 & 0 & 0 & 0 \\ c_{21} & c_{22} & 0 & 0 & c_{25} & c_{26} & c_{27} & c_{28} \end{bmatrix}$$

$$\mathbf{D} = \begin{bmatrix} 4/M & 1/M \\ -1/M & -7/12M \end{bmatrix}$$

The nonzero terms of the a_{ij} 's and c_{ij} 's are given in the Appendix.

2.3 AEROELASTIC MODEL

The aerodynamic equations in state-space form can be coupled to the structural equations of motion of an airfoil section with bending and torsional degrees of freedom. The equations of motion for the airfoil section shown in Fig. 2.1 can be written as

$$m\ddot{h} + S_\theta\ddot{\theta} + g_h\dot{h} + m\omega_h^2 h = Q_h$$

$$S_\theta\ddot{h} + I_\theta\ddot{\theta} + g_\theta\dot{\theta} + I_\theta\omega_\theta^2\theta = Q_\theta \quad (2.8)$$

where $m = \pi\mu\rho(c/2)^2$ is the mass per unit length, μ is the mass ratio, ρ is the air density, $I_\theta = m(c/2)^2 r_\theta^2$ is the polar moment of inertia about the quarter chord per unit length, r_θ is the radius of gyration about elastic axis, $S_\theta = m(c/2)x_\theta$ is the static mass moment, x_θ is the nondimensional distance in semichords from elastic axis to center of mass, c is the chord length, h is the plunge displacement (positive downward), θ is the pitch angle, ω_h and ω_θ are the bending and torsion frequencies respectively, g_h and g_θ are the structural damping coefficients in plunging and pitching respectively and Q_h and Q_θ are generalized aerodynamic forces in plunging and pitching respectively.

By defining the states

$$z_1 = h, \quad z_2 = \theta, \quad z_3 = \dot{h}, \quad z_4 = \dot{\theta}, \quad (2.9)$$

the above equations can be written as

$$\begin{bmatrix} \mathbf{I} & \mathbf{0} \\ \mathbf{0} & \mathbf{M} \end{bmatrix} \dot{\mathbf{z}} = \begin{bmatrix} \mathbf{0} & \mathbf{I} \\ -\mathbf{k} & -\mathbf{g} \end{bmatrix} \mathbf{z} + \begin{Bmatrix} \mathbf{0} \\ \mathbf{Q} \end{Bmatrix} \quad (2.10)$$

where

$$\begin{aligned} \mathbf{M} &= \begin{bmatrix} m & S_\theta \\ S_\theta & I_\theta \end{bmatrix} & \mathbf{g} &= \begin{bmatrix} g_h & 0 \\ 0 & g_\theta \end{bmatrix} \\ \mathbf{k} &= \begin{bmatrix} m\omega_h^2 & 0 \\ 0 & I_\theta\omega_\theta^2 \end{bmatrix} \\ \mathbf{Q} &= \begin{Bmatrix} -L \\ M \end{Bmatrix} = \frac{1}{2}\rho V^2 \begin{bmatrix} -c & 0 \\ 0 & c^2 \end{bmatrix} \begin{Bmatrix} C_N \\ C_M \end{Bmatrix} \end{aligned}$$

In order to couple the structural and aerodynamic equations, the input vector can be expressed in terms of the z states as given below

$$\begin{Bmatrix} \alpha \\ q \end{Bmatrix} = \begin{bmatrix} 0 & 1 & 1/V & 0 \\ 0 & 0 & 0 & c/V \end{bmatrix} \begin{Bmatrix} z_1 \\ z_2 \\ z_3 \\ z_4 \end{Bmatrix} \quad (2.11)$$

The aerodynamic state equations and the output equations then respectively become

$$\begin{aligned}\dot{\mathbf{x}} &= \mathbf{A}\mathbf{x} + [\mathbf{B}'_1 \ \mathbf{B}'_2]\mathbf{z} \\ \mathbf{Q} &= \mathbf{C}'\mathbf{x} + [\mathbf{D}'_1 \ \mathbf{D}'_2]\mathbf{z}\end{aligned}\tag{2.12}$$

where \mathbf{A} is a diagonal 8x8 matrix, \mathbf{B}'_1 and \mathbf{B}'_2 are 8x2 matrices, \mathbf{C}' is a 2x8 matrix and \mathbf{D}'_1 and \mathbf{D}'_2 are 2x2 matrices.

The resulting set of first-order differential equations in terms of the \mathbf{z} and \mathbf{x} states are given by

$$\begin{bmatrix} \mathbf{I} & 0 & 0 \\ 0 & \mathbf{M} & 0 \\ 0 & 0 & \mathbf{I} \end{bmatrix} \begin{Bmatrix} \dot{\mathbf{z}} \\ \dot{\mathbf{x}} \end{Bmatrix} = \begin{bmatrix} 0 & \mathbf{I} & 0 \\ \mathbf{D}'_1 - \mathbf{k} & \mathbf{D}'_2 - \mathbf{g} & \mathbf{C}' \\ \mathbf{B}'_1 & \mathbf{B}'_2 & \mathbf{A} \end{bmatrix} \begin{Bmatrix} \mathbf{z} \\ \mathbf{x} \end{Bmatrix}\tag{2.13}$$

which is a 12x12 system of linear equations. The stability of the system could be determined at different free-stream speeds by an eigenanalysis of the above system of equations. The flutter speed is that particular value of the free-stream speed at which the real part of the eigenvalue approaches zero.

2.4 SENSITIVITY EQUATIONS

The aeroelastic equations obtained as a set of first order ODEs is of the form

$$[\mathbf{P}]\dot{\mathbf{w}} = [\mathbf{Q}]\mathbf{w}\tag{2.14}$$

which could be written as

$$\dot{\mathbf{w}} = [\mathbf{E}]\mathbf{w}\tag{2.15}$$

where $[\mathbf{E}] = [\mathbf{P}]^{-1}[\mathbf{Q}]$

Since the flutter speed is determined by solving the eigenvalue problem, the derivatives of the eigenvalues have to be calculated for obtaining the flutter speed

derivatives. A number of papers [76–80] have been published on calculation of the derivatives of eigenvalues and eigenvectors of real, symmetric matrices as well as general matrices.

The derivative of the i th eigenvalue for the eigenproblem in equation (2.15) with respect to the flutter speed is given by [81]

$$\frac{\partial \lambda^i}{\partial V_f} = \frac{\{e_l^i\}^T \frac{\partial [E]}{\partial V_f} \{e_r^i\}}{\{e_l^i\}^T \{e_r^i\}} \quad (2.16)$$

where $\{e_l^i\}$ and $\{e_r^i\}$ are the i th left and right eigenvectors respectively, and $\frac{\partial [E]}{\partial V_f}$ is calculated analytically by differentiating the elements of the matrix with respect to V_f .

Similarly, the derivative of the i th eigenvalue with respect to any parameter p is given by

$$\frac{\partial \lambda^i}{\partial p} = \frac{\{e_l^i\}^T \frac{\partial [E]}{\partial p} \{e_r^i\}}{\{e_l^i\}^T \{e_r^i\}} \quad (2.17)$$

$\frac{\partial [E]}{\partial p}$ can be conveniently written as

$$\frac{\partial [E]}{\partial p} = \frac{\partial [P]^{-1}}{\partial p} [Q] + [P]^{-1} \frac{\partial [Q]}{\partial p} \quad (2.18)$$

and can be computed analytically, where

$$\frac{\partial [P]^{-1}}{\partial p} = -[P]^{-1} \frac{\partial [P]}{\partial p} [P]^{-1}. \quad (2.19)$$

The i th eigenvalue λ^i is a function of the speed V and the parameter p which are varied. That is,

$$\lambda^i = \lambda^i(V, p) \quad (2.20)$$

Therefore,

$$d\lambda^i = \frac{\partial \lambda^i}{\partial V} dV + \frac{\partial \lambda^i}{\partial p} dp \quad (2.21)$$

At the critical condition ($V = V_f$), the real part of the eigenvalue goes to zero.

Therefore,

$$\text{Real}(\lambda^i) = 0, \quad \text{Real}(d\lambda^i) = 0 \quad (2.22)$$

Thus we have,

$$0 = \text{Real}\left(\frac{\partial \lambda^i}{\partial V_f}\right) dV_f + \text{Real}\left(\frac{\partial \lambda^i}{\partial p}\right) dp \quad (2.23)$$

The analytical derivative of the flutter speed with respect to parameter p is then given by

$$\frac{dV_f}{dp} = -\frac{\text{Real}\left(\frac{\partial \lambda^i}{\partial p}\right)}{\text{Real}\left(\frac{\partial \lambda^i}{\partial V_f}\right)} \quad (2.24)$$

The $[E]$ matrix is composed of mass, stiffness and aerodynamic matrices. Obtaining the analytical derivatives of the mass, stiffness and aerodynamic terms with respect to any parameter p is straightforward for the typical section. This is done by computing analytically the derivatives of those terms that are explicit functions of the desired parameters.

2.5 AEROELASTIC ANALYSIS

An aeroelastic formulation in the time-domain leads to a set of first-order ordinary differential equations (ODEs) which can be solved by time-integration or as an eigenvalue problem to examine the stability of the system.

2.5.1 EIGENVALUE SOLUTION OF THE AEROELASTIC EQUATIONS

The flutter characteristics of the airfoil are found by calculating the complex eigenvalues $\lambda_k = \sigma_k + i\omega_k$ at various values of free stream velocity. Flutter occurs at the lowest speed for which any σ_k becomes positive.

The flutter speed was determined for the following case, the results for which have been presented by Leishman and Crouse [82]. The parameters used are $\mu = 100$, $x_\theta = 0.25$, $r_\theta = 0.5$, $\omega_h = 10 \text{ rad/s.}$, $\omega_\theta = 50 \text{ rad/s.}$, $a_h = -0.5$, $b = 5 \text{ in.}$, $C_{N_\alpha} = 14.65$, $x_{ac} = 0.286$, $M = 0.85$. Flutter was found to occur at 92.34 ft/s. , i.e., a non-dimensional speed of $V/b\omega_\theta=4.43$ which agrees well with the value of $V/b\omega_\theta=4.4$ reported in [82].

The damping ratio for each of the aeroelastic modes is given by

$$\zeta_k = -\frac{\sigma_k}{\sqrt{\sigma_k^2 + \omega_k^2}} \quad (2.25)$$

A plot of the variation of the damping ratio ζ with non-dimensional speed $V/b\omega_\theta$ is given in Fig. 2.2. Fig. 2.3 shows the variation of flutter speed predicted by this method for different values of ω_h/ω_θ .

2.5.2 TIME INTEGRATION OF THE AEROELASTIC EQUATIONS

Several numerical integration techniques [83–85] exist for step-by-step solution of these equations. The aeroelastic equations are integrated with respect to time using a time-integration scheme. The Wilson- θ method [85] was used for this purpose. A set of first order ODEs can be represented as

$$[R]\{u'\} = [S]\{u\} \quad (2.26)$$

In the Wilson- θ method, it is assumed that the variation of velocity from time t to $t + \theta\Delta t$, where $\theta \geq 1.37$, is linear. At time $(t + \theta\Delta t)$, then

$$\{u_{t+\theta\Delta t}\} = \{u_t\} + \frac{\theta\Delta t}{2}\{u'_{t+\theta\Delta t} + u'_t\} \quad (2.27)$$

Then equation (2.26) becomes

$$\left[[R] - [S]\frac{\theta\Delta t}{2} \right] \{u'_{t+\theta\Delta t}\} = [S]\left\{ u_t + \frac{\theta\Delta t}{2}u'_t \right\} \quad (2.28)$$

Using the starting values of $\{u_t\}$ and $\{u'_t\}$ at time t , $\{u'_{t+\theta\Delta t}\}$ is computed from equation (2.28). The vector $\{u_{t+\theta\Delta t}\}$ is then calculated from equation (2.27). The new values of $\{u_{t+\theta\Delta t}\}$ and $\{u'_{t+\theta\Delta t}\}$ are then used in equation (2.28) to update the $\{u'_{t+\theta\Delta t}\}$ vector. The step-by-step integration of the equations is done in this manner with respect to time by repeating the above process. The amplitudes of displacements are then monitored as time progresses.

Flutter for the typical section (see section 2.5.1) was found to occur at 92.34 ft/s., i.e., a non-dimensional speed of $V/b\omega_\theta=4.43$. A time-integration of the first order ODEs representing the aeroelastic system was done using the Wilson- θ method. The plunge and pitch amplitudes of motion are plotted with respect to time in Figs. 2.4 and 2.5 respectively, at three different non-dimensional speeds, including the flutter speed. It can be seen that at speeds below the flutter speed, the oscillations that are set in due to any initial disturbance given to the airfoil die out as time progresses, whereas, at speeds above the flutter speed, the displacement amplitudes increase with time, leading to instability. At the flutter speed, the oscillations are able to maintain a constant amplitude, denoting a neutrally stable condition.

2.6 SENSITIVITY RESULTS

The sensitivity of flutter speed with various parameters namely μ , x_θ , r_θ , ω_h and ω_θ was calculated by both analytical and finite difference methods. In the analytical method, the derivatives of the [E] matrix (see section 2.4) with respect to the above mentioned parameters were calculated analytically. The finite difference derivatives were calculated for step sizes of 1%, 0.1% and 0.01%. The parameters were perturbed one at a time using these step sizes and the flutter speed recomputed. A forward difference scheme was then applied to compute the derivatives. It can be seen from the results shown in Table 2.1 that the forward difference derivatives obtained using a step size of 0.01% have good agreement with the analytical values.

Figs. 2.6–2.10 show the variation of flutter speed obtained by eigenanalysis with respect to various parameters. In each case, the sensitivity derivative computed at the baseline configuration is also shown. The sensitivity derivative computed forms a tangent to the flutter speed curve at the baseline, and in some cases, the linear approximation given by the sensitivity analysis approximates the flutter speed curve very closely, over the entire range of the parameter that is varied.

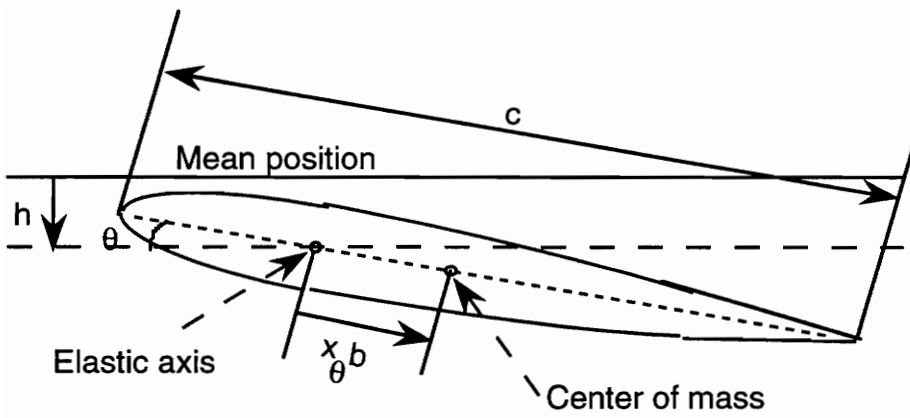


Fig. 2.1 Two degree of freedom airfoil

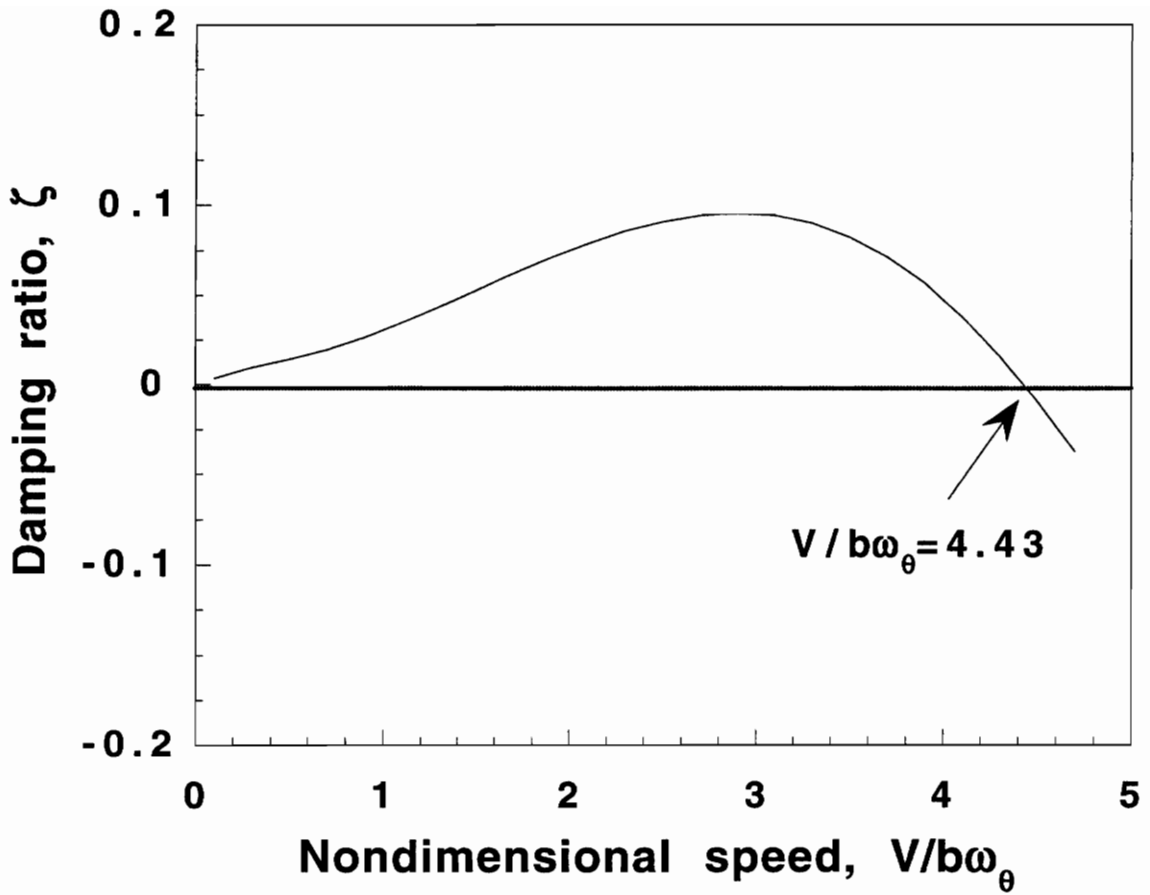


Fig. 2.2 Variation of damping ratio, ζ with nondimensional speed, $V/b\omega_\theta$

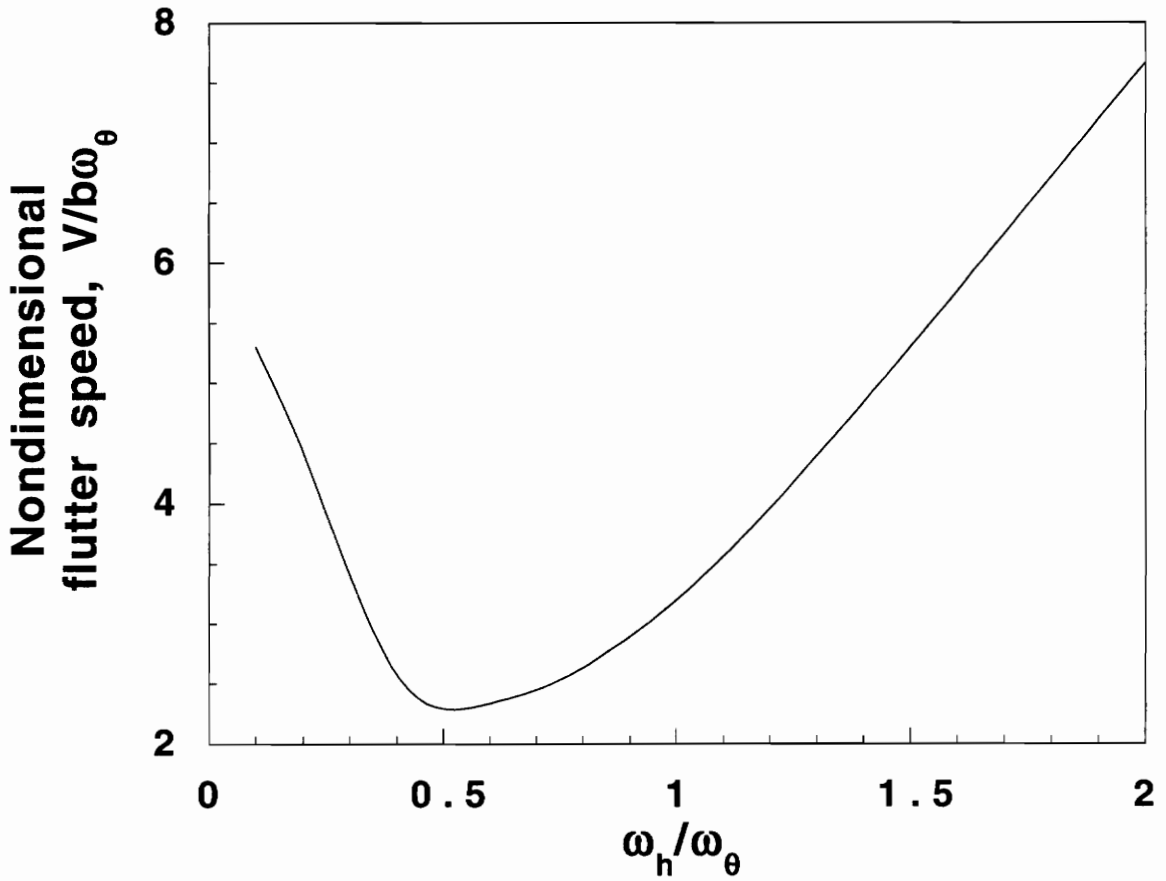


Fig. 2.3 Variation of nondimensional speed, $V/b\omega_\theta$ with ratio of frequencies, ω_h/ω_θ

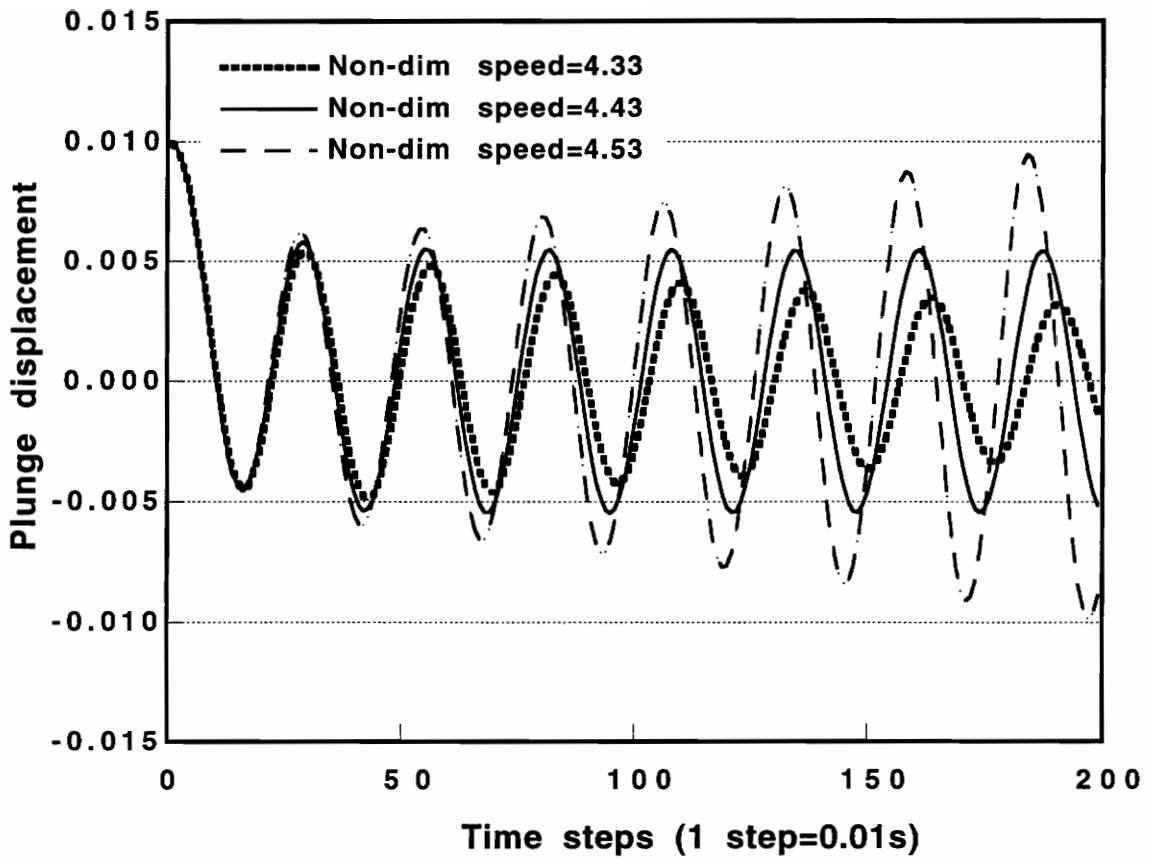


Fig. 2.4 Plunge displacement vs time

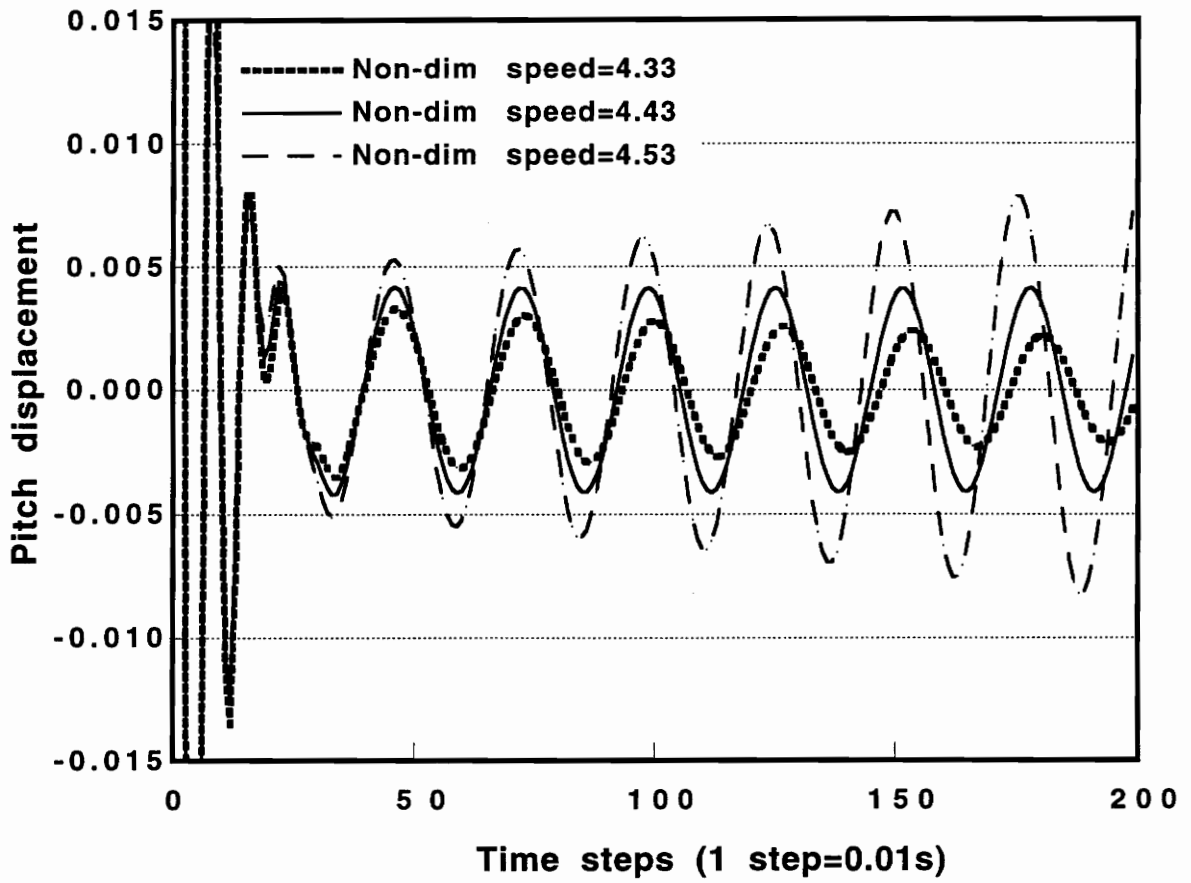


Fig. 2.5 Pitch displacement vs time

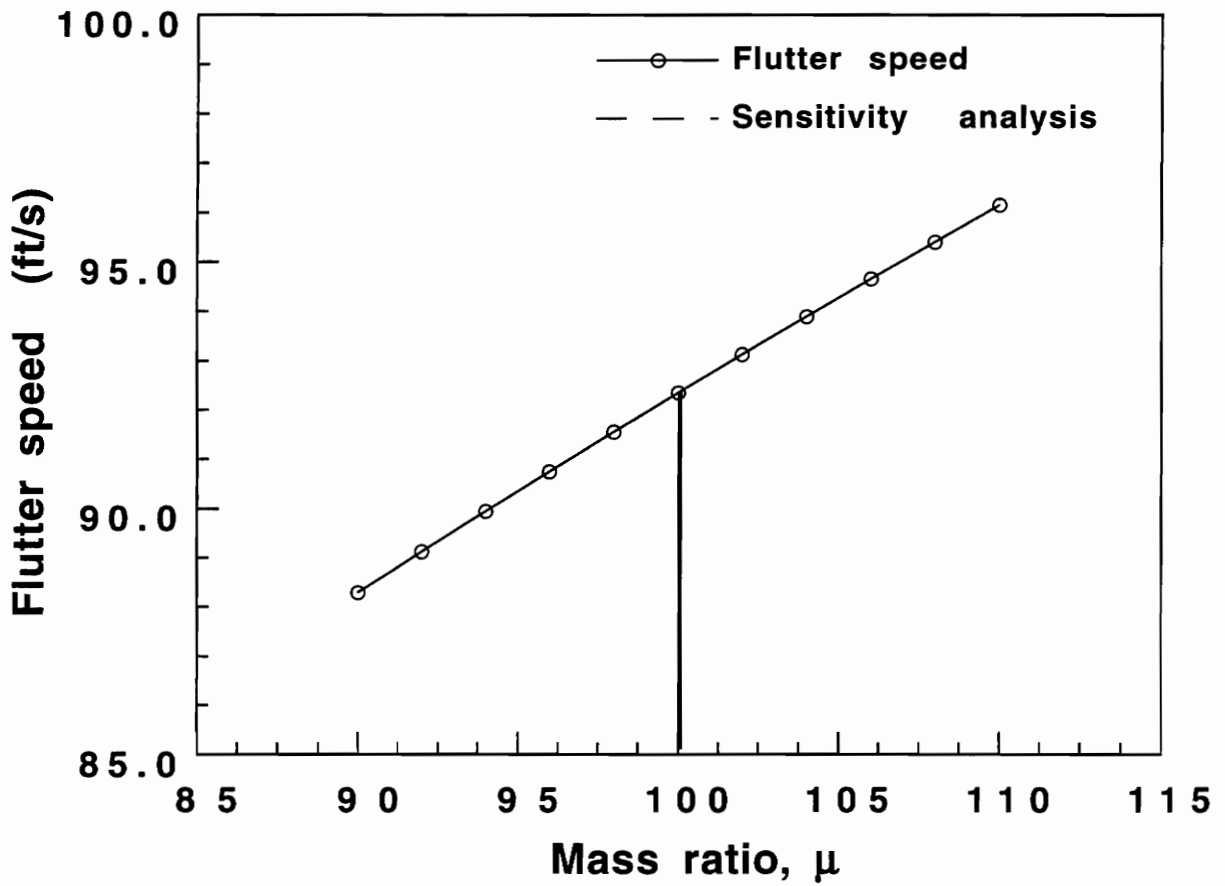


Fig. 2.6 Flutter speed vs Mass ratio (M=0.85)

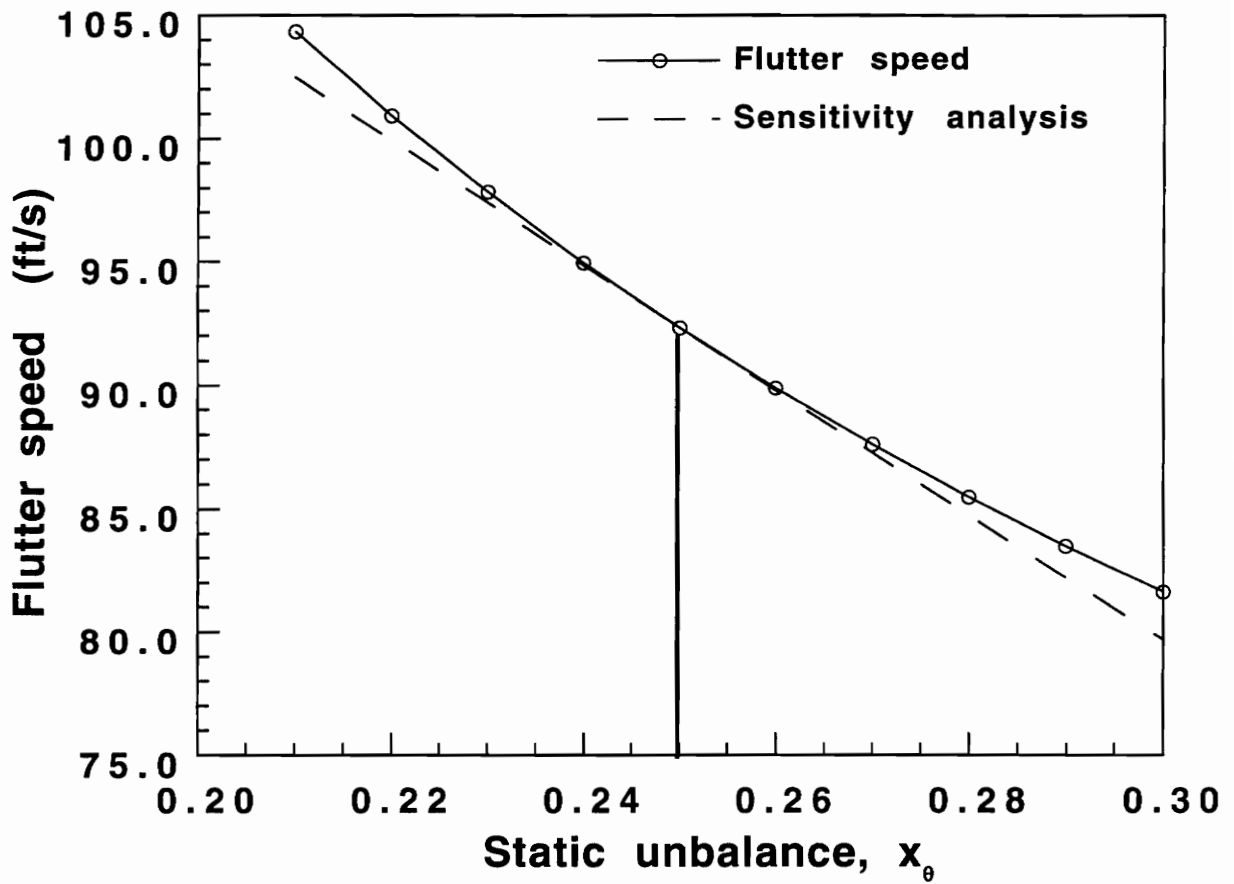


Fig. 2.7 Flutter speed vs Static unbalance (M=0.85)

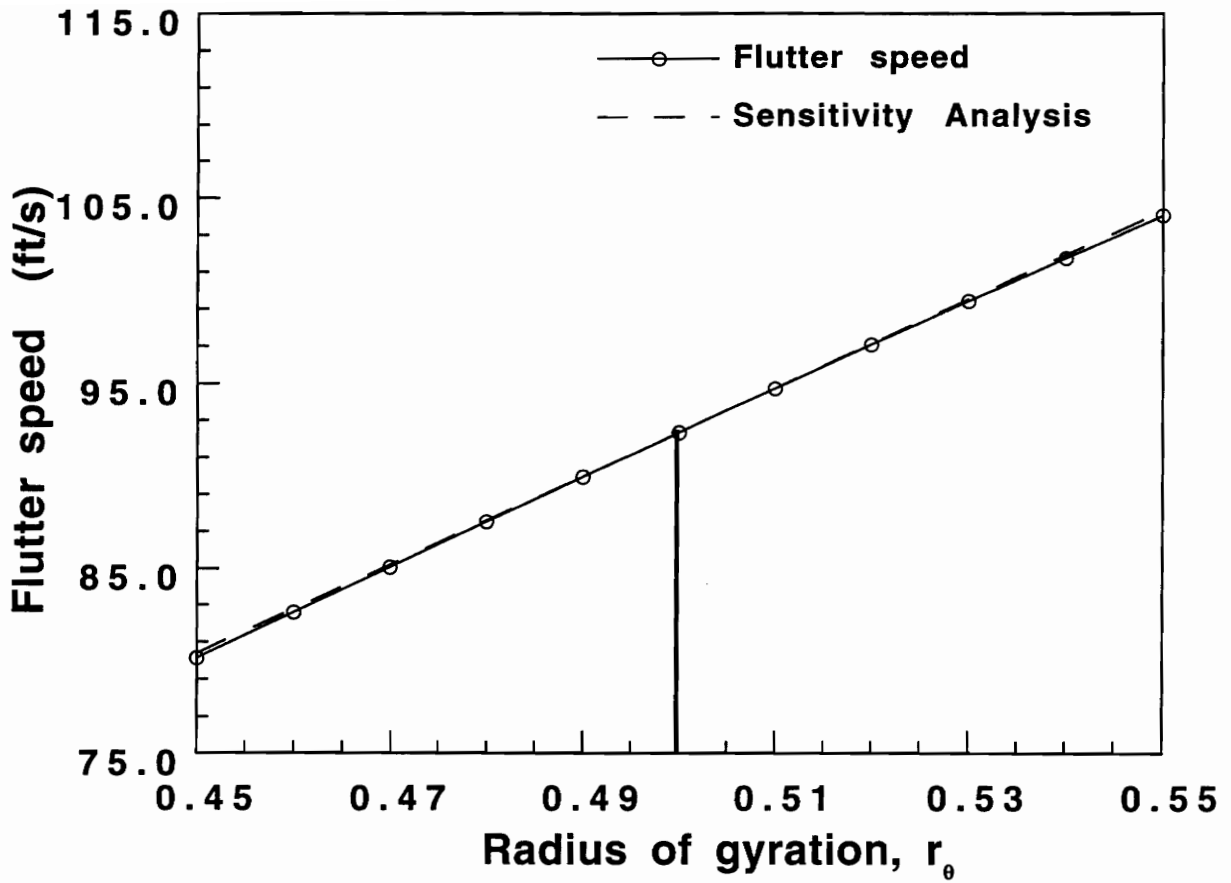


Fig. 2.8 Flutter speed vs Radius of gyration (M=0.85)

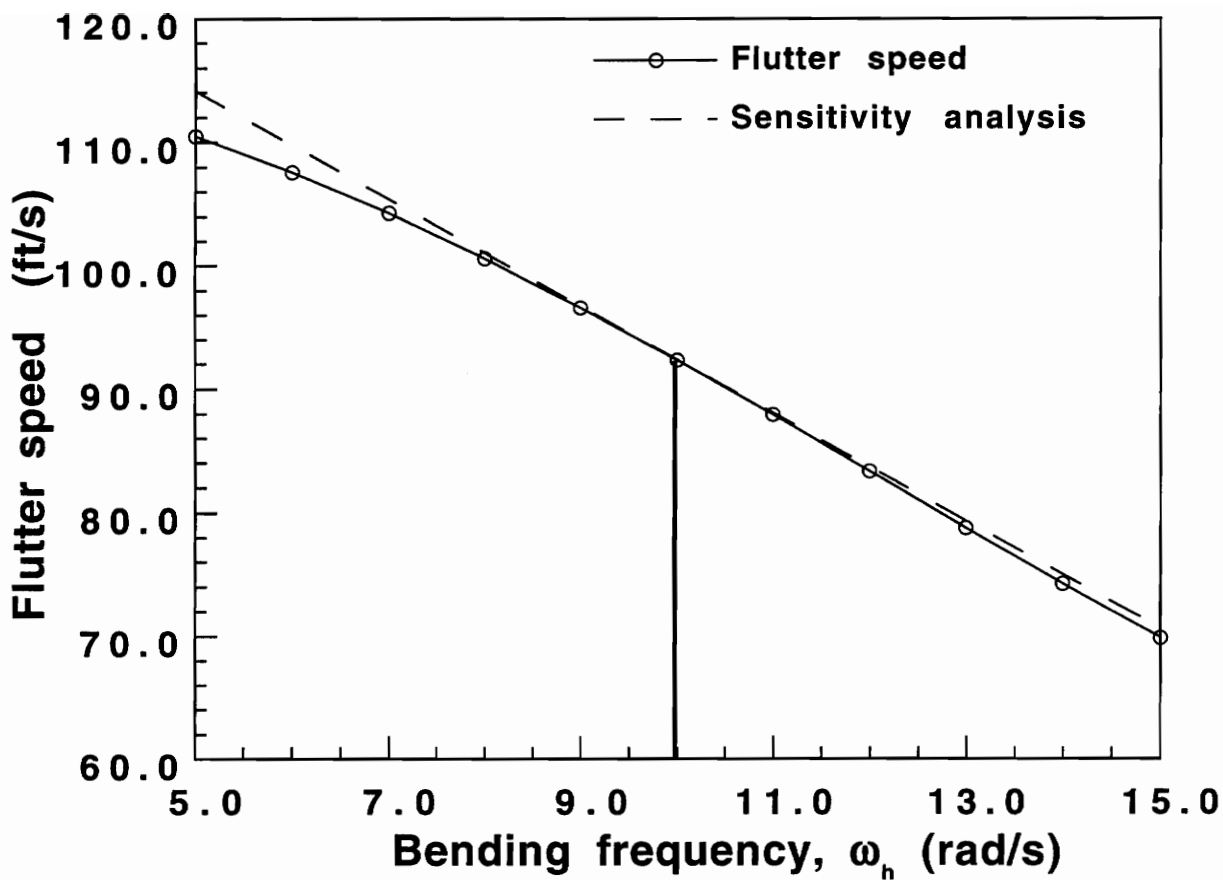


Fig. 2.9 Flutter speed vs Bending frequency (M=0.85)

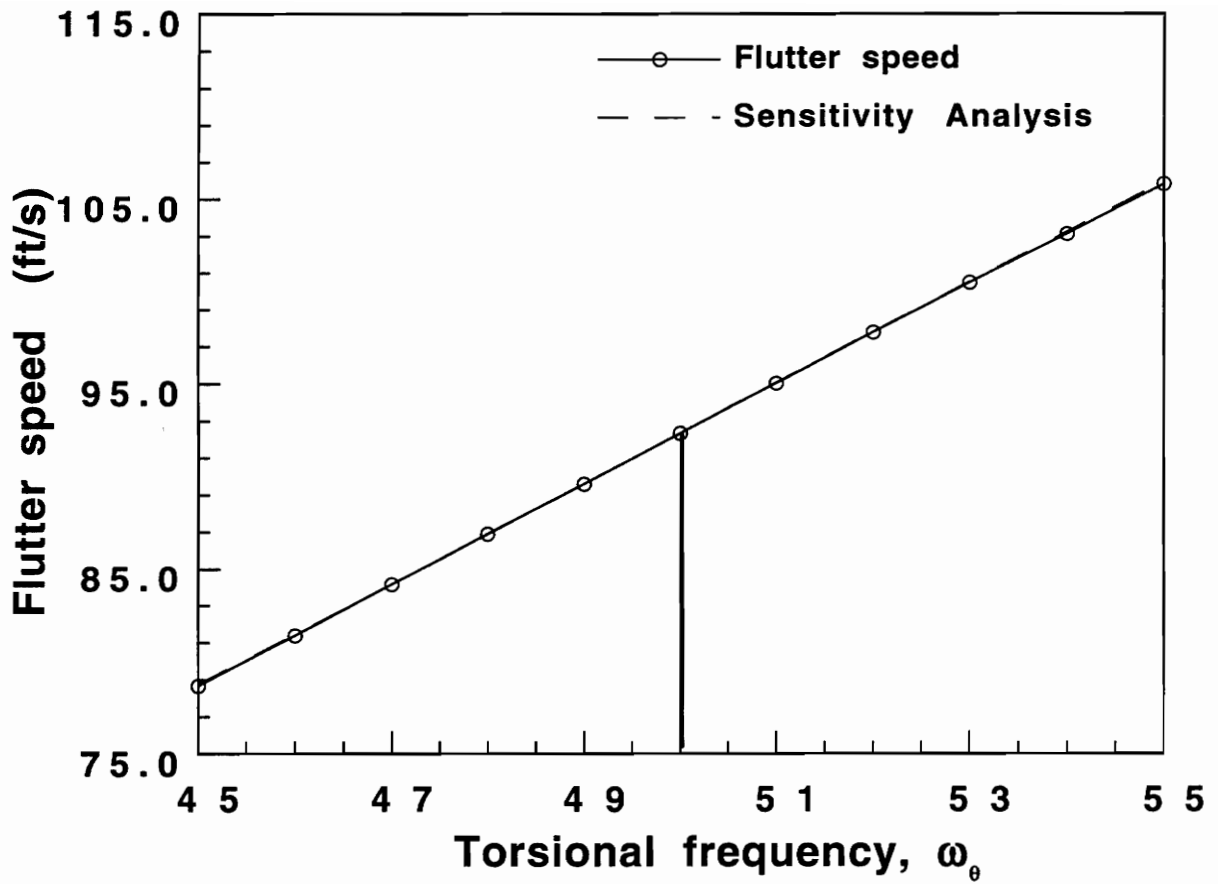


Fig. 2.10 Flutter speed vs Torsional frequency (M=0.85)

Table 2.1 Sensitivity of flutter speed with respect to various parameters at M=0.85 (Logarithmic derivatives)

($\mu = 100$, $x_\theta = 0.25$, $r_\theta = 0.5$, $\omega_h = 10$ rad/sec., $\omega_\theta = 50$ rad/sec.,
 $b = 5$ in., $a_h = -0.5$, $V_f = 92.34$ ft/sec)

Parameter	Analytic derivative	Finite Difference derivative		
		1% ^a	0.1%	0.01%
μ	0.42556	0.42016	0.42499	0.42548
x_θ	-0.68661	-0.67349	-0.68525	-0.68644
r_θ	1.29638	1.28080	1.29474	1.29615
ω_h	-0.47110	-0.46741	-0.47071	-0.47104
ω_θ	1.47113	1.45548	1.46948	1.47089

^a indicates step size

CHAPTER 3

SENSITIVITY OF AEROELASTIC RESPONSE OF A WING USING TIME DOMAIN APPROACH

3.1 OVERVIEW

In the previous chapter, a state-space model for the unsteady aerodynamics was used for aeroelastic analysis of a typical section and the sensitivity of flutter response to airfoil parameters were computed analytically. An aircraft during flight is subjected to unsteady airloads and the unsteady lift forces and moments at any spanwise station of the wing can be represented by the state-space formulation for the typical section presented earlier. A strip-theory formulation is thus developed in this chapter, to represent the unsteady aerodynamic forces on the wing. The wing structure is modeled using classical plate theory and is based on a Rayleigh-Ritz formulation using Chebyshev polynomials for the wing displacements. The structural equations are coupled with the aerodynamic state equations and the resulting aeroelastic equations are solved as an eigenvalue problem to examine the onset of aeroelastic instability. The equations are also integrated with respect to time to observe the aeroelastic phenomena in real time, at speeds close to the critical speed. The structural and aerodynamic characteristics of the wing are functions of its shape and hence the flutter response is sensitive to changes in shape parameters. In this chapter, the sensitivity of aeroelastic response of the wing with respect to the shape parameters, namely, aspect ratio, area, taper ratio and sweep angle are calculated analytically.

3.2 STRUCTURAL MODEL FOR THE WING

The structural formulation is based on a Ritz solution technique using the energy functionals for a laminated plate which includes the bending and stretching of the reference surface. The planform geometry can be represented by any generally tapered skewed configuration. The original rectangular (x, y) coordinate system and the transformed (η, ξ) coordinate system of the wing are shown in Fig. 3.1. The x - y plane is the mid-plane of the wing and the z axis is normal to the wing. For an unswept wing the fiber angle is measured counterclockwise from the positive y axis. As the wing is swept, the fiber angle is also rotated correspondingly.

In the Rayleigh-Ritz formulation, Chebyshev polynomials T_i are used to represent the displacements at any point on the wing [86]. The Chebyshev polynomials are given by

$$\begin{aligned}
 T_0(\psi) &= 1 \\
 T_1(\psi) &= \psi \\
 T_i(\psi) &= 2\psi T_{i-1} - T_{i-2} \quad -1 \leq \psi \leq 1
 \end{aligned} \tag{3.1}$$

The displacements are expressed in terms of the Chebyshev polynomials as shown

$$\begin{aligned}
 U(\eta, \xi) &= \sum_{i=0}^I \sum_{j=0}^J R_{ij} T_i(\eta) T_j(\xi) \\
 V(\eta, \xi) &= \sum_{k=0}^K \sum_{l=0}^L S_{kl} T_k(\eta) T_l(\xi) \\
 W(\eta, \xi) &= \sum_{m=0}^M \sum_{n=0}^N P_{mn} T_m(\eta) T_n(\xi) \quad -1 \leq \eta, \xi \leq 1
 \end{aligned} \tag{3.2}$$

It has been shown by Singhvi and Kapania [86] that for free vibrations of the laminated composite wing (*i.e.*, in the absence of aerodynamic forces) the equations of motion can be derived using classical plate theory in the form

$$[M]\{\ddot{q}\} + [\bar{K}]\{q\} = 0 \quad (3.3)$$

where $[\bar{K}]$ and $[M]$ are the stiffness and mass matrices, respectively. The vector $\{q\}$ is defined as

$$\{q\} = (R_{00}, R_{01}, \dots, R_{ij}; S_{00}, S_{01}, \dots, S_{kl}; P_{00}, P_{01}, \dots, P_{mn})^T \quad (3.4)$$

Linear and rotational springs of large magnitude are placed at the wing root to approximately satisfy the clamped boundary conditions. The stiffness matrix for the plate alone (*i.e.*, excluding the springs) is

$$[\bar{K}] = \int_{-1}^1 \int_{-1}^1 [B]^T [T]^T \begin{bmatrix} A & B \\ B & D \end{bmatrix} [T][B] |J| d\eta d\xi \quad (3.5)$$

where $[B]$ is the matrix whose elements consist of the partial derivatives of the Chebyshev polynomials with respect to the natural coordinates η and ξ and is defined by

$$\begin{pmatrix} \epsilon' \\ \kappa' \end{pmatrix} = [B]\{q\} \quad (3.6)$$

where

$$\begin{pmatrix} \epsilon' \\ \kappa' \end{pmatrix}^T = (u_\eta \quad u_\xi \quad v_\eta \quad v_\xi \quad w_\eta \quad w_{\eta\eta} \quad w_{\xi\xi} \quad w_{\eta\xi})$$

The $[T]$ in equation(3.5) is the transformation matrix that relates the strain and curvature vector in the (x, y) coordinate system to the strain and curvature vector

in the (η, ξ) coordinate system and J is the Jacobian of the transformation. The strain transformation is given by

$$\begin{pmatrix} \epsilon \\ \kappa \end{pmatrix} = [T] \begin{pmatrix} \epsilon' \\ \kappa' \end{pmatrix} \quad (3.7)$$

where

$$\begin{pmatrix} \epsilon \\ \kappa \end{pmatrix}^T = (u_x \quad v_y \quad u_y + v_x \quad w_{xx} \quad w_{yy} \quad 2w_{xy})$$

The details of the $[T]$ and $[B]$ matrices and J are given in [87]. A typical element of the mass matrix $[M]$ is given by

$$M_{ij} = \rho_m t \int_{-1}^1 \int_{-1}^1 T_k(\eta) T_l(\xi) T_o(\eta) T_p(\xi) |J| d\eta d\xi \quad (3.8)$$

The coefficients R_{ij} and S_{kl} in $\{q\}$ corresponding to the inplane displacements in equation(3.3) are condensed out using static condensation to the form

$$[M]\{\ddot{P}_{mn}\} + [K]\{P_{mn}\} = 0 \quad (3.9)$$

where $[M]$ is the mass matrix and $[K]$ is the stiffness matrix of order $(M+1) \times (N+1)$ (see equation(3.2)) with generalized coefficients $\{P_{mn}\}$. In the present work, a value of 5 is chosen for both M and N .

3.3 AEROELASTIC MODEL FOR THE WING

The aerodynamic state space model which was used for the aeroelastic analysis of a typical section is extended to represent the unsteady aerodynamic forces acting on a wing. The lift and moment forces on a typical section acting at the quarter chord are given by equation(2.10) as

$$L = \frac{1}{2} \rho V^2 c C_N$$

$$M = \frac{1}{2} \rho V^2 c^2 C_M$$

When extending this compressible aerodynamic theory to a finite span wing, the lift forces are assumed to be distributed along the quarter chord line (reference line) and the moments act about the reference line. Since the lift and moment forces are non-conservative forces, using the principle of virtual work, we get

$$\delta W_{nc} = \int_0^l -L\delta h d\bar{y} + \int_0^l M\delta\theta d\bar{y} \quad (3.10)$$

where l is the length of the quarter chord line, δh and $\delta\theta$ are virtual displacements and \bar{y} is the coordinate along the reference line.

The displacement at any location \bar{y} is given by

$$h(\bar{y}) = w(\eta, \xi) \quad (3.11)$$

where η and ξ are the natural coordinates corresponding to the (x, y) coordinates of the point at distance \bar{y} from the origin.

The rotation about the reference line (positive wing leading edge up) is given by

$$\theta(\bar{y}) = w_{,x} \cos\Lambda - w_{,y} \sin\Lambda \quad (3.12)$$

To facilitate numerical integration using Gaussian quadrature, the limits of integration along the reference line are transformed in the range of -1 to 1 by $\bar{y} = l(1 + \psi)/2$, where $-1 \leq \psi \leq 1$

Substituting the expressions for the lift and moment on the wing and the wing deflection, we have

$$\begin{aligned} & \int_0^l L\delta h d\bar{y} \\ &= \frac{l}{2} \int_{-1}^1 L\delta h d\psi \\ &= \frac{l}{2} \left(\frac{1}{2}\rho V^2\right) \sum_{i=0}^m \sum_{j=0}^n \left[\int_{-1}^1 c \left([C_{1p}]\{x\} + [D_{1p'}] \begin{bmatrix} H_{ij} & 0 \\ 0 & H_{ij} \end{bmatrix} \begin{Bmatrix} P_{ij} \\ \dot{P}_{ij} \end{Bmatrix} \right) w_{1,ij} d\psi \right] \delta P_{ij} \end{aligned}$$

and

$$\begin{aligned}
& \int_0^l M \delta \theta d\bar{y} \\
&= \frac{l}{2} \int_{-1}^1 M \delta \theta d\psi \\
&= \frac{l}{2} \left(\frac{1}{2} \rho V^2 \right) \sum_{i=0}^m \sum_{j=0}^n \left[\int_{-1}^1 c^2 \left([C_{2p}] \{x\} + [D_{2p'}] \begin{bmatrix} H_{ij} & 0 \\ 0 & H_{ij} \end{bmatrix} \begin{Bmatrix} P_{ij} \\ \dot{P}_{ij} \end{Bmatrix} \right) w_{2ij} d\psi \right] \delta P_{ij}
\end{aligned} \tag{3.13}$$

where m and n represent the order of the Chebyshev polynomial used in the displacement function. The row vectors $[C_{1p}]$ and $[C_{2p}]$ are the elements of the $[C]$ matrix (see section 2.2) where $p = 1, 2, \dots, 8$. The row vectors $[D_{1p'}]$ and $[D_{2p'}]$ are the elements of the matrix given by

$$[D] = \begin{bmatrix} 4/M & 1/M \\ -1/M & -7/12M \end{bmatrix} \begin{bmatrix} 0 & 1 & 1/V & 0 \\ 0 & 0 & 0 & c/V \end{bmatrix} \tag{3.14}$$

where $p' = 1, \dots, 4$.

The variables w_{1ij} and w_{2ij} in equation(3.13) are given by

$$\begin{aligned}
w_{1ij} &= T_i(\eta)T_j(\xi) \\
w_{2ij} &= \cos\Lambda(T_{i,\eta}T_j\eta_{,x} + T_iT_{j,\xi}\xi_{,x}) - \sin\Lambda(T_{i,\eta}T_j\eta_{,y} + T_iT_{j,\xi}\xi_{,y})
\end{aligned} \tag{3.15}$$

where Λ is the sweep angle.

$[H_{ij}]$ in equation(3.13) is a matrix of order $2xN$ where $N = (m + 1)(n + 1)$.

A typical column of the matrix is given by

$$H_k = \left\{ \begin{array}{c} T_i T_j \\ \cos\Lambda(T_{i,\eta}T_j\eta_{,x} + T_iT_{j,\xi}\xi_{,x}) - \sin\Lambda(T_{i,\eta}T_j\eta_{,y} + T_iT_{j,\xi}\xi_{,y}) \end{array} \right\} \tag{3.16}$$

where $k = 1, 2, \dots, N$.

The column vector $\{x\}$ in equation(3.13) is the vector of aerodynamic state variables and $\{P_{ij} \dot{P}_{ij}\}^T$ is the vector of generalized displacements.

Using equations (3.11), (3.12) and (3.13), equation(3.10) can be written as

$$\delta W_{nc} = \sum_{i=1}^N Q_i \delta P_i \quad , \quad N = (m+1)(n+1) \quad (3.17)$$

where

$$Q_i = [C']\{x\} + [D'_1 \ D'_2] \begin{Bmatrix} P_{ij} \\ \dot{P}_{ij} \end{Bmatrix} \quad (3.18)$$

The aerodynamic state equations(2.6) for a typical section perpendicular to the quarter chord line were in the form

$$\{\dot{x}\} = [A]\{x\} + [B]\{u\}$$

An integration of these state equations along the quarter chord line to consider the effect of finite span yields

$$\begin{aligned} \{\dot{x}\} &= \frac{1}{2} \int_{-1}^1 \left[[A]\{x\} + [B] \begin{bmatrix} H_{ij} & 0 \\ 0 & H_{ij} \end{bmatrix} \begin{Bmatrix} P_{ij} \\ \dot{P}_{ij} \end{Bmatrix} \right] d\psi \\ &= [A']\{x\} + [B'_1 \ B'_2] \begin{Bmatrix} P_{ij} \\ \dot{P}_{ij} \end{Bmatrix} \end{aligned} \quad (3.19)$$

Equations(3.9) can be written as a set of first order ODE's in $\{P_{ij}\}$ and $\{\dot{P}_{ij}\}$ which will be represented by $\{p_i\}$ and $\{q_i\}$, respectively. It can be coupled with equations(3.18) and (3.19) to generate the aeroelastic equations of the wing in the form

$$\begin{bmatrix} I & 0 & 0 \\ 0 & M & 0 \\ 0 & 0 & I \end{bmatrix} \begin{Bmatrix} \dot{p}_i \\ \dot{q}_i \\ \dot{x} \end{Bmatrix} = \begin{bmatrix} 0 & I & 0 \\ D'_1 - K & D'_2 & C' \\ B'_1 & B'_2 & A' \end{bmatrix} \begin{Bmatrix} p_i \\ q_i \\ x \end{Bmatrix} \quad (3.20)$$

Since a Chebyshev polynomial of order 5 is chosen for the displacement function in η and ξ , we have 36 generalized coefficients $\{p_i\}$, their 36 time derivatives $\{q_i\}$ and the 8 aerodynamic state variables $\{x\}$. The stability of this system can be determined by solving this 80x80 eigenvalue problem.

3.4 NUMERICAL EXAMPLES

The natural frequencies and flutter speeds predicted by this aeroelastic state-space formulation are compared with previously published results. The aeroelastic equations are solved as an eigenvalue problem and also using a time-integration scheme.

3.4.1 EIGENVALUE SOLUTION OF THE AEROELASTIC EQUATIONS

Before performing the sensitivity calculations of the flutter speed of the wing with respect to shape parameters, comparison of natural frequencies and predicted flutter speeds was made with other results. The first three natural frequencies of an unswept wing and its flutter speed in subsonic flow were compared with results reported by Landsberger and Dugundji [88] for different laminate sequences in Table 3.1 and Table 3.2. The material used for the wing is Hercules Graphite Epoxy (AS1/3501-6) with properties: $E_1 = 98 \times 10^9 \text{ Pa}$, $E_2 = 7.9 \times 10^9 \text{ Pa}$, $\nu_{12} = 0.28$, $G_{12} = 5.6 \times 10^9 \text{ Pa}$ and $\rho = 1520 \text{ kg/m}^3$. The thickness of each ply is $0.134 \times 10^{-3} \text{ m}$. The flutter data used for comparison [88] are the experimental results from the wind tunnel tests performed in the MIT Acoustic wind tunnel. The results agree fairly well.

3.4.2 TIME INTEGRATION OF THE AEROELASTIC EQUATIONS

The aeroelastic equations are integrated with respect to time to examine the effect of time-dependent airloads on the vibration characteristics of the structure. This gives insight into the type of response that can be expected from a flexible

structure operating at conditions on the verge of instability. One of the features of time-integration is that one can observe the aeroelastic response in real time (important for studying fatigue) at different airspeeds (*i.e.*, at different freestream velocities), than just determining the critical speed at the onset of instability.

The aeroelastic response of the wing shown in Fig. 3.2 is examined. The wing skins are made of 0 deg. laminated Graphite/Epoxy (*T300/N5208*) with the following material properties: $E_1 = 181 \times 10^9 \text{ Pa}$, $E_2 = 10.3 \times 10^9 \text{ Pa}$, $\nu_{12} = 0.28$, $G_{12} = 7.17 \times 10^9 \text{ Pa}$ and $\rho = 1600 \text{ kg/m}^3$. The aeroelastic analysis is carried out at Mach number of 0.7 and $\rho_{air} = 0.6 \text{ kg/m}^3$. In order to observe the aeroelastic phenomena in real time, one of the coefficients of the displacement function was perturbed and the system of equations was integrated with respect to time using the Wilson- θ method, described in Section 2.5.2. The wing tip displacement is plotted as a function of time at different speeds in Figs. 3.3–3.9. The tip displacement of the 5° swept wing at the divergence speed is shown in Fig. 3.3. It can be seen that the displacement approaches a constant amplitude at this speed and does not decrease to the zero mean value. Above this speed, the displacement increases with time as shown in Fig. 3.4. This is characteristic of divergence which is a static instability, and hence of a non-oscillatory nature. The small wiggles in the response are due to the dynamic effects. For the 20° swept wing, the displacement slowly approaches a constant value at the divergence speed as shown in Fig. 3.5. The oscillatory nature is due to the fact that the flutter and divergence speeds are close enough. It can be seen that the oscillations die down since the dynamic instability has not yet set in. Fig. 3.6 shows the flutter

condition for the 20° swept wing. Since the wing has already diverged at a lower speed, we see the constant amplitude oscillations about a diverging mean position. This is the condition when a static mode has become unstable and the oscillatory mode is neutrally stable. Figs. 3.7, 3.8 and 3.9 show the tip displacement of the 30° swept wing below the flutter speed, at the flutter speed and above the flutter speed, respectively. The oscillations are damped out at low speeds, but at the critical speed the structure is able to maintain self-sustained oscillations, and at higher speeds, the amplitudes of oscillations rapidly increase with time.

3.5 SENSITIVITY RESULTS

The aeroelastic equations (3.20) are a set of first-order ordinary differential equations and the procedure for analytically determining the sensitivity of the flutter speed is described in section 2.4. The expressions for the analytical derivatives of the $[\bar{K}]$ and $[M]$ matrices (equations(3.5) and (3.8)) are given in [87]. Since the reduced stiffness matrix $[K]$ is obtained from $[\bar{K}]$ by static condensation the analytical derivative $\frac{\partial[K]}{\partial p}$ is obtained by a succession of differentiations using the chain rule. The derivatives of the aerodynamic terms are obtained by taking the analytical derivatives of those terms that are explicit functions of the shape parameters, given in Appendix A.

Sensitivity analysis of the flutter speed of the wing with respect to shape parameters is carried out for the wing shown in Fig. 3.2. The wing skins are made of 0° laminated Graphite/Epoxy (*T300/N5208*) with the following material properties: $E_1 = 181 \times 10^9 \text{ Pa}$, $E_2 = 10.3 \times 10^9 \text{ Pa}$, $\nu_{12} = 0.28$, $G_{12} = 7.17 \times$

$10^9 Pa$ and $\rho = 1600 kg/m^3$. The flutter speed calculated using this strip-theory formulation is compared with the flutter speed obtained using a lifting-surface unsteady aerodynamic theory (FAST) in Fig. 3.10 for the wing at Mach 0.7 and a range of values of aspect ratio. The results agree fairly well, with the strip-theory predicting higher values for the flutter speed. The critical airspeed of the wing is shown in Fig. 3.11 as a function of the quarter-chord sweep angle. As seen from the graph, divergence (zero frequency flutter) instability is critical upto a sweep angle of about 20° and for higher sweep angles, the flutter mode is the unstable mode. The shape sensitivity derivatives of the divergence speeds and flutter speeds of the wing at Mach 0.7 and $\rho_{air} = 0.6 kg/m^3$ are computed analytically.

The critical speeds of the wing obtained by perturbing one shape parameter at a time from the baseline configuration are shown in Figs. 3.12–3.19. The prediction of critical speed by analytical sensitivity calculations is also superposed. The sensitivity derivative obtained forms a tangent to the critical speed curve at the value of the shape parameter at which it is computed.

It is observed from Fig. 3.12 and Fig. 3.16 that the divergence and flutter speeds, respectively, drop as the aspect ratio increases. Physically, as the wing is made more slender, the instability sets in at a lower speed. As the area of the wing is increased, the divergence and flutter speeds are found to decrease as shown in Fig. 3.13 and Fig. 3.17, respectively. The greater the area of the wing, the greater the unsteady aerodynamic forces acting on it, causing the aeroelastic instability to occur at a lower speed. The analytical sensitivity gives a good linear approximation of the critical speeds over the range the aspect ratio and area of the wing are varied.

The divergence speed of the wing is not affected much as the taper ratio is increased from 0.4 to 0.6 as seen from Fig. 3.14. The flutter speed of the wing decreases as the taper ratio is increased as shown in Fig. 3.18. The flutter speed curve can be approximated linearly as indicated by the sensitivity prediction.

It can be seen from Fig. 3.15 that the divergence speed increases as the wing is swept backwards. The flutter speed does not vary much with increasing sweep angle about the 15° swept configuration as seen from Fig. 3.19. By performing one sensitivity calculation at the baseline analytically, this method gives a linear approximation to the critical speeds of the wing for changes in the wing shape parameters about the baseline. This information is useful for preliminary design purposes, as it avoids the necessity of a reanalysis for small changes in any of the shape parameters.

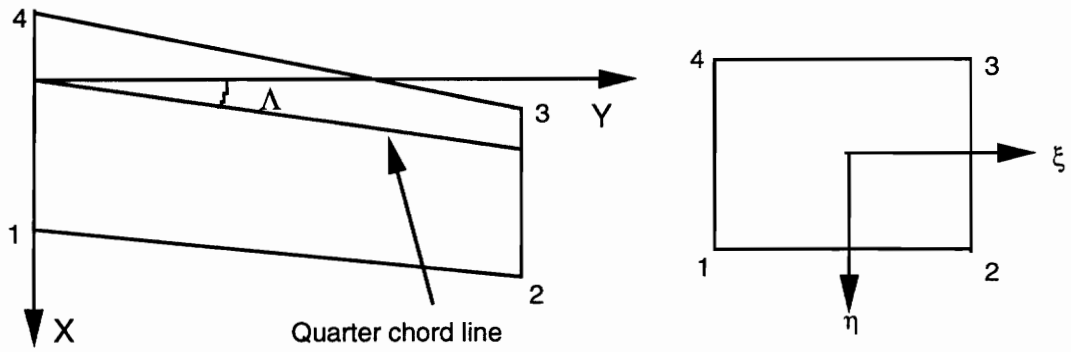


Fig. 3.1 Original and Transformed Coordinate Systems

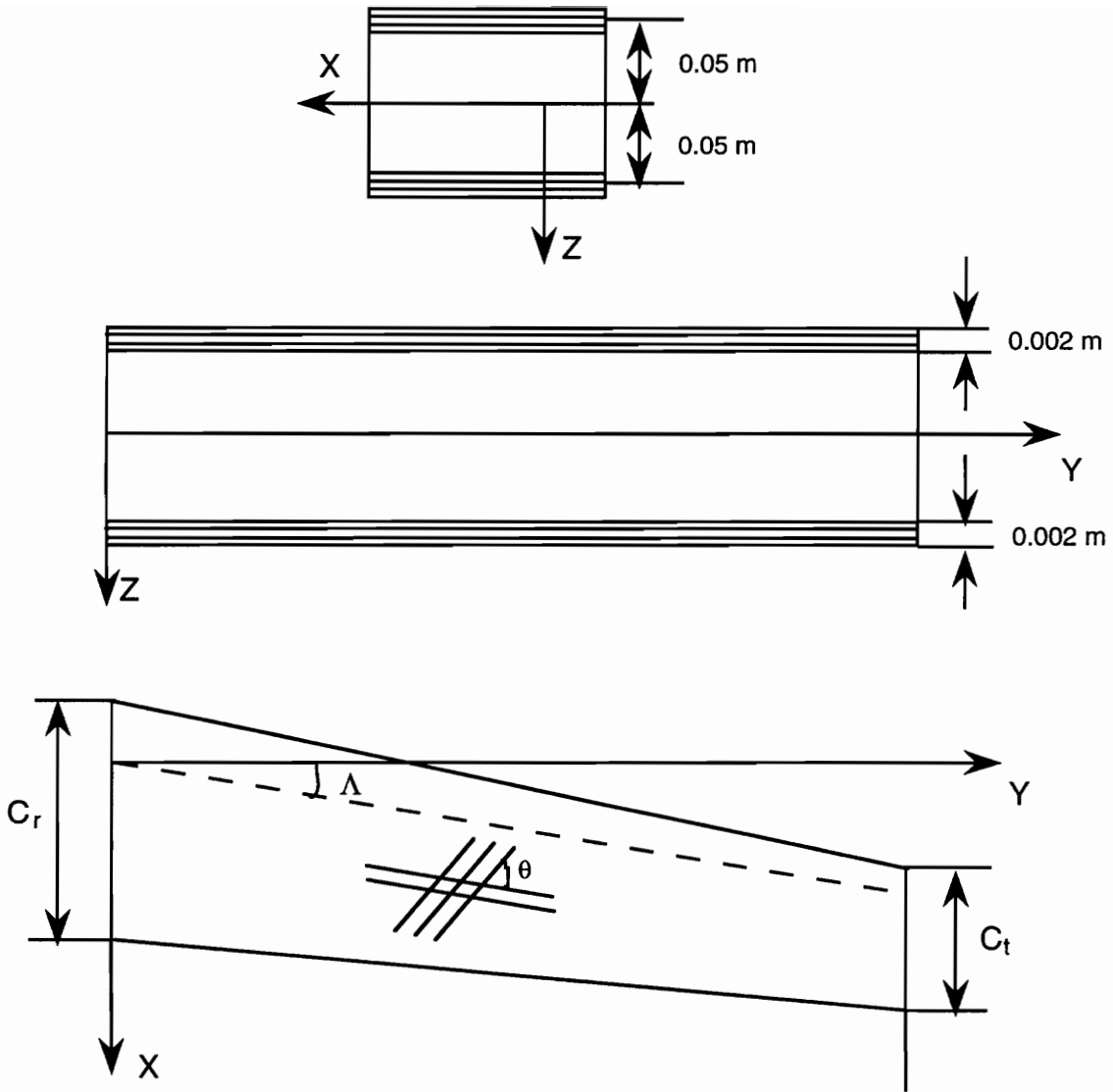


Fig. 3.2 Wing section used

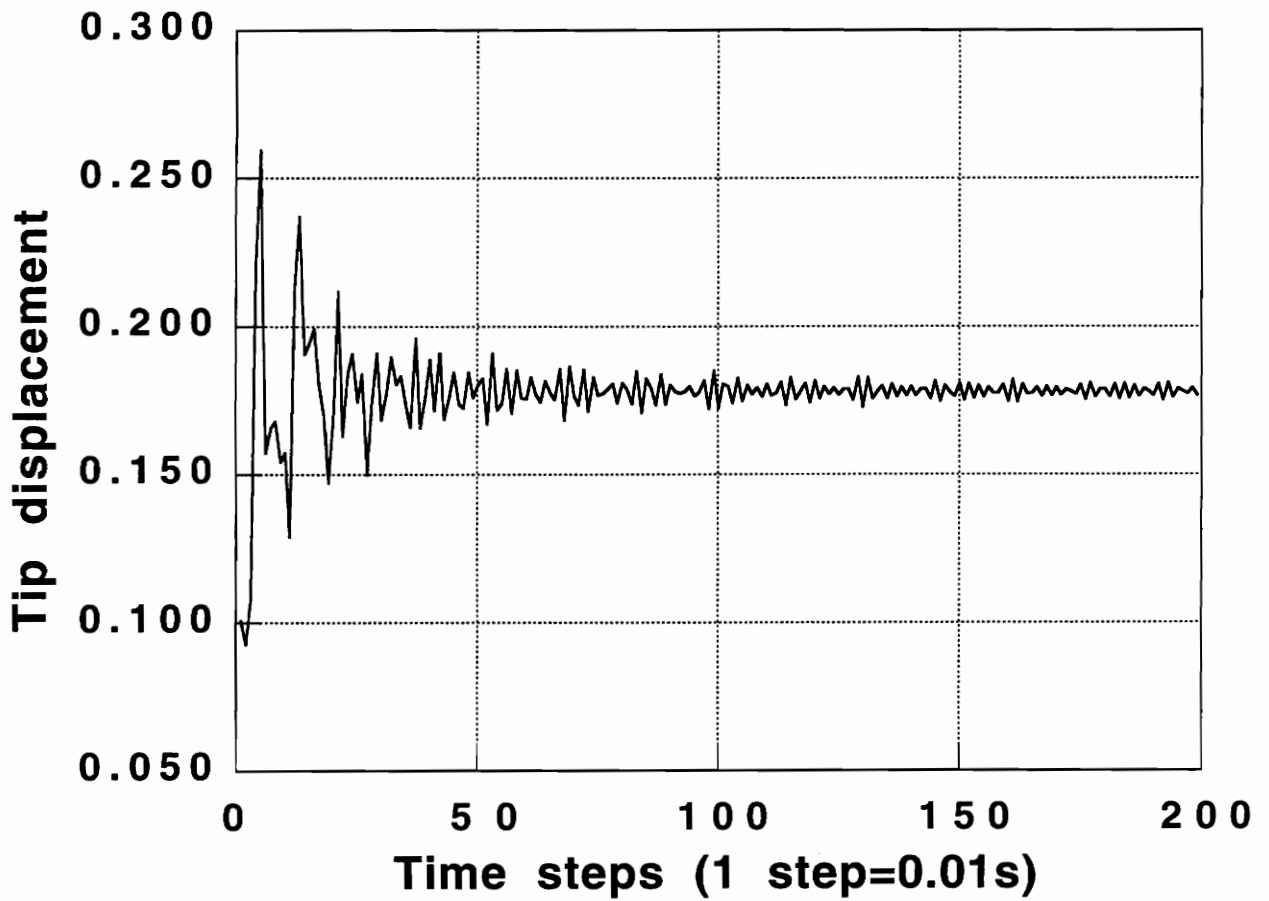


Fig. 3.3 Displacement vs Time at $V=66.24$ m/s
($AR=10$, $Area=20m^2$, $TR=0.5$, $Sweep=5^\circ$)

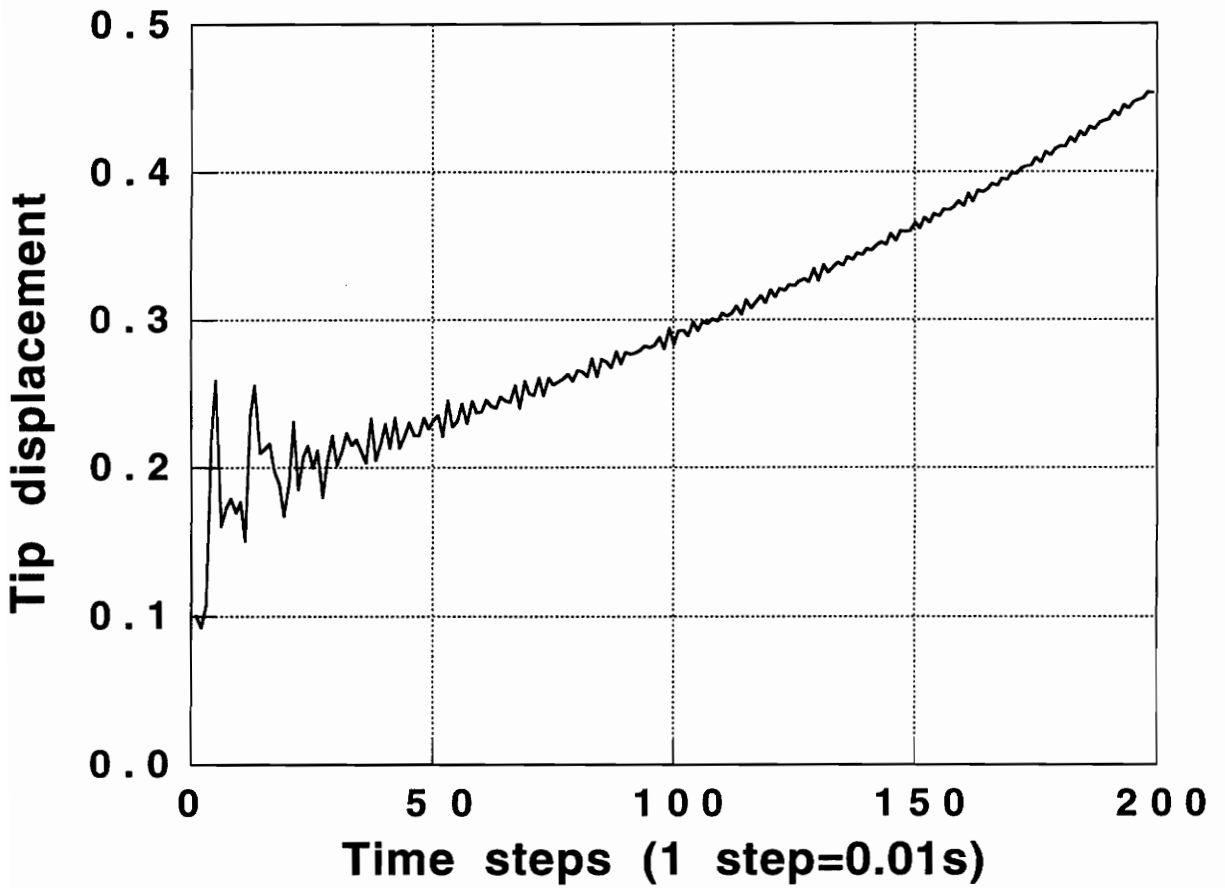


Fig. 3.4 Displacement vs Time at $V=70.0$ m/s
($AR=10$, $Area=20m^2$, $TR=0.5$, $Sweep=5^\circ$)

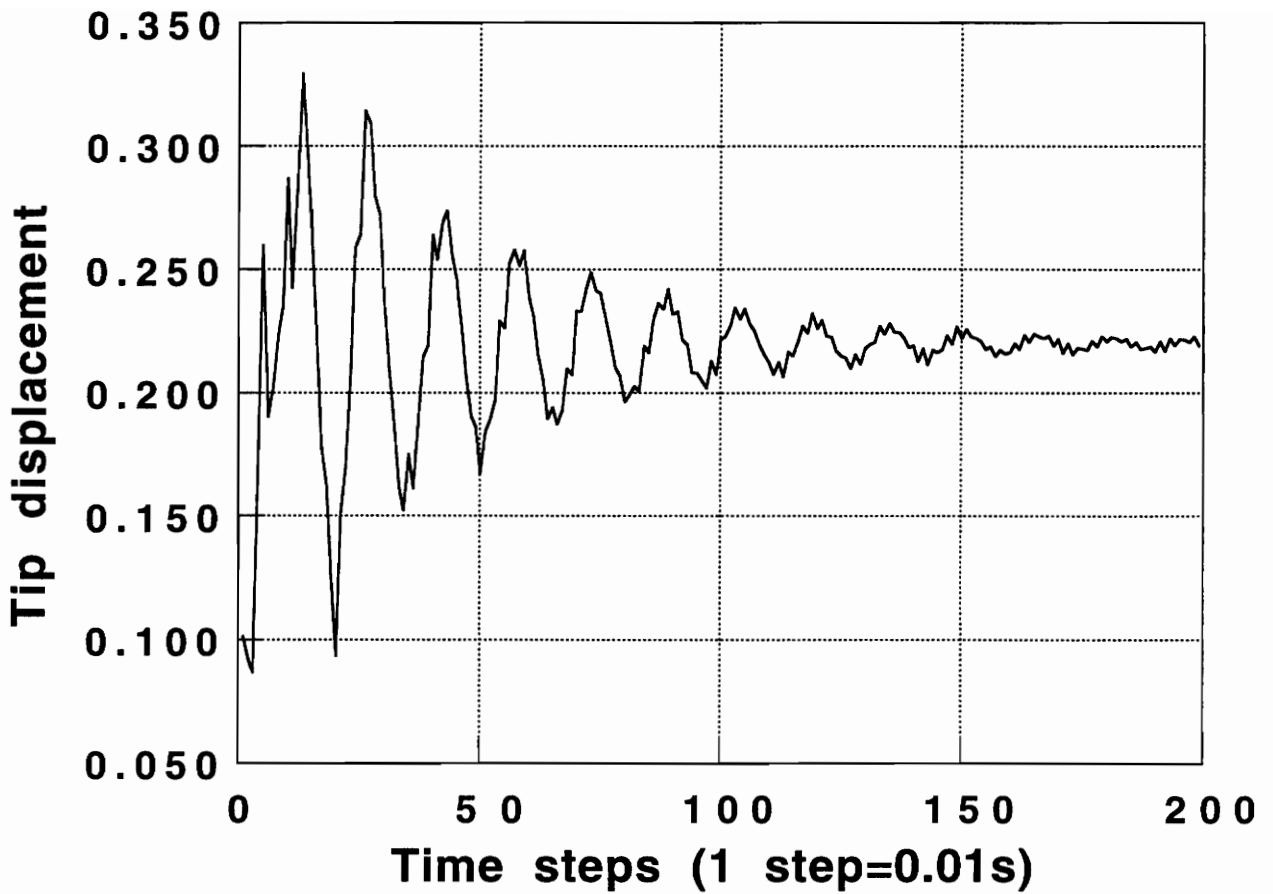


Fig. 3.5 Displacement vs Time at $V=92.64$ m/s
($AR=10$, $Area=20m^2$, $TR=0.5$, $Sweep=20^\circ$)

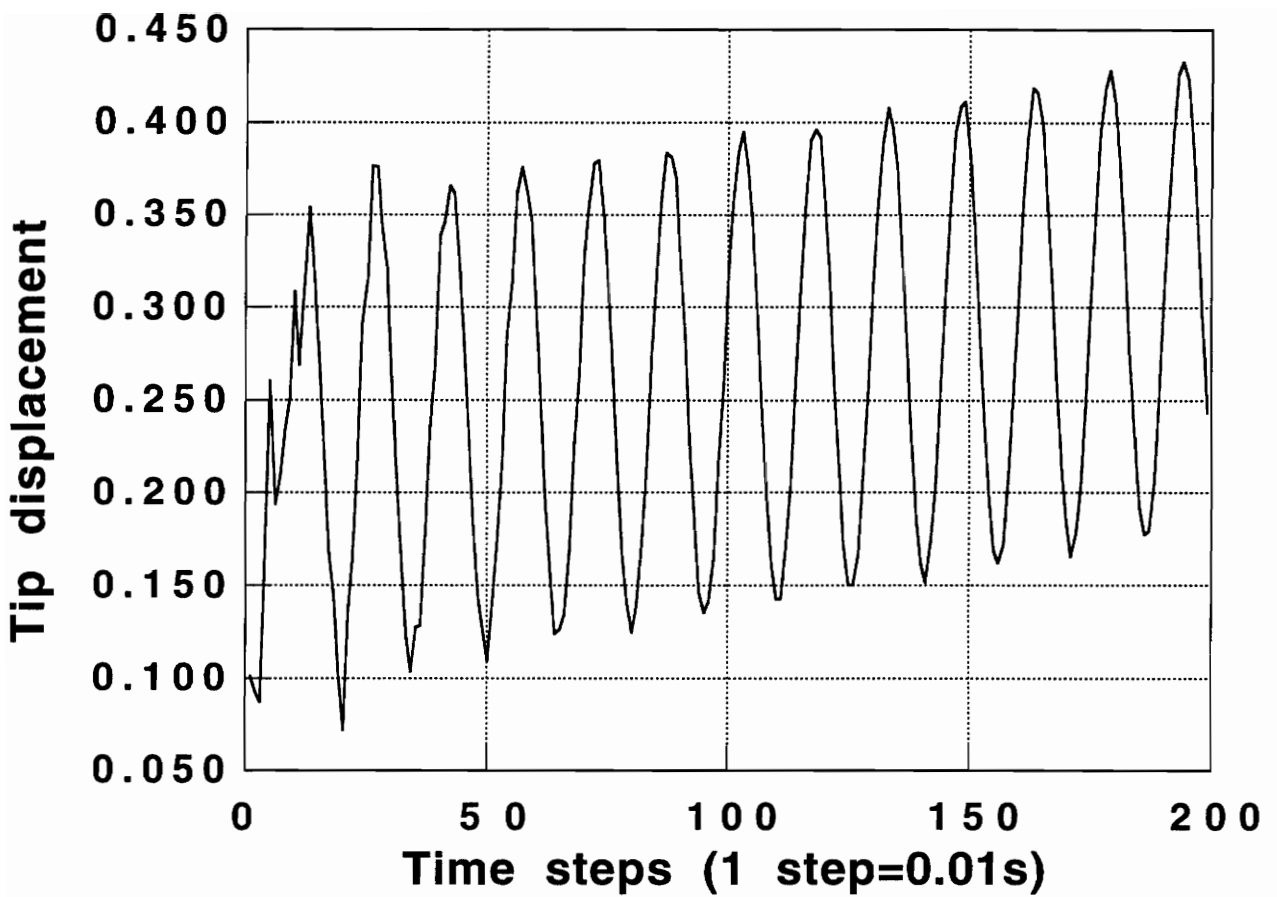


Fig. 3.6 Displacement vs Time at $V=95.90$ m/s
($AR=10$, $Area=20m^2$, $TR=0.5$, $Sweep=20^\circ$)

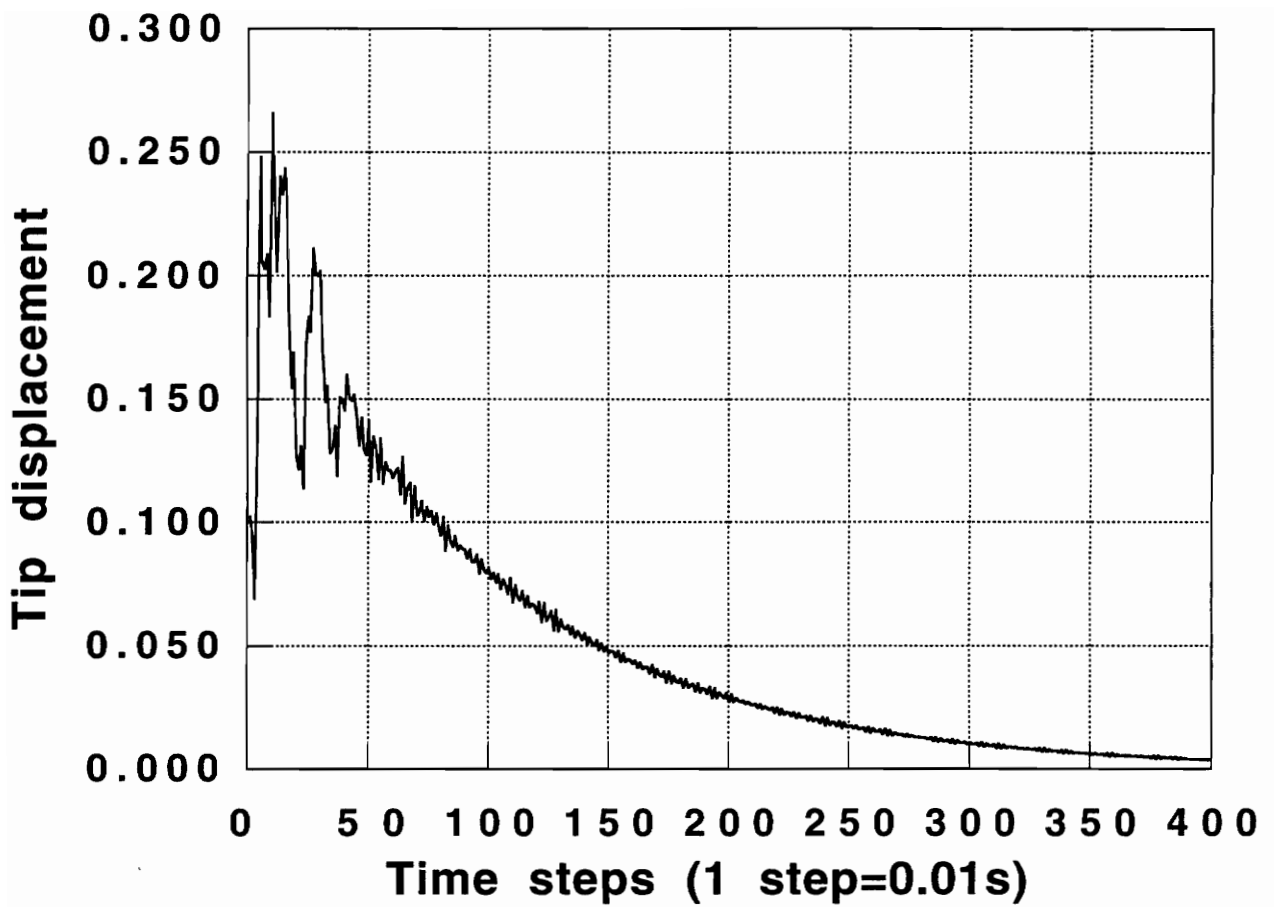


Fig. 3.7 Displacement vs Time at $V=90.0$ m/s
($AR=10$, $Area=20m^2$, $TR=0.5$, $Sweep=30^\circ$)

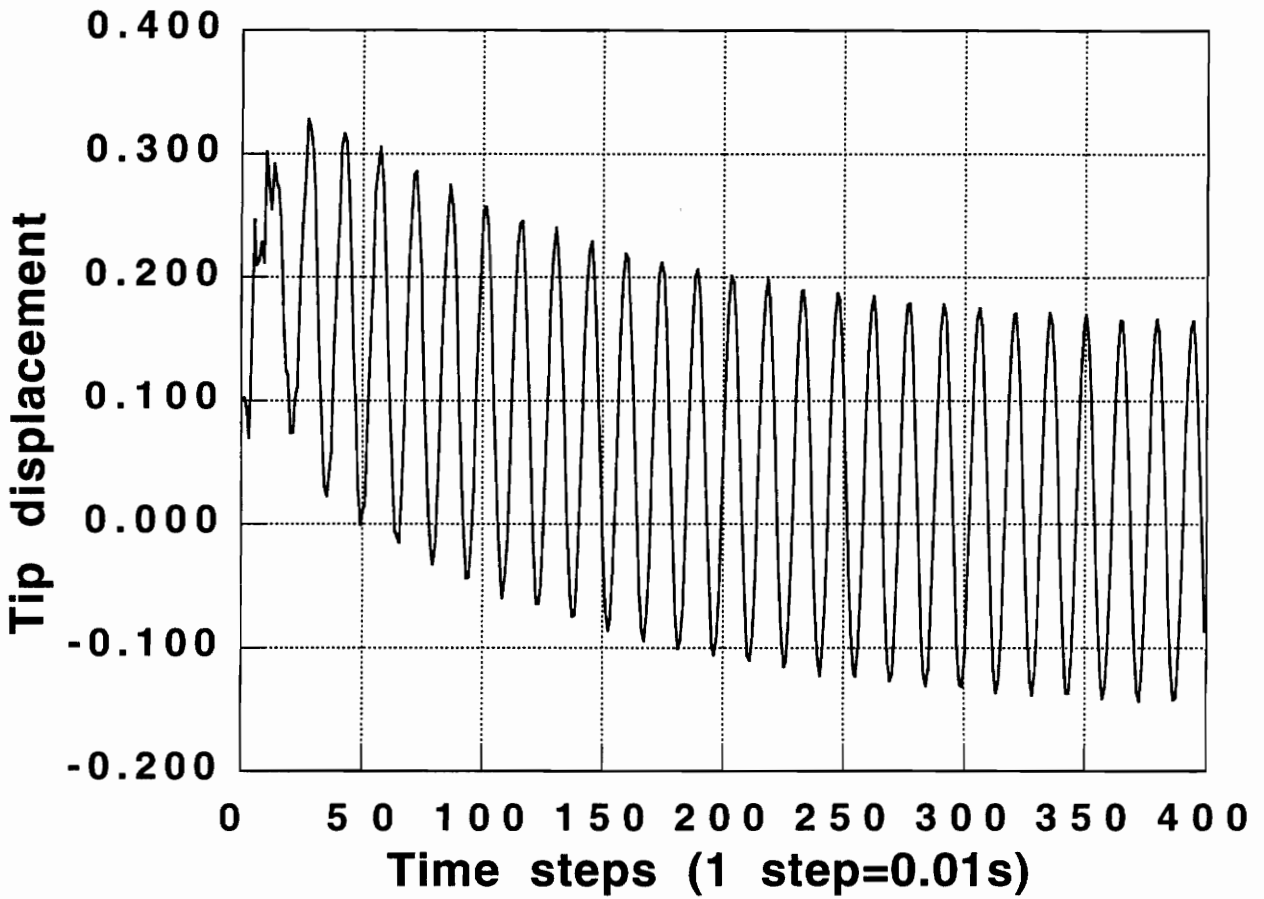


Fig. 3.8 Displacement vs Time at $V=98.87$ m/s
($AR=10$, $Area=20m^2$, $TR=0.5$, $Sweep=30^\circ$)

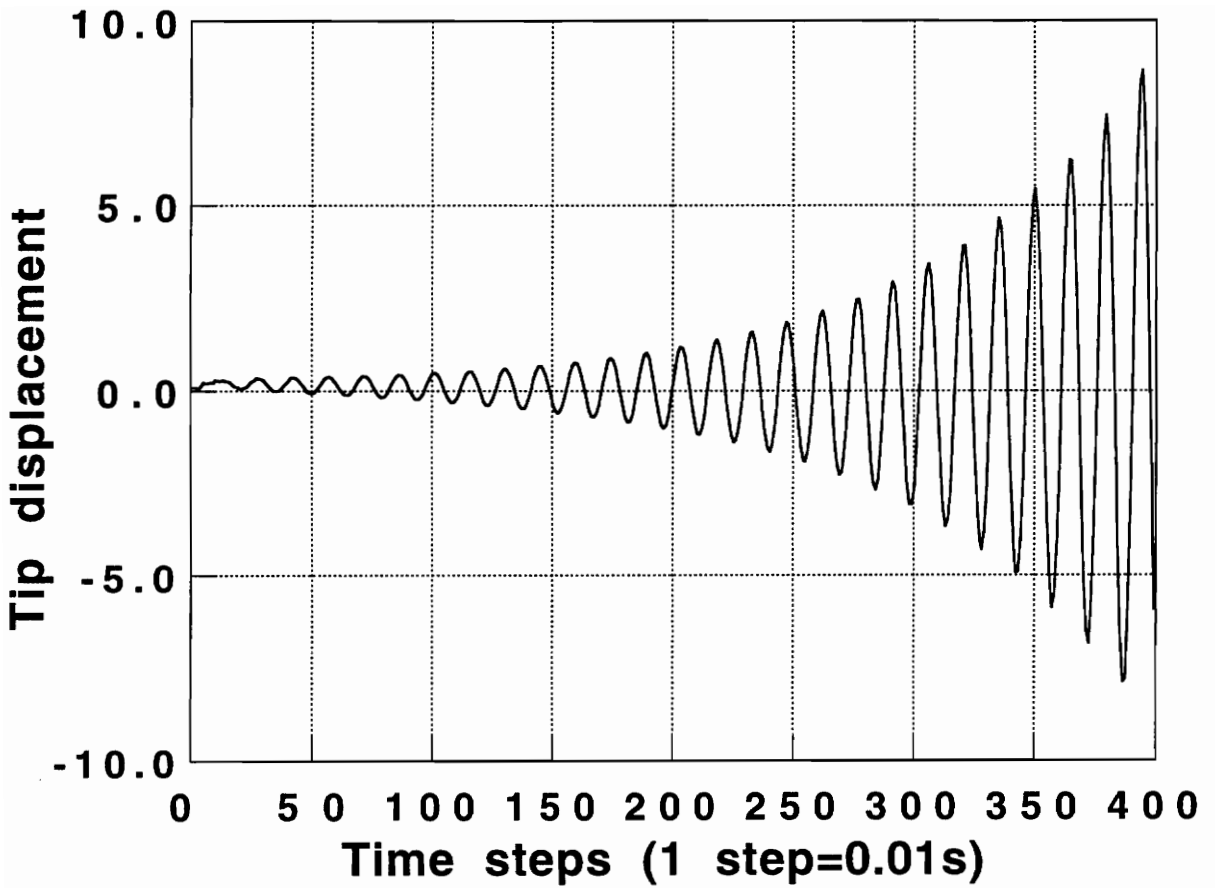


Fig. 3.9 Displacement vs Time at $V=100.0$ m/s
($AR=10$, $Area=20m^2$, $TR=0.5$, $Sweep=30^\circ$)

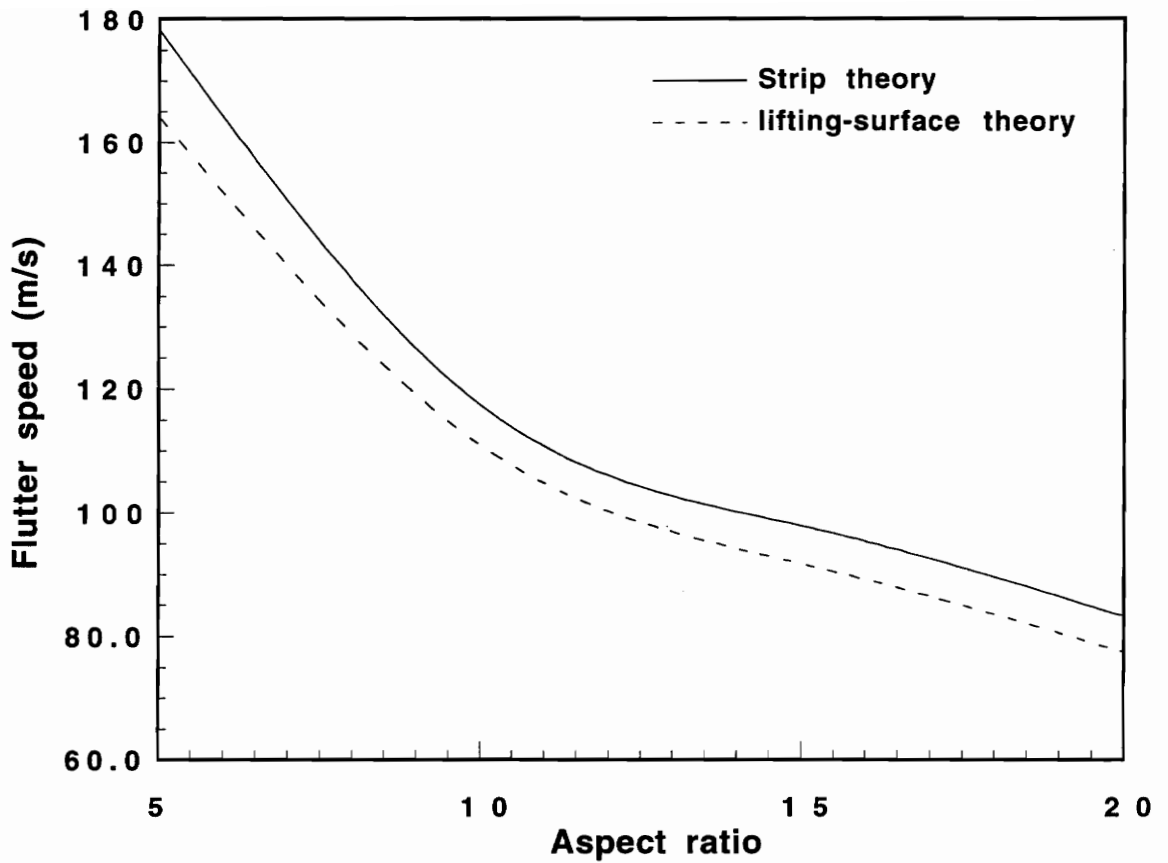


Fig. 3.10 Flutter speed from strip-theory (state-space aerodynamics) compared to lifting-surface theory (FAST)

(M=0.7, Area=20m², TR=0.5, Sweep=0°)

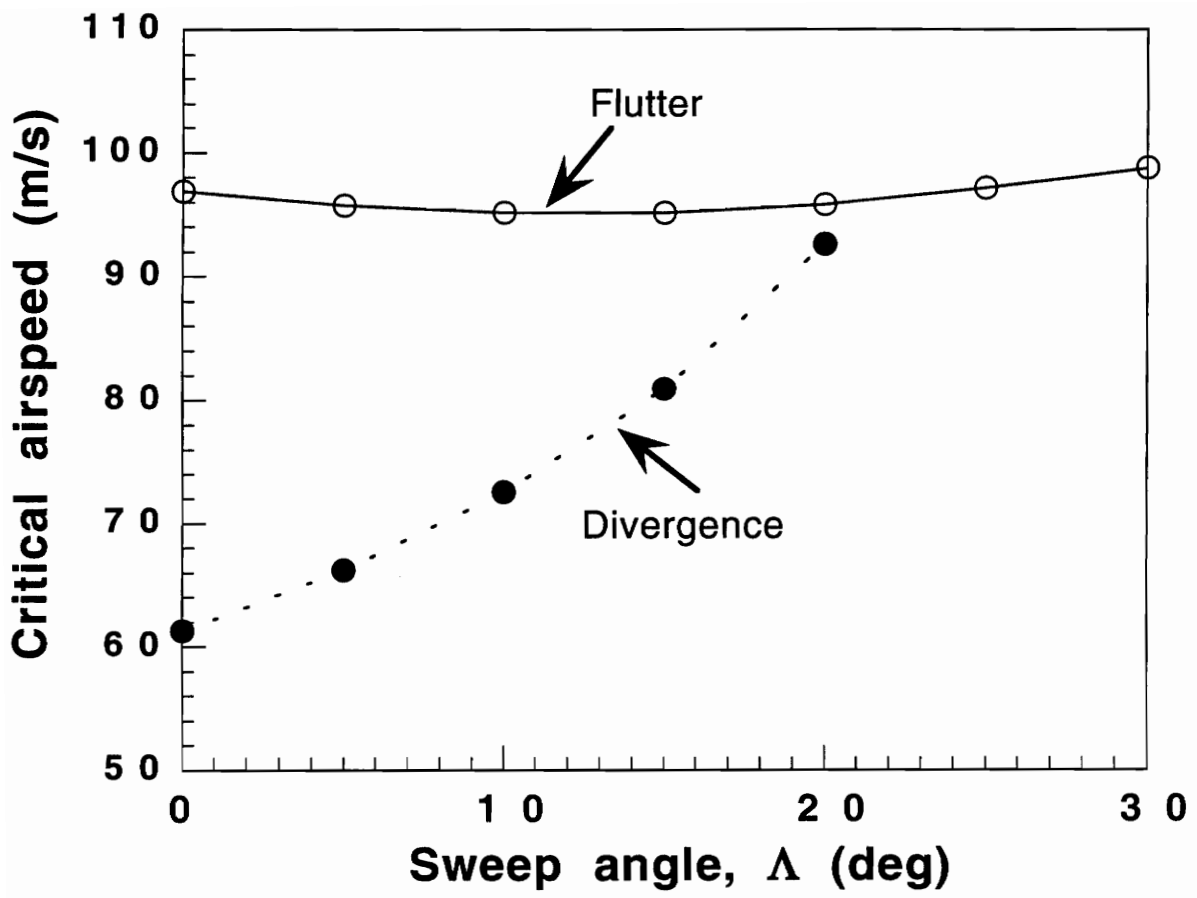


Fig. 3.11 Critical speed vs Sweep Angle
(AR=10, Area=20 m², TR=0.5)

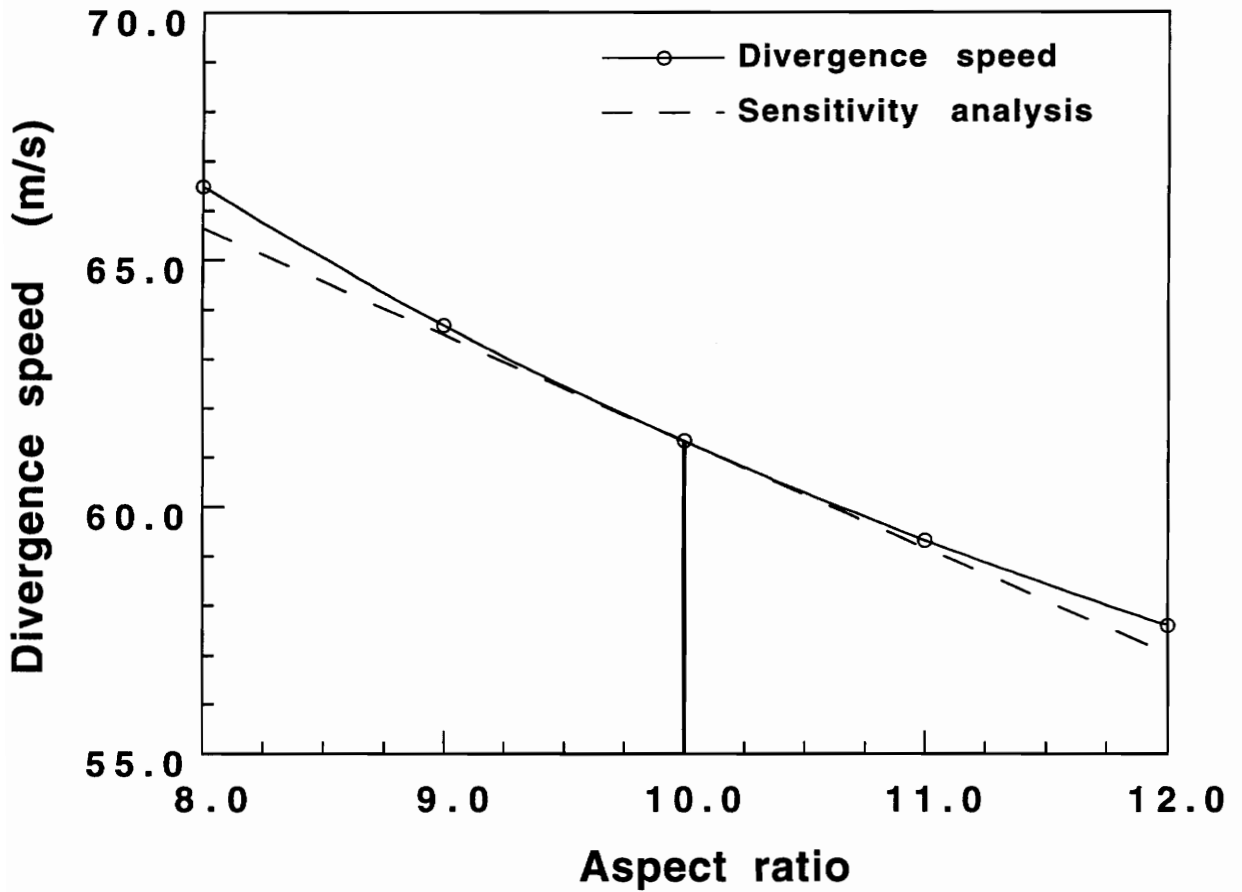


Fig. 3.12 Divergence speed vs Aspect ratio (M=0.7)
(AR=10, Area=20m², TR=0.5, Sweep=0°)

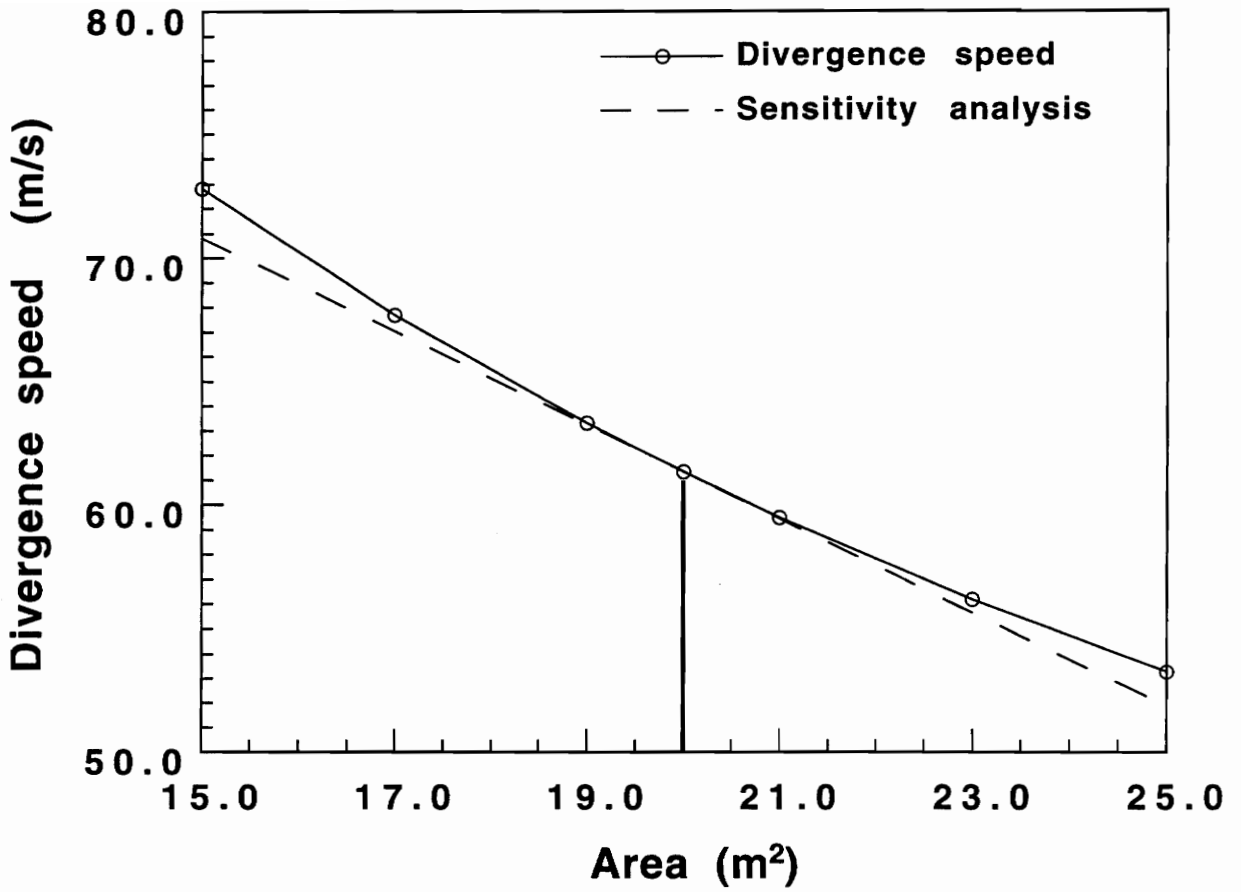


Fig. 3.13 Divergence speed vs Area (M=0.7)
(AR=10, Area=20m², TR=0.5, Sweep=0°)

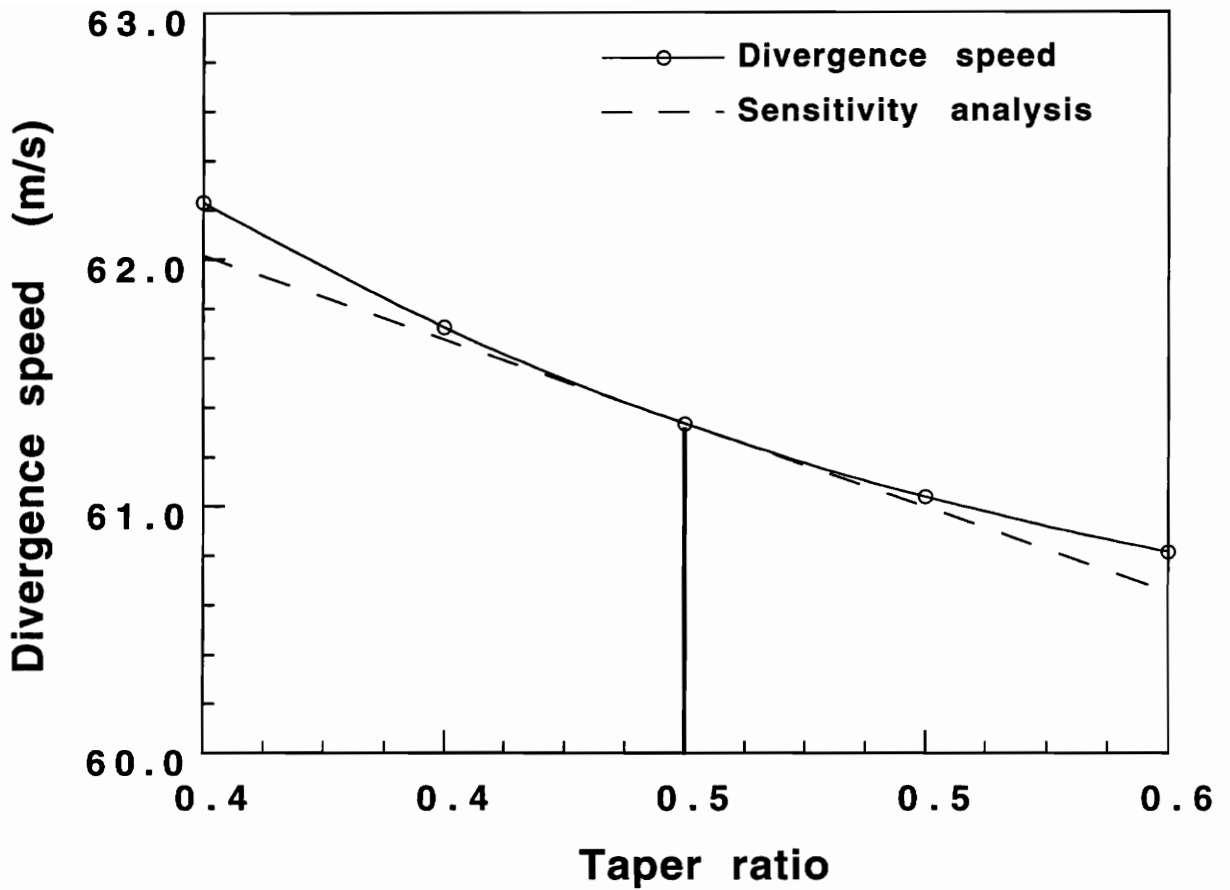


Fig. 3.14 Divergence speed vs Taper ratio ($M=0.7$)
($AR=10$, $Area=20m^2$, $TR=0.5$, $Sweep=0^\circ$)

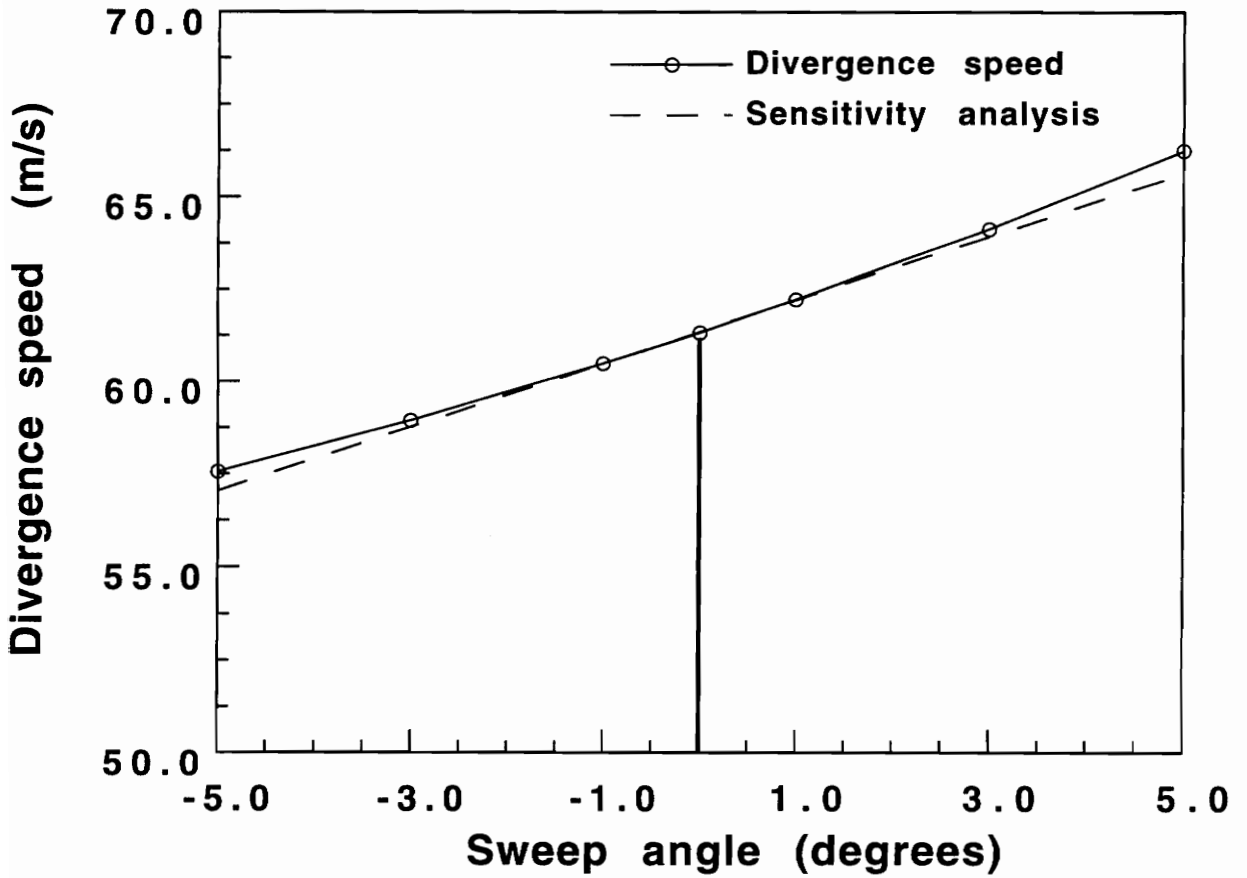


Fig. 3.15 Divergence speed vs Sweep angle ($M=0.7$)
($AR=10$, $Area=20m^2$, $TR=0.5$, $Sweep=0^\circ$)

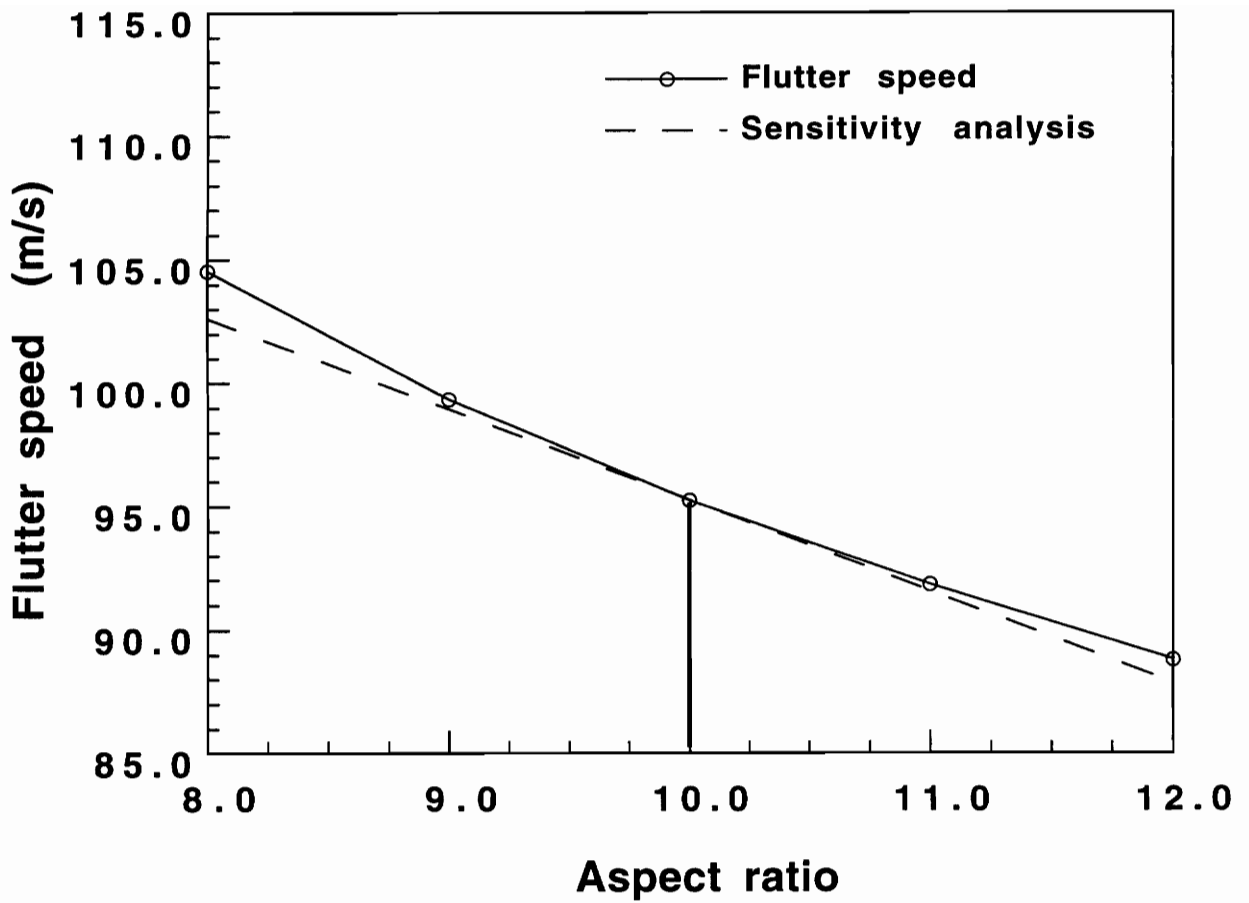


Fig. 3.16 Flutter speed vs Aspect ratio ($M=0.7$)
($AR=10$, $Area=20m^2$, $TR=0.5$, $Sweep=15^\circ$)

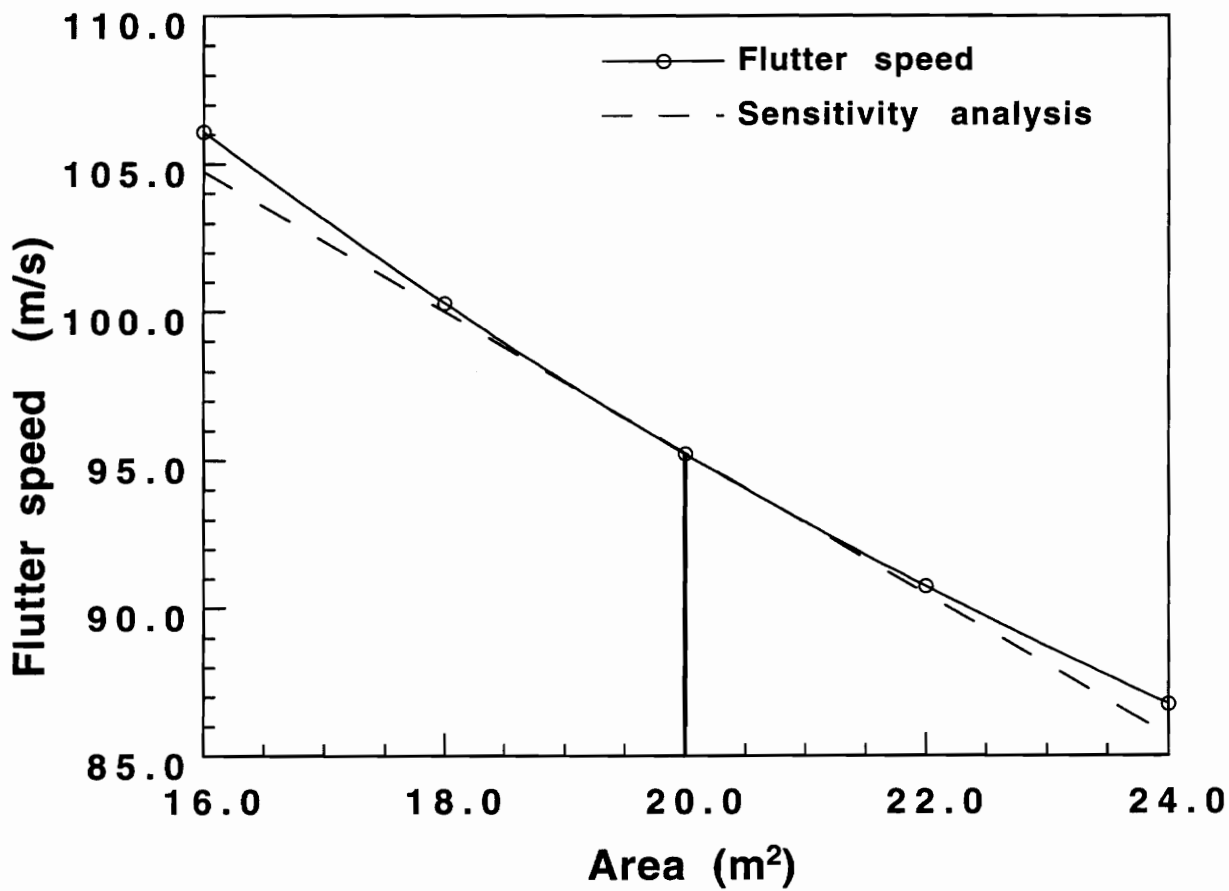


Fig. 3.17 Flutter speed vs Area (M=0.7)
(AR=10, Area=20m², TR=0.5, Sweep=15°)

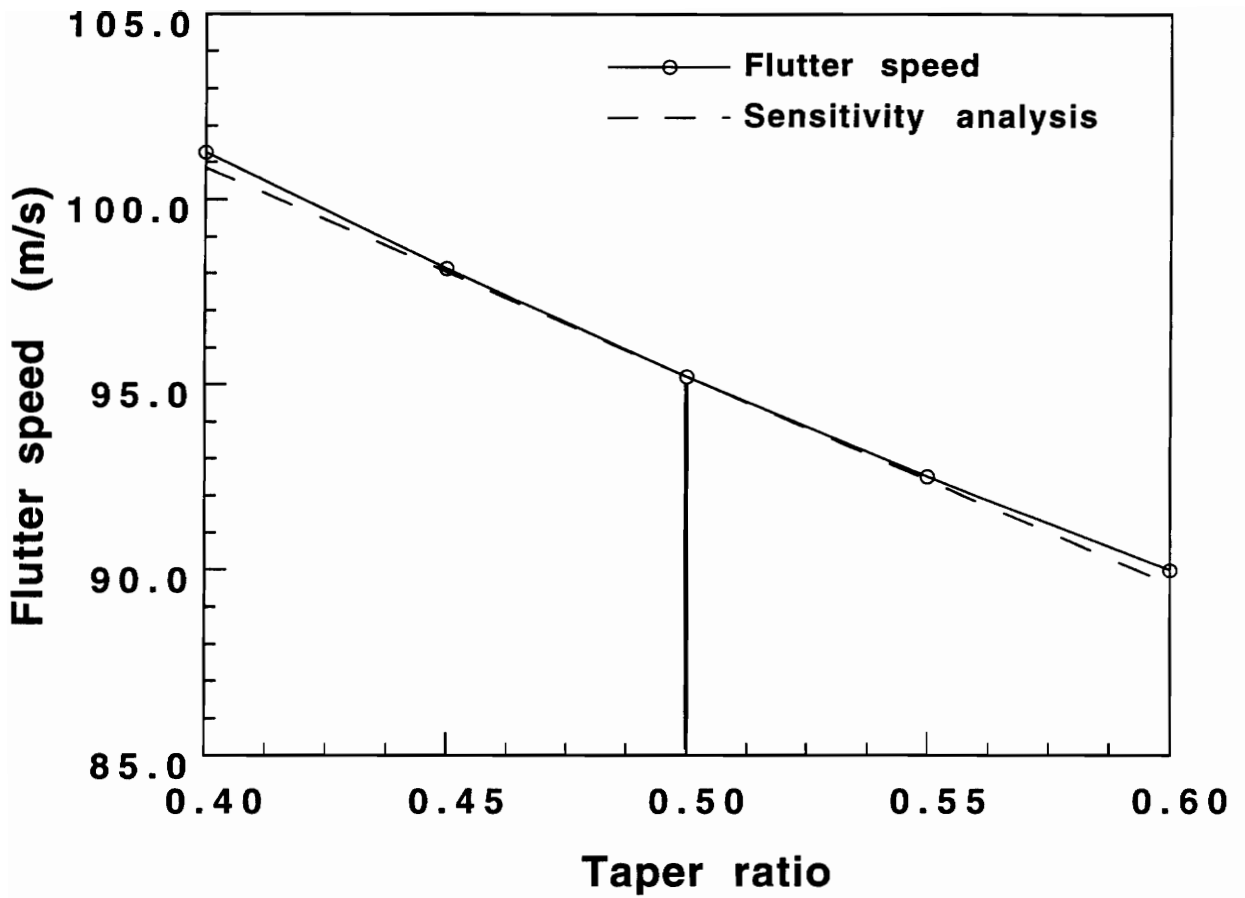


Fig. 3.18 Flutter speed vs Taper ratio (M=0.7)
(AR=10, Area=20m², TR=0.5, Sweep=15°)

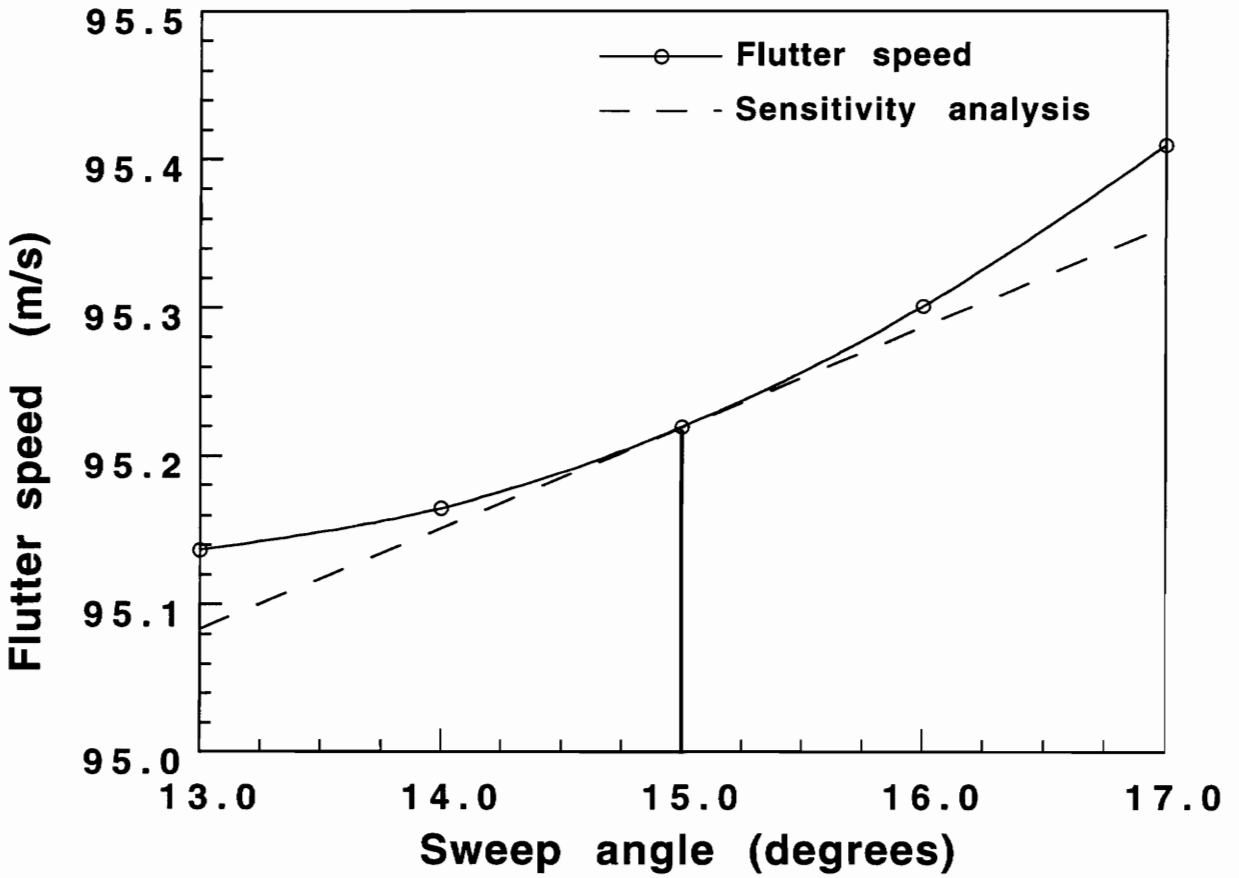


Fig. 3.19 Flutter speed vs Sweep angle (M=0.7)
(AR=10, Area=20m², TR=0.5, Sweep=15°)

Table 3.1 Comparison of natural frequencies of an unswept wing
 (*Area* = 0.02318 m², *Aspect ratio* = 4.0132, *Taper ratio* = 1.0)
 for different laminate sequences

Laminate sequence	Natural frequencies (Hz.)					
	Present			Landsberger and Dugundji [88]		
	First	Second	Third	First	Second	Third
[0 ₂ /90] _s	11.03	39.30	69.06	10.8	39	67
[15 ₂ /0] _s	8.86	42.62	63.25	8.5	48	58
[±15/0] _s	10.12	48.9	64.94	9.9	50	63
[+30 ₂ /0] _s	6.21	37.57	57.78	6.0	41	60
[±30/0] _s	7.73	48.76	64.42	7.8	50	65

Table 3.2 Comparison of flutter speed of an unswept wing
 (*Area* = 0.02318 m², *Aspect ratio* = 4.0132, *Taper ratio* = 1.0)
 in subsonic flow

Laminate sequence	Flutter speed (m/s)	
	Present	Experimental [88]
[0 ₂ /90] _s	24.9	26
[15 ₂ /0] _s	23.2	25
[±15/0] _s	28.1	28
[∓15/0] _s	18.9	21
[+30 ₂ /0] _s	28.8	29

CHAPTER 4

SENSITIVITY OF AEROELASTIC RESPONSE OF A WING USING FREQUENCY DOMAIN APPROACH

4.1 OVERVIEW

The problem of flutter instability was studied in Chapter 3 using a state-space unsteady aerodynamic representation and a Rayleigh-Ritz structural formulation. The sensitivity of flutter speed to shape parameters of the wing were obtained analytically. In this Chapter, the same Rayleigh-Ritz structural formulation is adopted, but the aeroelastic analysis is carried out using lifting-surface unsteady aerodynamics using modules from a system of programs [89] called FAST (Flutter Analysis System). Flutter speeds are obtained using a V-g type of solution. The derivatives of the flutter speed with respect to shape parameters of the wing are calculated using automatic differentiation (ADIFOR). In order to determine the importance of a particular mode to flutter, derivatives of the flutter speed with respect to natural frequencies, generalized mass and generalized aerodynamic forces are computed using ADIFOR.

Automatic differentiation is emerging as a valuable tool for sensitivity calculations. ADIFOR, GRESS, PADRE-2, Power Calculus and ODYSEE are some of the automatic differentiation packages [90] developed for differentiating FORTRAN77 codes. ADIFOR (Automatic Differentiation of FORtran) is a joint venture of Rice University and Argonne National Laboratory. ADIFOR processes a given Fortran code and generates a Fortran code for computing the derivatives

of the desired output variables with respect to the independent variables by applying the chain rule of differentiation. Differentiating large codes by hand is cumbersome, divided differences are dependent on choice of step size and symbolic programs may be infeasible for large codes. Automatic differentiation, on the other hand, can handle codes of arbitrary size and produce exact derivatives of the discrete system with no truncation error.

4.2 AEROELASTIC MODEL

The equivalent plate model described in section (3.2) based on a Rayleigh-Ritz formulation using Chebyshev polynomials for the wing displacements is used for structural modeling. Flutter calculations are performed using FAST [89], a system of programs based on the subsonic kernel function lifting-surface aerodynamic theory. A free vibration analysis of the wing is performed and the vibration modes from this analysis are fed into the modes processing module from FAST. The subsonic kernel function matrix program then solves the subsonic downwash integral equation for the oscillating planar wing lifting surface. The generalized force module from FAST then computes the aerodynamic forces from the subsonic kernel matrices. The flutter speed of the wing is obtained using a V-g type of solution. The generalized aerodynamic forces are determined for a specific Mach number and for a range of values of the reduced frequency for the specified downwash distribution. These values are then interpolated to get aerodynamic forces for closely spaced values of the reduced frequency. The flutter equation solved by the program is

$$[\omega^2 - \omega_i^2(1 + ig)]M_i q_i + \sum_{j=1}^n A_{ij} q_j = 0, \quad i = 1, n \quad (4.1)$$

where ω is the vibration frequency, ω_i is the frequency of the i th natural vibration mode, M_i is the generalized mass associated with the i th natural vibration mode, g is the incremental damping, A_{ij} are the generalized aerodynamic forces resulting from the pressure induced by the j th mode acting through the displacements of the i th mode and q_i is the i th component of the flutter eigenvector.

In terms of the non-dimensional generalized aerodynamic forces \bar{A}_{ij} , the above equation can be written as an eigenvalue problem in the form,

$$\sum_{j=1}^n (C_{ij} - \delta_{ij}\Omega)q_j = 0, \quad i = 1, n \quad (4.2)$$

where the eigenvalue Ω is given by

$$\Omega = \left(\frac{\omega_o b_o}{V} \right)^2 (1 + ig) \quad (4.3)$$

and

$$C_{ij} = \left(\frac{\omega_o}{\omega_i} \right)^2 \left[\frac{\rho b_o^3 \bar{A}_{ij}}{2M_i} + \delta_{ij}k^2 \right] \quad (4.4)$$

where ω_o is a reference frequency, b_o is the reference length, usually root semichord, k is the reduced frequency, ρ is the air density and V is the airspeed.

The above eigenvalue problem is solved for a range of values of the reduced frequency and monitored for crossings on the V - g plane when the incremental damping g goes to zero. At each of these crossings, the values of the airspeed and the frequency are noted. The critical flutter speed is the lowest speed at which the damping of the structure goes to zero.

4.3 SENSITIVITY ANALYSIS USING AUTOMATIC DIFFERENTIATION

The sensitivity of flutter speed of the wing to shape parameters namely aspect ratio, area, taper ratio and sweep angle is computed using ADIFOR. In order to examine the importance of a particular mode to flutter, the sensitivity of flutter speed with respect to the modal parameters, namely, natural frequency, generalized mass and generalized aerodynamic forces is calculated using ADIFOR.

4.3.1 AUTOMATIC DIFFERENTIATION

Once the input variables and output variables of interest are identified, ADIFOR can be used to differentiate FORTRAN codes. ADIFOR propagates derivative values rather than formulas as in an analytic derivation. Only those intermediate variables that are functions of the input variables and are required in the computation of the output variables are identified and differentiated by ADIFOR.

A small example of an ADIFOR-generated FORTRAN code to compute the derivatives from a simple program **main.f** with one call made to the subroutine **func.f** is given in Appendix B. ADIFOR generates the code **g_func.f** which has statements to compute the derivatives of the output variable y with respect to the input variable array $x(3)$.

4.3.2 SENSITIVITY TO SHAPE PARAMETERS

For all the results presented, the wing shown in Fig. 3.2 is used with the wing skins made of 0 deg. laminated Graphite/Epoxy ($T300/N5208$) with the

following material properties: $E_1 = 181 \times 10^9 \text{ Pa}$, $E_2 = 10.3 \times 10^9 \text{ Pa}$, $\nu_{12} = 0.28$, $G_{12} = 7.17 \times 10^9 \text{ Pa}$ and $\rho = 1600 \text{ kg/m}^3$.

The sensitivity derivatives of the flutter speed with respect to shape parameters are calculated using ADIFOR. The sensitivity results and the results from reanalysis are shown in Figs. 4.1–4.4 for the wing at $M = 0.6$ and $\rho_{air} = 0.8 \text{ kg/m}^3$. The decrease in flutter speed due to increasing aspect ratio is seen to be gradual from $AR = 8$ to $AR = 10$ in Fig. 4.1. Then, a more sharper drop in flutter speed is seen as the AR is increased to 12. The sensitivity derivative however predicts the trend seen at the baseline configuration. The flutter speed decreases with increase in area and taper ratio as shown in Figs. 4.2 and 4.3. Increasing the sweep angle has the effect of increasing the flutter speed about the 30° swept-back configuration as shown in Fig. 4.4. By performing one sensitivity calculation at the baseline, this method gives a linear approximation to the flutter speeds of the wing for changes in the wing shape parameters about the baseline. This information is useful for preliminary design purposes, as it avoids the necessity of a reanalysis for small changes in any of the shape parameters.

4.3.3 SENSITIVITY TO MODAL PARAMETERS

Complex wing structures are often modeled with a large number of degrees of freedom and a vibration analysis yields a large number of free vibration modes. A certain number of these modes have to be fed into FAST to generate the generalized aerodynamic forces required for flutter analysis. Some of these modes do not actively participate in the flutter and using several modes to determine flutter

instability leads to larger computational cost. In situations, where the natural frequencies and mode shapes of the wing are measured from experiments, one has large amount of modal data and has to determine the number of modes that are required for reasonably estimating the flutter speed. One could make a judicious choice of the number of modes that are required for flutter analysis, based on the sensitivity derivatives of the flutter speed with respect to the modal parameters of the wing.

The sensitivity of flutter speed to modal parameters were obtained using ADIFOR. The derivatives of the flutter speed with respect to natural frequencies of the wing are shown in Fig. 4.5. Nine modes were used for the flutter analysis. It can be seen that if the third natural frequency is increased by 1 rad/s , then the flutter speed increases by 1.5 m/s . It is also seen that higher modes do not contribute much to the flutter. The derivatives of the flutter speed with respect to generalized mass are given in Fig. 4.6 and the flutter speed sensitivity to the real and imaginary parts of the generalized aerodynamic forces (GAF) is given in Fig. 4.7. The (i, j) term in Fig. 4.7 stands for the non-dimensional generalized aerodynamic force resulting from the pressure induced by the j th mode acting through the displacements of the i th mode. The sensitivities of flutter speed with respect to modal parameters give an estimate of the importance of a particular mode to flutter.

In order to obtain a quantitative estimate of the contribution of a particular mode to flutter, one can use the sensitivity information which gives the variation of flutter speed with the natural frequency, generalized mass and real and imaginary parts of the generalized aerodynamic forces associated with that mode. It is

possible to construct a logarithmic derivative and sum up the absolute values of these derivatives, which reflects the change in flutter speed due to changes in modal parameters associated with a particular mode. Having obtained all the derivatives one could construct a parameter P_i for each mode i given by

$$P_i = \left| \frac{\omega_i}{V_f} \frac{\partial V_f}{\partial \omega_i} \right| + \left| \frac{M_i}{V_f} \frac{\partial V_f}{\partial M_i} \right| + \sum_{j=0}^N \left[\left| \frac{Re(Q_{ij})}{V_f} \frac{\partial V_f}{\partial Re(Q_{ij})} \right| + \left| \frac{Im(Q_{ij})}{V_f} \frac{\partial V_f}{\partial Im(Q_{ij})} \right| \right] \quad (4.5)$$

where V_f is the flutter speed, ω_i is the natural frequency, M_i is the generalized mass and $Re(Q_{ij})$ and $Im(Q_{ij})$ are the real and imaginary parts of the generalized aerodynamic forces for an aeroelastic analysis using N vibration modes. The values of this parameter P_i for the nine modes used in the analysis are given in Table 4.1. It can be seen that the higher modes do not contribute significantly to the flutter phenomenon. Based on this information, flutter analysis of the same wing was carried out using fewer modes (5 modes) and the flutter speed obtained was 100.338 m/s compared to a value of 100.404 m/s using 9 modes, which is not a significant drop in flutter speed. The differences in the values of the derivatives of the flutter speed computed using fewer modes are found to be insignificant compared to the derivative values using more number of modes.

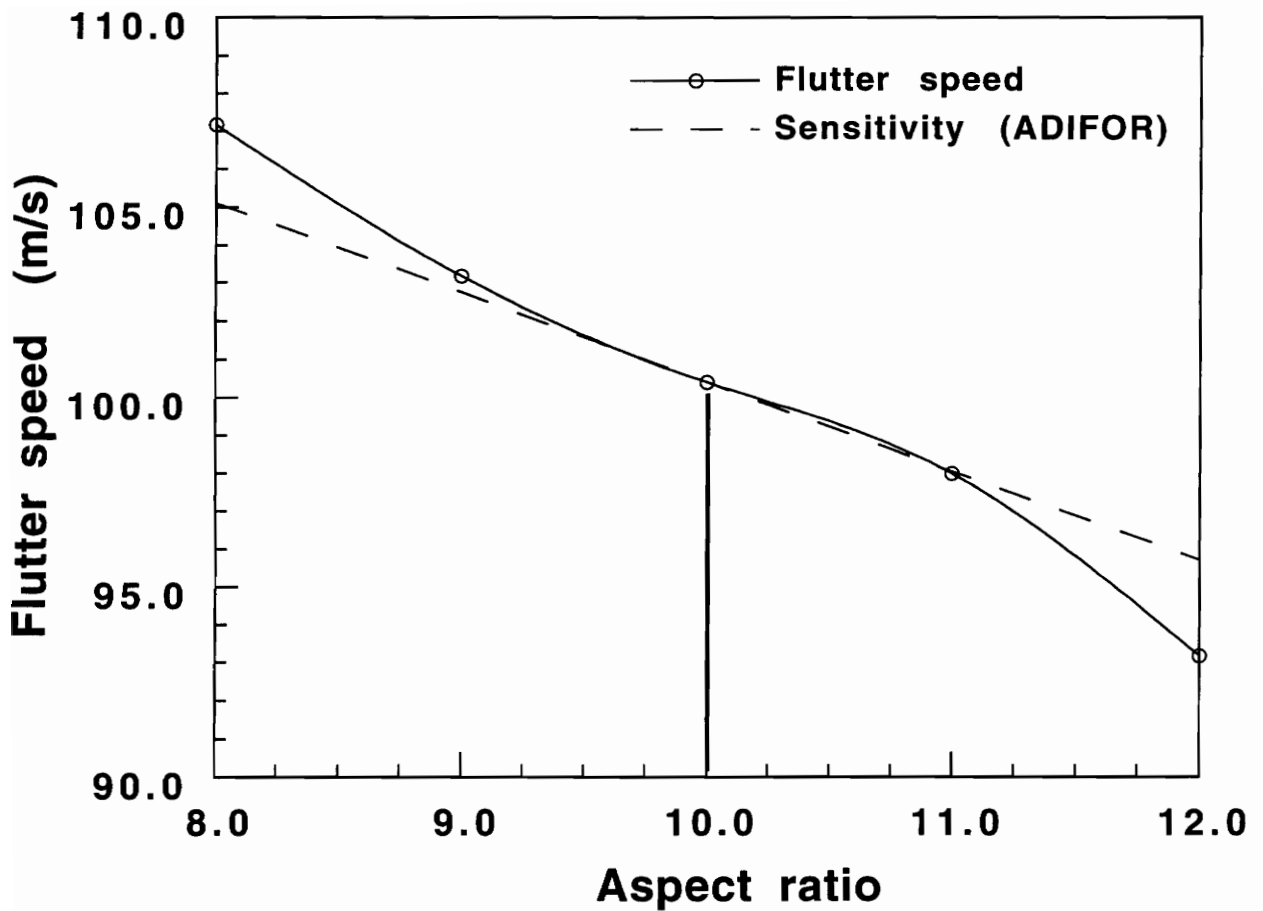
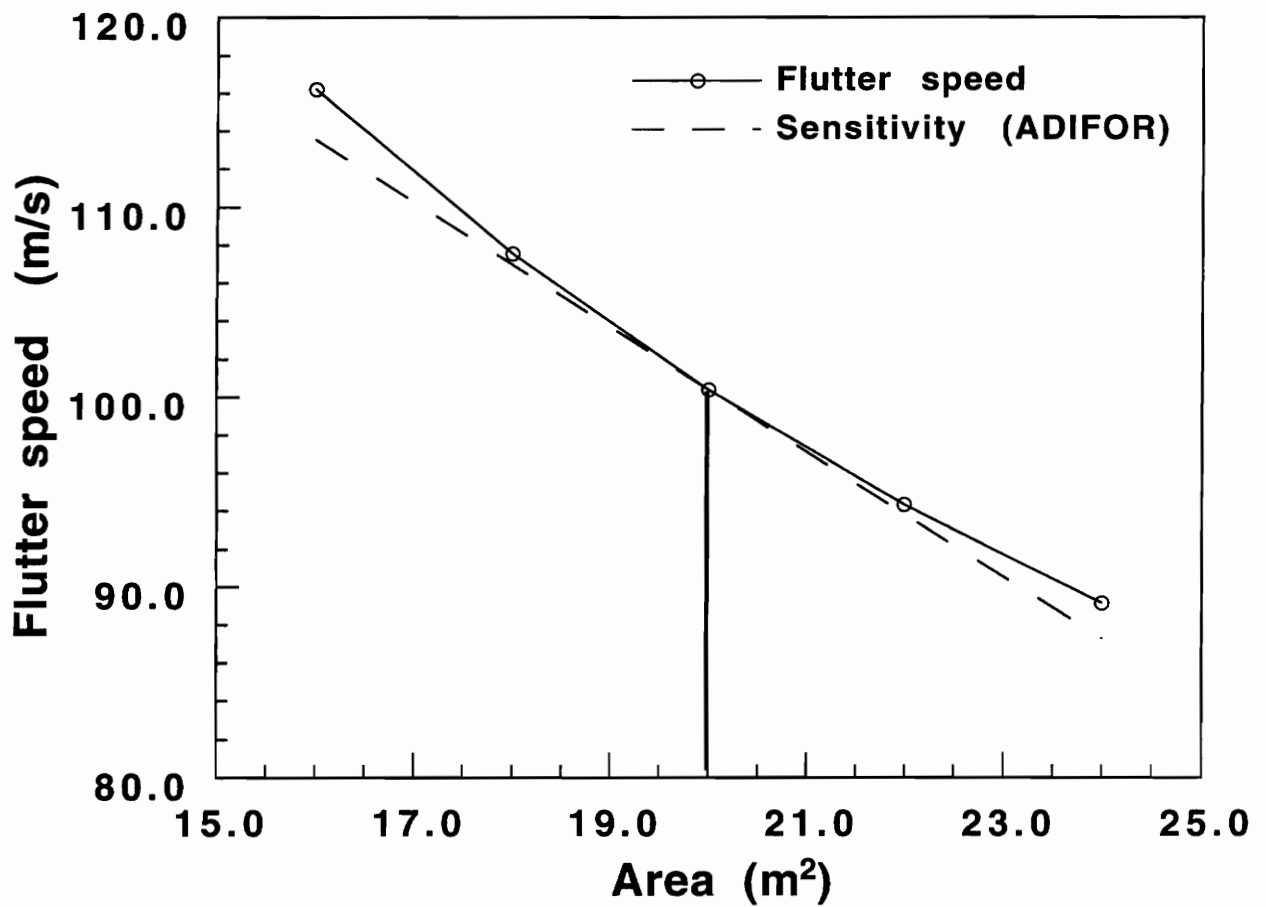


Fig. 4.1 Flutter speed vs Aspect ratio (M=0.6) from FAST

(AR=10, Area=20m², TR=0.5, Sweep=30°)



**Fig 4.2 Flutter speed Vs Area (M=0.6)
from FAST**

(AR=10, Area=20m², TR=0.5, Sweep=30°)

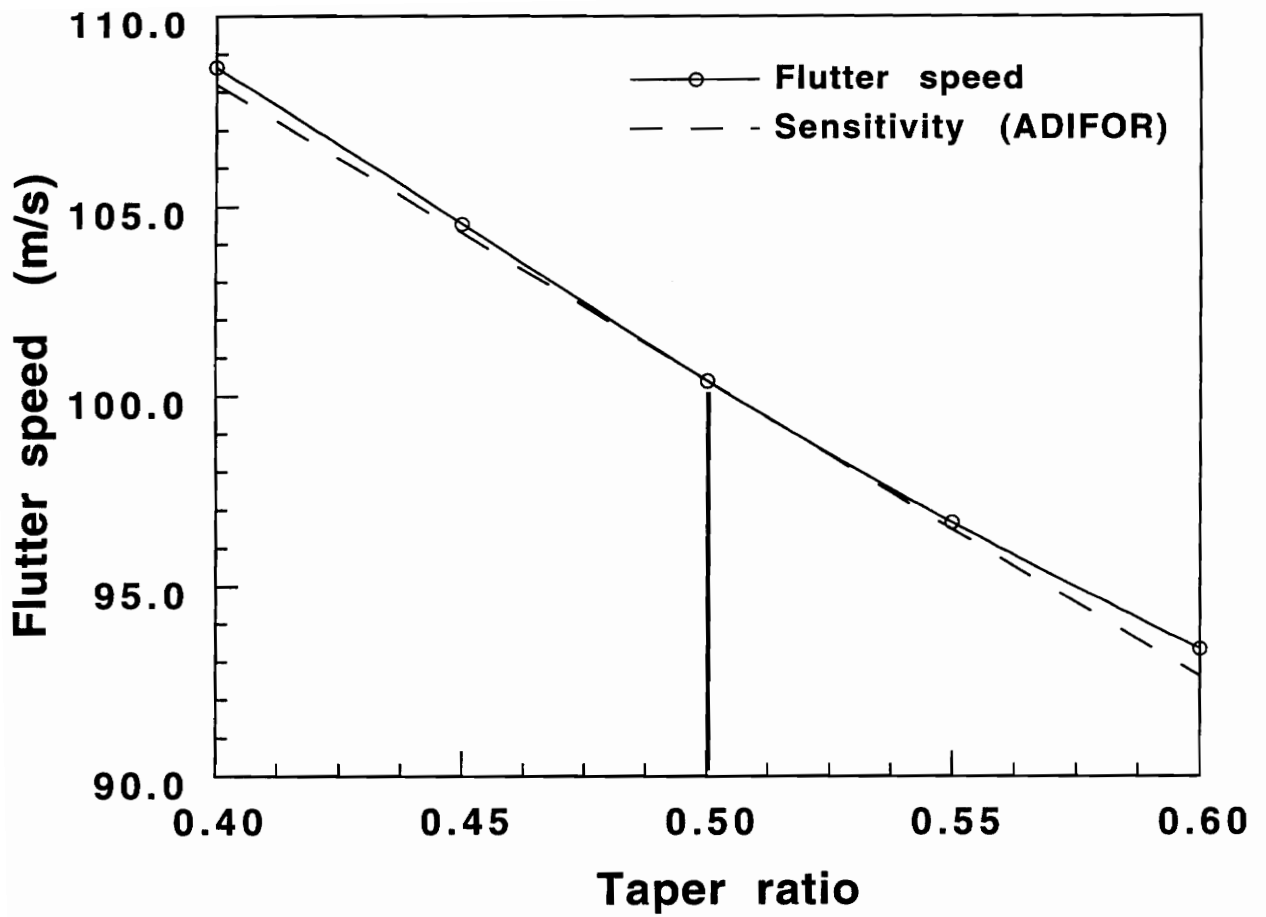


**Fig. 4.3 Flutter speed vs Taper ratio (M=0.6)
from FAST**

(AR=10, Area=20m², TR=0.5, Sweep=30°)

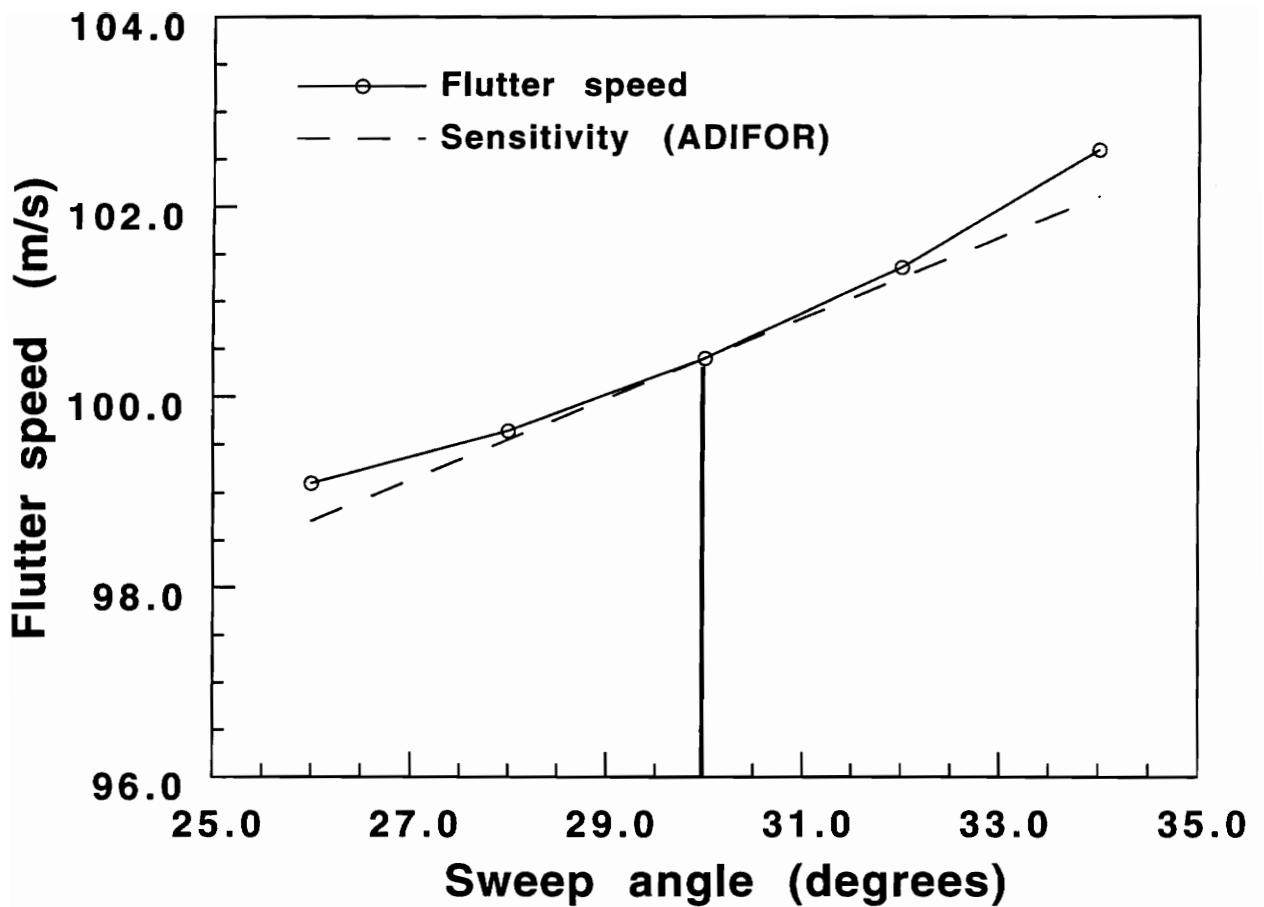


**Fig. 4.4 Flutter speed vs Sweep angle (M=0.6)
from FAST**

(AR=10, Area=20m², TR=0.5, Sweep=30°)

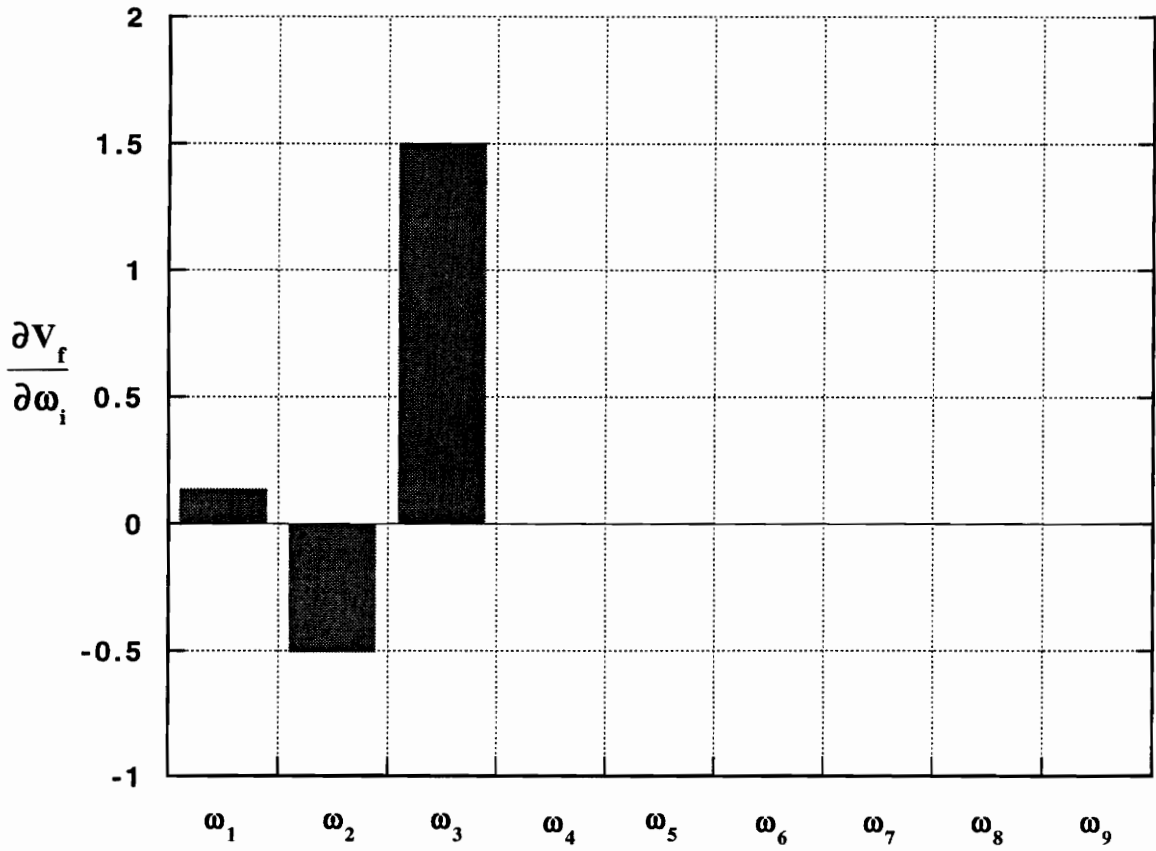
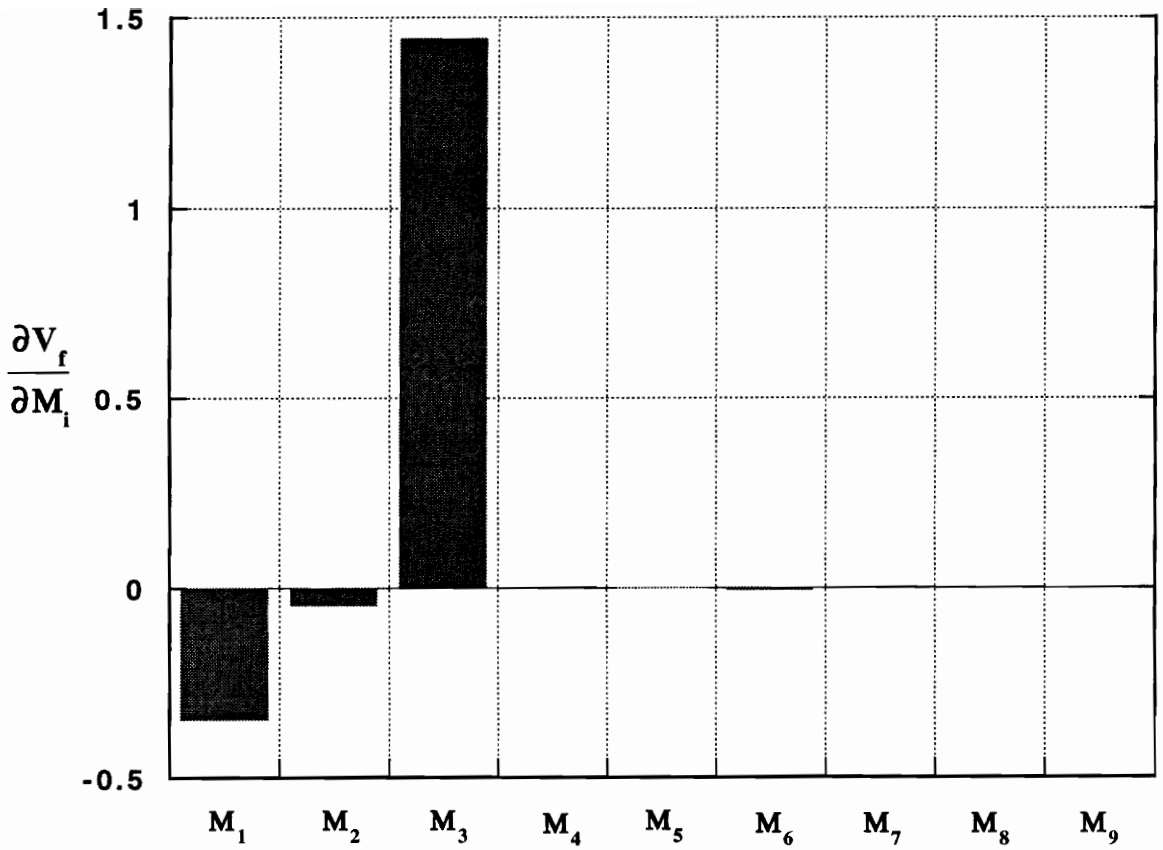


Fig. 4.5 Flutter speed sensitivity to natural frequency (M=0.6)
in (m/s)/(rad/s)
(AR=10, Area=20m², TR=0.5, Sweep=30°)



**Fig. 4.6 Flutter speed sensitivity to generalized mass (M=0.6)
in (m/s)/(kg)**
(AR=10, Area=20m², TR=0.5, Sweep=30°)

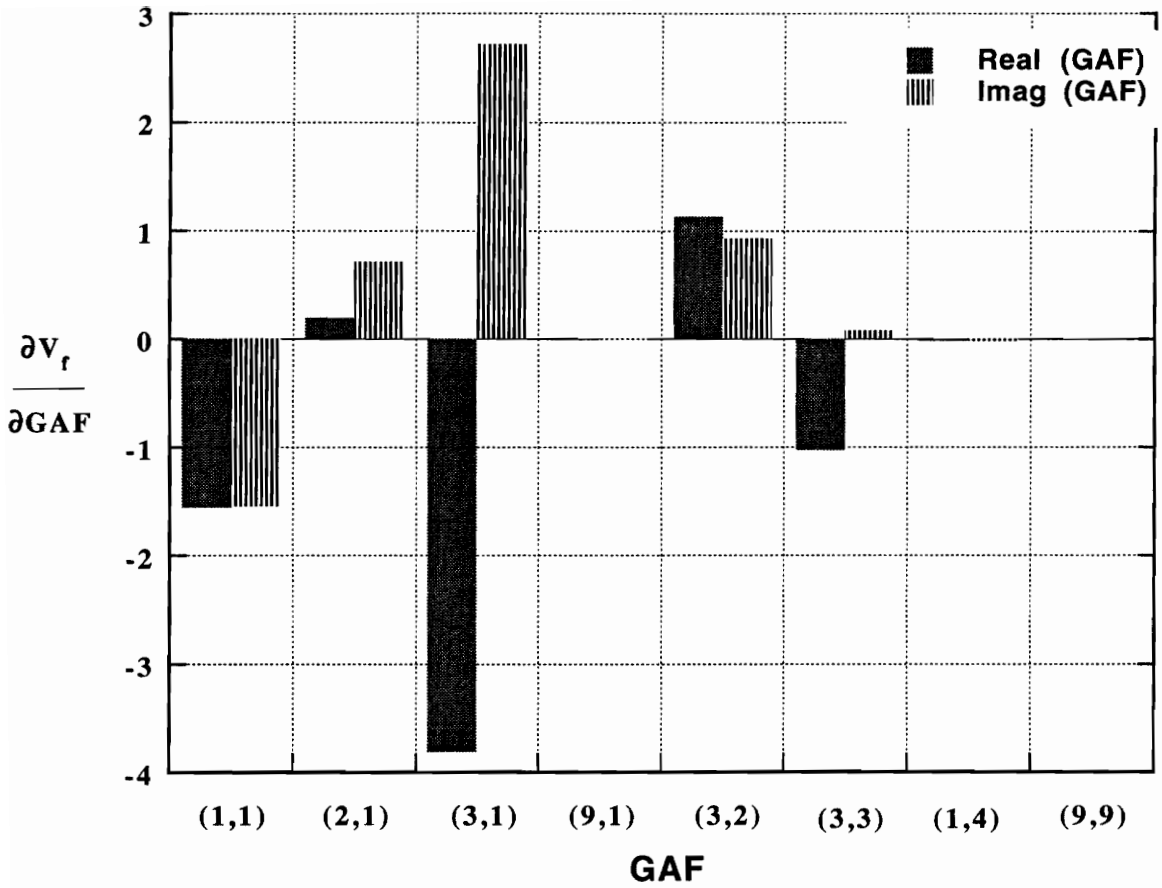


Fig. 4.7 Flutter speed sensitivity to nondimensional generalized aerodynamic forces (GAF) ($M=0.6$) in (m/s)
($AR=10$, $Area=20m^2$, $TR=0.5$, $Sweep=30^\circ$)

**Table 4.1 Sum of the absolute values of the logarithmic derivatives
(Parameter P_i for each mode i)**

Mode i	Parameter P_i
1	$0.603527579439D + 00$
2	$0.423090289768D + 00$
3	$0.232364489123D + 01$
4	$0.689605102271D - 02$
5	$0.175814335457D - 01$
6	$0.339129036750D - 02$
7	$0.518670036226D - 04$
8	$0.176862340452D - 03$
9	$0.432725654009D - 03$

CHAPTER 5

FINITE ELEMENT WING MODELING USING NASTRAN FOR AEROELASTIC SENSITIVITY CALCULATIONS

5.1 OVERVIEW

In previous chapters, to obtain sensitivity of aeroelastic response of a wing to shape and modal parameters, a Rayleigh-Ritz based equivalent plate model was used for analyzing the wing structure. Though equivalent plate representation in conjunction with global Ritz analysis techniques are relatively inexpensive for mathematical modeling of wings to study aeroelasticity, finite element methods [91–93] are being used in the industry for structural modeling of aircraft wings.

Several commercial finite element codes like ABAQUS, ANSYS, EAL, IDEAS and NASTRAN exist for finite element analysis of structures. The current work focusses on modeling the wing structure using NASTRAN [94]. One of the features of using FEM is that any planform shape and wing cross-section could be analyzed as opposed to the Rayleigh-Ritz formulation based equivalent plate model used in Chapters 3 and 4, where only a trapezoidal skewed configuration of uniform thickness and layerwise construction could be analyzed. The wing skins, spars and ribs of an airplane wing can be modeled using shell and beam elements in NASTRAN. The free vibration modes of the wing can be fed into the unsteady aerodynamics code to generate the aerodynamic forces for aeroelastic analysis. The sensitivity of flutter speed of the wing to shape and modal parameters is

computed using a combination of the central difference scheme and the automatic differentiation software ADIFOR.

5.2 NASTRAN ELEMENTS USED IN THIS STUDY

In this study, the CQUAD4 and CTRIA3 shell elements, the CBAR beam elements and the CSHEAR shear panel elements are used. A description of these elements is given below.

5.2.1 CQUAD4 SHELL ELEMENT

The CQUAD4 element is one of the isoparametric quadrilateral shell elements in NASTRAN with optional coupling of bending and membrane stiffness. The element coordinate system for quadrilateral shell element is shown in Fig. 5.1. The integers 1, 2, 3 and 4 refer to the order of the connected grid points on the connection entries defining the elements. The angle, THETA, is the orientation angle for material properties. The CQUAD4 element is a 4-noded, 24 degrees of freedom element with 6 degrees of freedom per node ($u, v, w, \theta_x, \theta_y, \theta_z$).

5.2.2 CTRIA3 SHELL ELEMENT

The CTRIA3 element is one of the isoparametric triangular shell elements in NASTRAN with optional coupling of bending and membrane stiffness. The element coordinate system for triangular shell element is shown in Fig. 5.2. The integers 1, 2 and 3 refer to the order of the connected grid points on the connection entries defining the elements. The angle, THETA, is the orientation angle for material properties. The CTRIA3 element is a 3-noded, 18 degrees of freedom element with 6 degrees of freedom per node ($u, v, w, \theta_x, \theta_y, \theta_z$).

5.2.3 CBAR BEAM ELEMENT

The CBAR element is a one-dimensional bending element which is prismatic, and for which the elastic axis, gravity axis, and shear center all coincide. The bar element coordinate system is shown in Fig. 5.3. The CBAR element is a 2-noded, 12 degree of freedom element with 6 degrees of freedom per node ($u, v, w, \theta_x, \theta_y, \theta_z$).

5.2.4 CSHEAR SHEAR PANEL ELEMENTS

The CSHEAR shear panel element is a two-dimensional structural element that resists the action of tangential forces applied to its edges, and the action of normal forces if effectiveness factors are used. The use of proper effectiveness factors to account for the normal forces on the elements are described in section 5.3.2 where shear panels are used to model the spar and rib webs. The structural and non-structural mass of the shear panel is lumped at the connected grid points. The element coordinate system for a shear panel is shown in Fig. 5.4a. The labels G1, G2, G3 and G4 refer the order of the connected grid points. The element forces are shown in Fig. 5.4b, which consist of the forces applied to the element at the corners in the direction of the sides, kick forces at the corners in a direction normal to the plane formed by the two adjacent edges, and shear flows (force per unit length) along the four edges.

5.3 NUMERICAL EXAMPLES

In order to validate the finite element modeling, static analysis of a box-beam is performed using NASTRAN and the results compared with Euler-Bernoulli solution. Both static and dynamic analysis of a swept-back wing are carried out using NASTRAN and the wing deflections and frequencies are compared with previously published results.

5.3.1 FINITE ELEMENT BOX-BEAM MODEL USING NASTRAN

As a first example, a cantilevered box-beam shown in Fig. 5.5 was analyzed. The box-beam is modeled with CQUAD4 shell elements and CBAR beam elements. A total of 70 plate elements and 60 beam elements were used for the discretization. The dimensions of the box-beam are as follows:

Thickness of the plate elements, $t = 5mm$

Length of the beam, $L = 4m$

Width of the beam, $b = 0.8m$

Height of the beam, $h = 0.4m$

Area of the beam elements, $A_b = 900mm^2$

Young's Modulus, $E = 210GPa$

Poisson's ratio, $\nu = 0.3$

Moment of inertia, $I = 586 \times 10^{-6}m^4$

The box-beam was subjected to two loadings: (i) a tip load of $P = 300N$, and (ii) a distributed load of $q = 80N/m$ (corresponding to a uniform pressure load of $100N/m^2$ on the beam $0.8m$ wide). The tip deflection results from NASTRAN, at nodes 1 to 6 (see Fig. 5.5) on the tip of the beam, were compared with Euler-Bernoulli beam-theory solution for a beam given below:

For a tip load,

$$w = \frac{PL^3}{3EI} \quad (5.1)$$

For a distributed load,

$$w = \frac{qL^4}{8EI} \quad (5.2)$$

The results are shown in Fig. 5.6. There is good agreement between the finite element solution and the beam-theory solution.

5.3.2 STATIC AND DYNAMIC ANALYSIS OF A SWEPT WING

In order to validate the modeling, a swept back wing model reported in Ref. 95 published for AGARD is analyzed. It is an all aluminum wing, swept back by 30 deg. and has 5 identical spars and 3 identical ribs bonded to the top and bottom cover skins. The dimensions of the wing and its cross-section properties are given in Fig. 5.7. The finite element discretization of the wing is given in Fig. 5.8.

The wing is subjected to a tip load of 1 *lb.* at the trailing edge as shown in Fig. 5.9. The wing skins are modeled using CQUAD4 and CTRIA3 shell membrane-bending elements. The spar and rib webs are modeled using CSHEAR panel elements and the spar and rib caps are modeled using CBAR beam elements. The computed deflections from NASTRAN of the front and rear spars along the span are plotted in Fig. 5.9. The measured deflection from Ref. 95 is also shown. The results agree fairly well.

Next, the natural frequencies of the wing are calculated using NASTRAN. The wing skins are modeled using CQUAD4 and CTRIA3 shell membrane-bending

elements and the spar and rib caps are modeled using CBAR beam elements as before. However, the spar and rib webs are modeled in two different ways: (i) using CSHEAR shear panel elements and (ii) CQUAD4 shell membrane-bending elements. The natural frequencies of the wing are compared in Table 5.1 to the results reported in Ref. 96 which were computed using ELFINI finite element package. It should be noted that in the finite element model reported in Ref. 96, the webs act only in shear. The results obtained using shear panels for the webs compare well with ELFINI results. When shear panels are used to model the webs, it is assumed that the webs act only in shear and the required axial stiffness at the edges are provided to support the corner forces. However, these webs also contribute to the stiffness of the structure in a small way. Hence, the spar and rib webs are modeled using CQUAD4 shell membrane-bending elements and the first five frequencies are given in Table 5.1. The CQUAD4 element for the webs gives stiffer solutions as can be seen from Table 5.1 (the frequencies of transverse vibration are about 2-3 % higher, especially in the bending modes, and the inplane frequency is also higher).

When using the CSHEAR element in NASTRAN (see Fig. 5.4), appropriate factors F_1 and F_2 have to be specified for providing extensional stiffness along the sides of the element to handle the corner forces which are parallel to the sides of the element. Factor F_1 is the effectiveness factor for extensional stiffness along edges 1-2 and 3-4 and F_2 is the effectiveness factor for extensional stiffness along edges 2-3 and 1-4. The effective extensional area is defined by means of extensional rods on the perimeter of the element. Thus, if $F_1 = 1.0$, the panel

is fully effective for extension in the 1-2 and 3-4 direction. The areas of the rods on the edges 1-2 and 3-4 are set equal to $(0.5 F_1 T w_1)$, where w_1 is the average width of the panel and T is the thickness of the panel. Proper selection of the effectiveness factors is important when using the shear panel elements. Three different cases were examined using the effectiveness factors. If the default values of $F_1 = F_2 = 0.0$ are used, then the computed frequencies are very small, since the shear panel elements have no axial stiffness along the edges. If the panels are made fully effective for extension in both directions, then the solution obtained is much stiffer than that obtained using CQUAD4 shell membrane-bending elements for the webs. The proper choice is to make the panel (for spar and rib webs) fully effective for extension in the transverse direction of the wing and let the spar and rib caps carry the load in the other direction. This gives frequencies which agree well with the frequencies reported in Ref. 96 using ELFINI.

5.4 SENSITIVITY OF FLUTTER SPEED

The structural modeling of the wing is done using NASTRAN. The airfoil shape is generated by transforming a circle into an airfoil using the Joukowski transformation, so that shapes of varying thickness and camber can be obtained by varying the parameters. Finite element discretization of the wing skins, spars and ribs is done and a free vibration analysis of the wing is performed. The natural frequencies and mode shapes obtained are used to generate the generalized aerodynamic forces required for flutter analysis using FAST. The sensitivity of flutter speed to shape and modal parameters is computed using a combination of central difference scheme and ADIFOR.

5.4.1 AIRFOIL COORDINATES FOR THE WING

It is beneficial if the airfoil shape generation for the wing cross-section is parameterized so that shapes of varying thickness and camber can be generated. In order to generate the co-ordinates of the wing cross-section, a transformation of a circle into an airfoil using the Joukowski transformation is carried out. The equation of the circle in the ζ -plane shown in Fig. 5.10 is

$$(\xi - p)^2 + (\eta - q)^2 = a^2 \quad (5.3)$$

with center at $\mu = p + iq$ and radius a .

For points on the circle,

$$\left. \begin{array}{l} \xi = p + a\cos\theta \\ \eta = q + a\sin\theta \end{array} \right\} \quad 0 \leq \theta \leq 2\pi \quad (5.4)$$

Therefore,

$$\zeta = \xi + i\eta = (p + a\cos\theta) + i(q + a\sin\theta) \quad (5.5)$$

The circle is transformed into an airfoil in the z -plane using the Joukowski transformation

$$z = \zeta + \frac{c^2}{\zeta} \quad (5.6)$$

Substituting for ζ from equation(5.5) and denoting

$$D = p^2 + q^2 + a^2 + 2ap\cos\theta + 2aq\sin\theta \quad (5.7)$$

we have

$$\frac{z}{c} = \left(\frac{p}{c} + \frac{a}{c}\cos\theta\right)\left(1 + \frac{c^2}{D}\right) + i\left(\frac{q}{c} + \frac{a}{c}\sin\theta\right)\left(1 - \frac{c^2}{D}\right) \quad (5.8)$$

A number of different airfoil shapes can be generated by varying the values of p and q . Choosing $p = -c/12$ and $q = 0$, the airfoil generated is shown in Fig. 5.10.

5.4.2 FREE VIBRATION MODES OF THE WING

Before performing a flutter analysis using the lifting-surface unsteady aerodynamic program FAST, the free vibration analysis of the wing structure has to be performed. The finite element discretization of the wing is shown in Fig. 5.11, with the coordinates of the upper and lower skins of the wing obtained from equation (5.8). The airfoil thickness at any chord location varies linearly from the root of the wing to the tip. The wing is modeled using 4 spars (placed at $0.05c$, $0.2c$, $0.5c$ and $0.8c$ location) and 10 ribs (placed equidistant along the span). A total of 190 CQUAD4 and CTRIA3 shell elements and 200 CBAR beam elements were used to model the wing structure. The dimensions of the wing are as follows:

Wing span, $L = 5m$

Area, $A = 7.5m^2$

Root chord, $C_r = 2m$

Tip chord, $C_t = 1m$

Wing skin thickness, $t = 3mm$

Area of beam elements, $A_b = 75mm^2$

Young's Modulus, $E = 70GPa$

Poisson's ratio, $\nu = 0.3$

Material density, $\rho = 2700kg/m^3$

The natural frequencies and the mode shapes of the wing are obtained from NASTRAN and the first six frequencies and the corresponding free vibration modes of the wing are given in Fig. 5.12.

5.4.3 SENSITIVITY TO SHAPE AND MODAL PARAMETERS

In order to perform the aeroelastic analysis using FAST, six vibration modes of the wing are used. The modal information from NASTRAN finite element analysis is input into FAST to generate the flutter speed. The sensitivity analysis is carried out in two steps – a finite difference calculation followed by automatic differentiation. Since the new coordinates of the finite element nodal points are generated by perturbing the value of the shape parameter and these are input into NASTRAN in an 8-column format, it was observed that the precision of the numbers was not good enough which could lead to errors during finite differencing. So the central difference method was preferred over the forward finite difference method. One of the shape parameters of the wing is perturbed by a small positive value and the free vibration modes of the new wing configuration are obtained from NASTRAN. Again, the shape parameter is perturbed by a small negative value from its nominal value and modal analysis is carried out. It should be noted that the repeated finite element calculation is not very expensive, because the analysis can be performed to yield only a certain number of modes which are required for the flutter analysis, rather than compute all the frequencies. The derivatives of the modal frequency and mode shapes are calculated using a central difference scheme

$$\frac{\partial f}{\partial x} = \frac{f(x + \Delta x) - f(x - \Delta x)}{2\Delta x} \quad (5.9)$$

When the modal information is read into FAST for flutter analysis, the corresponding derivative information is also read in. These derivative values are then propagated and the derivatives of the subsequent active variables are calculated using automatic differentiation.

The sensitivity of flutter speed to shape parameters is plotted in Figs. 5.13–5.16 for $M = 0.6$ and $\rho_{air} = 0.8 \text{ kg/m}^3$ along with the flutter speed calculated from a reanalysis by changing one shape parameter at a time. The shape sensitivity derivatives give the trend that can be expected in the flutter speed variation for small changes in shape parameters about the baseline configuration. The derivatives of the flutter speed with respect to modal parameters are also calculated using ADIFOR, and the results are given in Figs. 5.17–5.19. It can be seen that the higher modes do not actively participate in flutter as evidenced by the sensitivity of the flutter speed to the modal parameters of the higher modes.

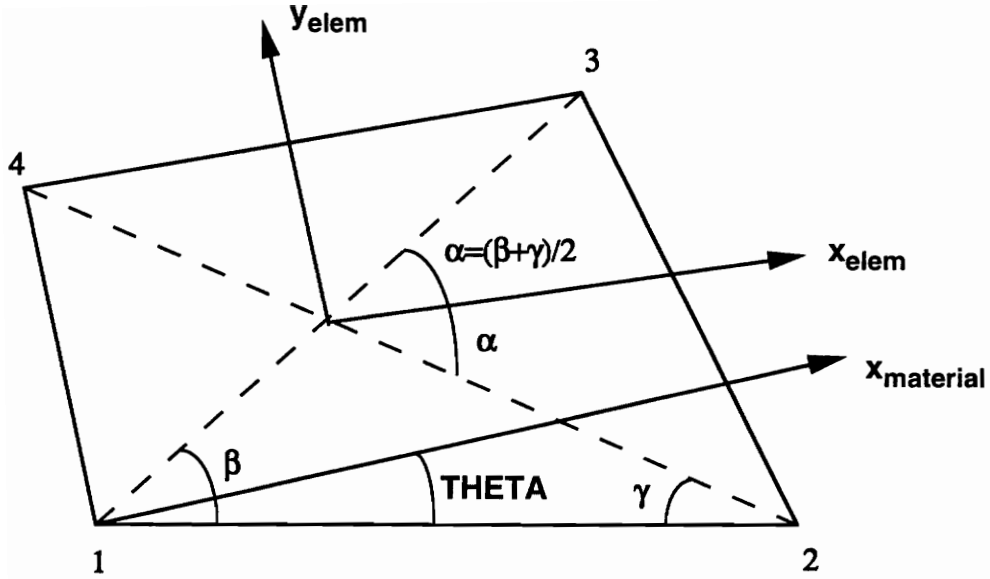


Fig. 5.1 CQUAD4 shell element

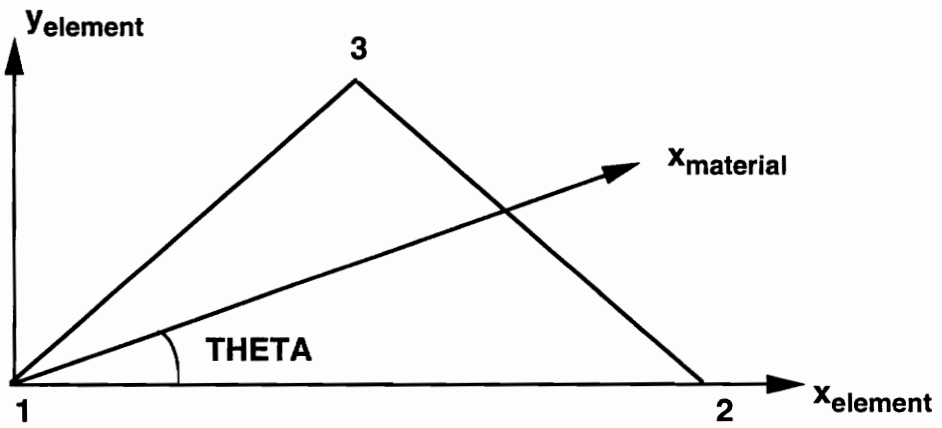


Fig. 5.2 CTRIA3 shell element

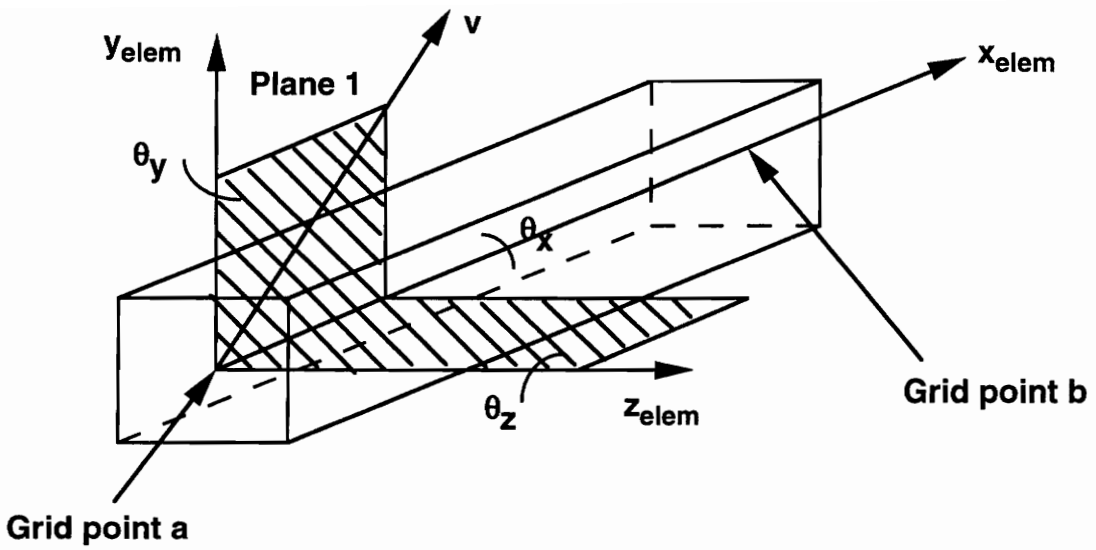


Fig. 5.3 CBAR beam element

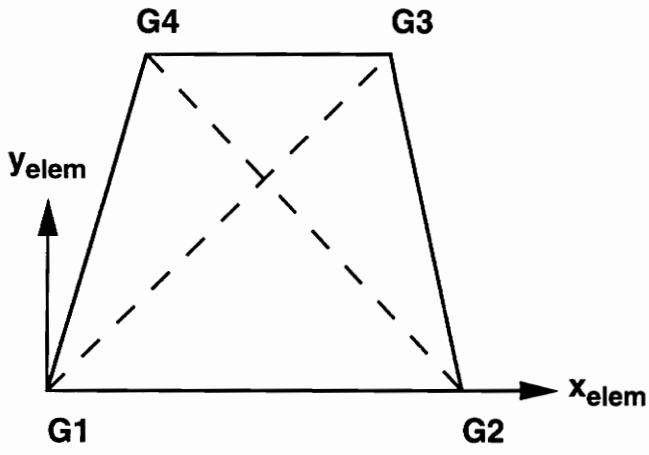


Fig. 5.4a CSHEAR element coordinate system

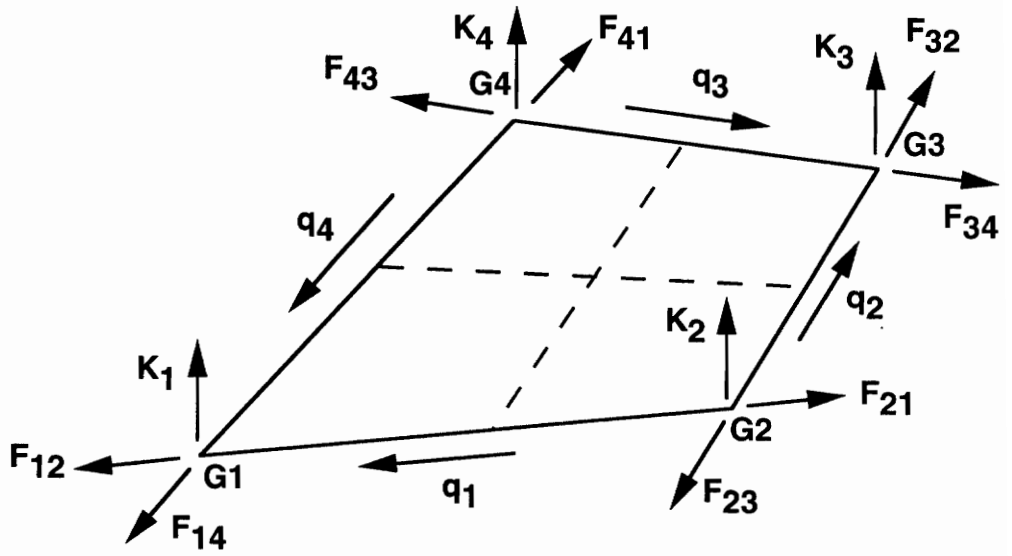


Fig. 5.4b CSHEAR element forces

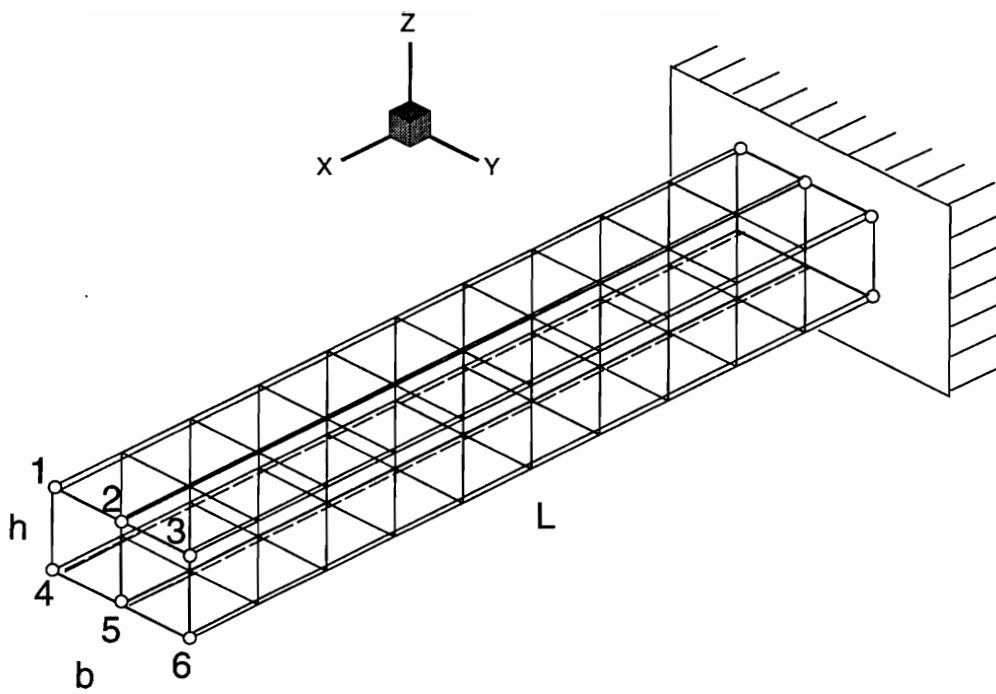


Fig. 5.5 Cantilevered Box-beam

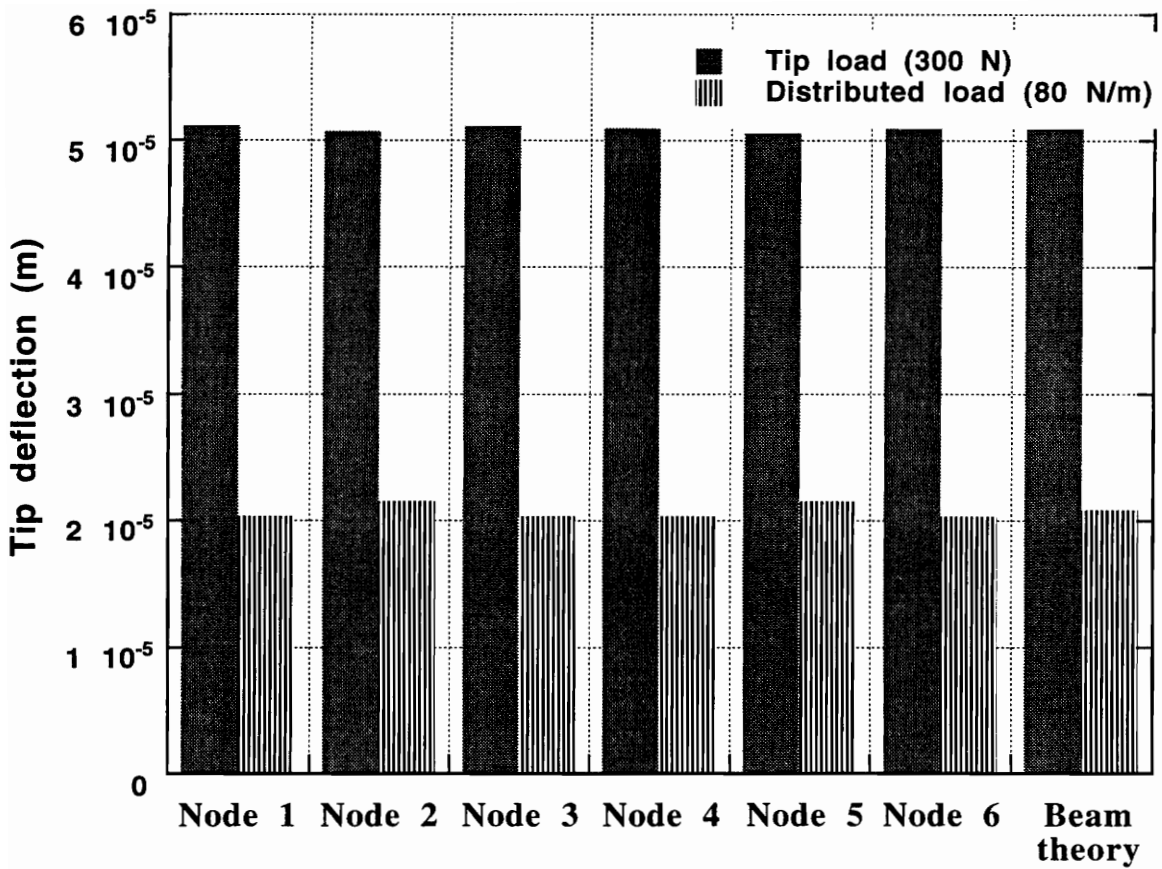
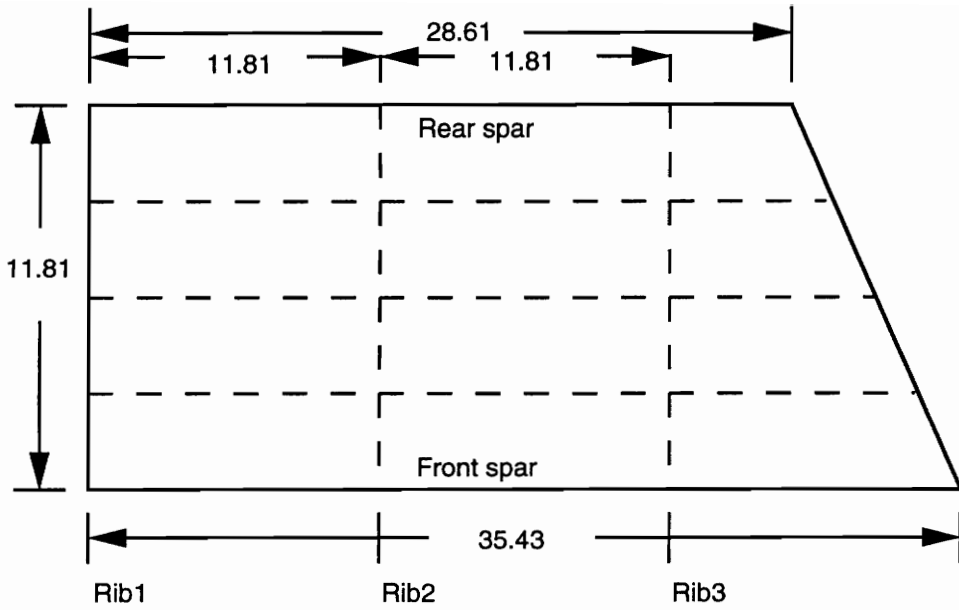
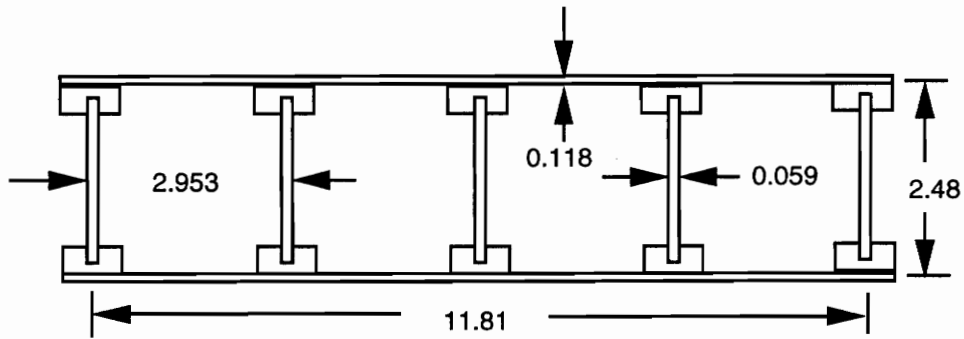


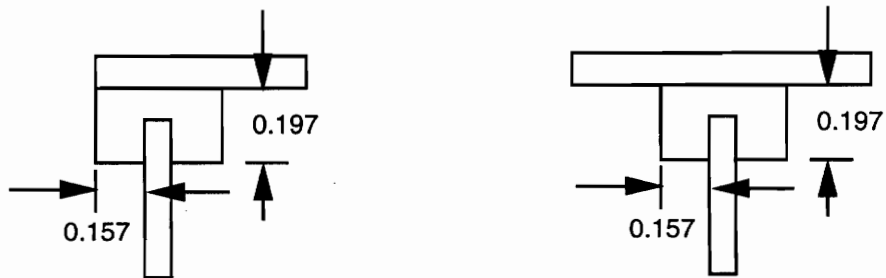
Fig. 5.6 Static deflection of the box-beam for two load cases



PLANFORM DIMENSIONS



TYPICAL CHORDWISE SECTION THROUGH MODEL



DETAILS OF ATTACHMENT OF SPAR AND RIB WEBS TO COVER SKIN
ALL DIMENSIONS ARE IN INCHES

Fig. 5.7 Planform dimensions and cross-section properties of the wing

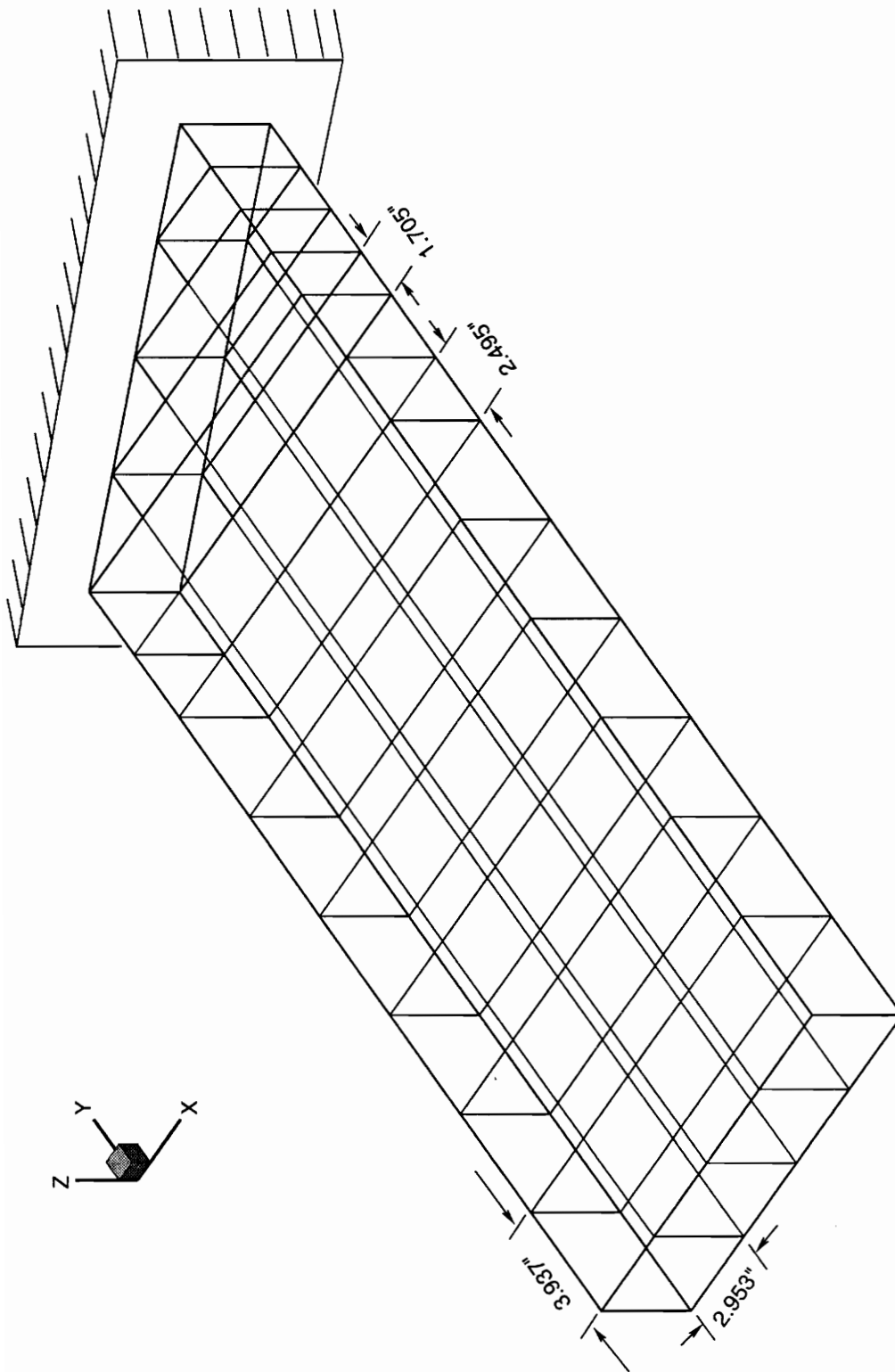


Fig. 5.8 Finite element discretization of the AGARD swept back wing model

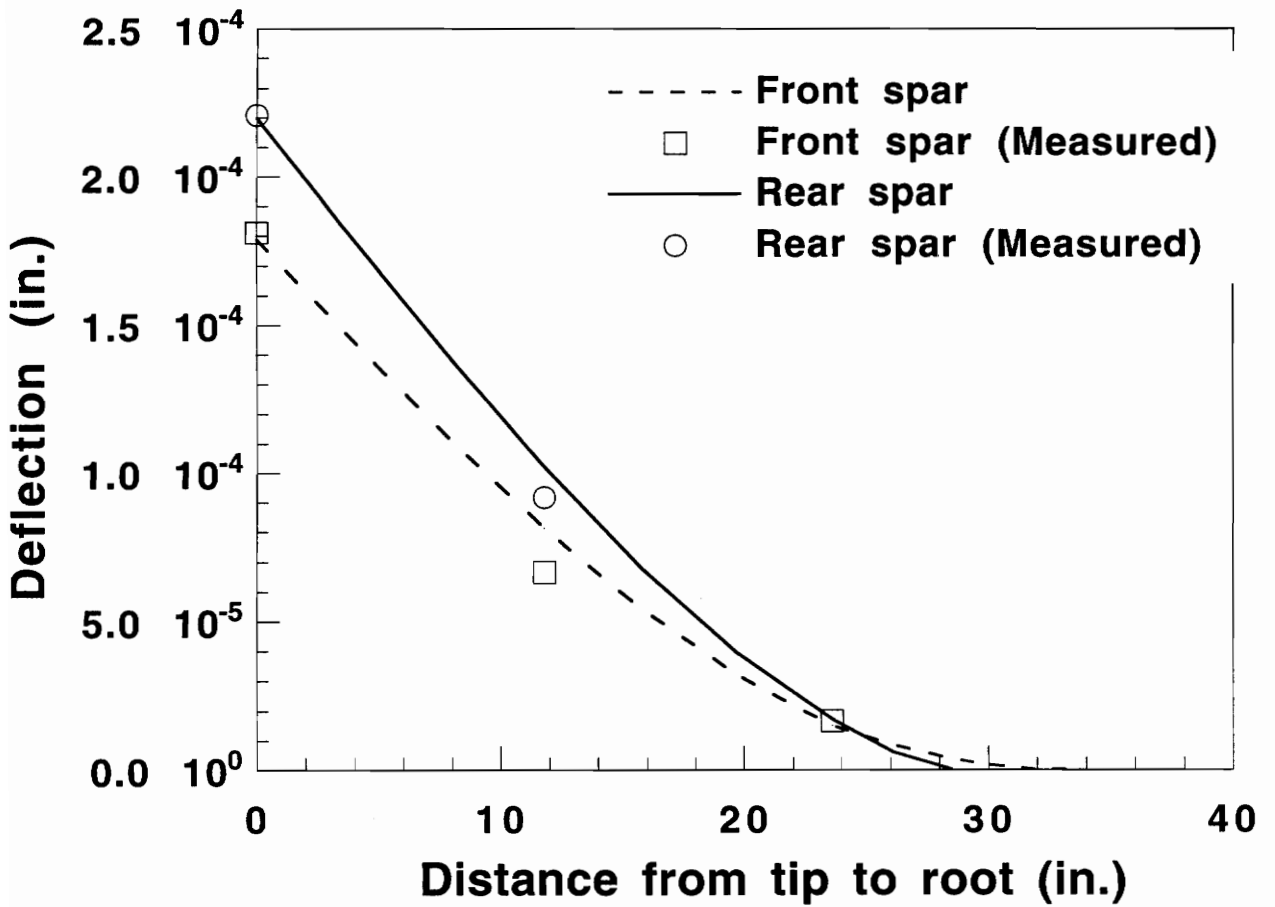
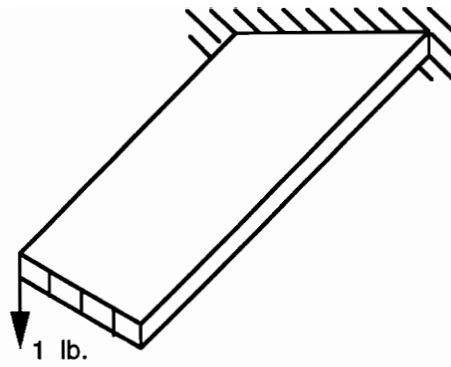


Fig. 5.9 Deflection of front and rear spar for a tip load of 1 lb. at the rear spar.

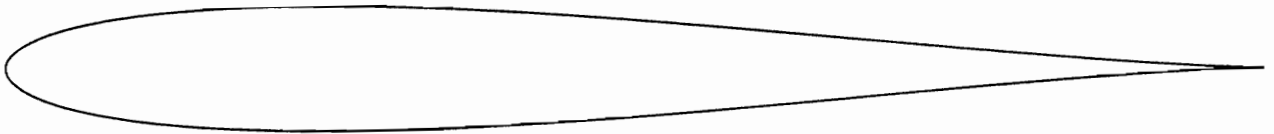
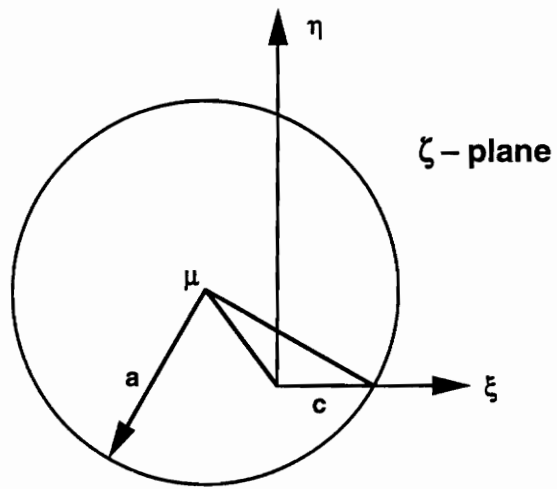


Fig. 5.10 Airfoil generated by transformation from a circle

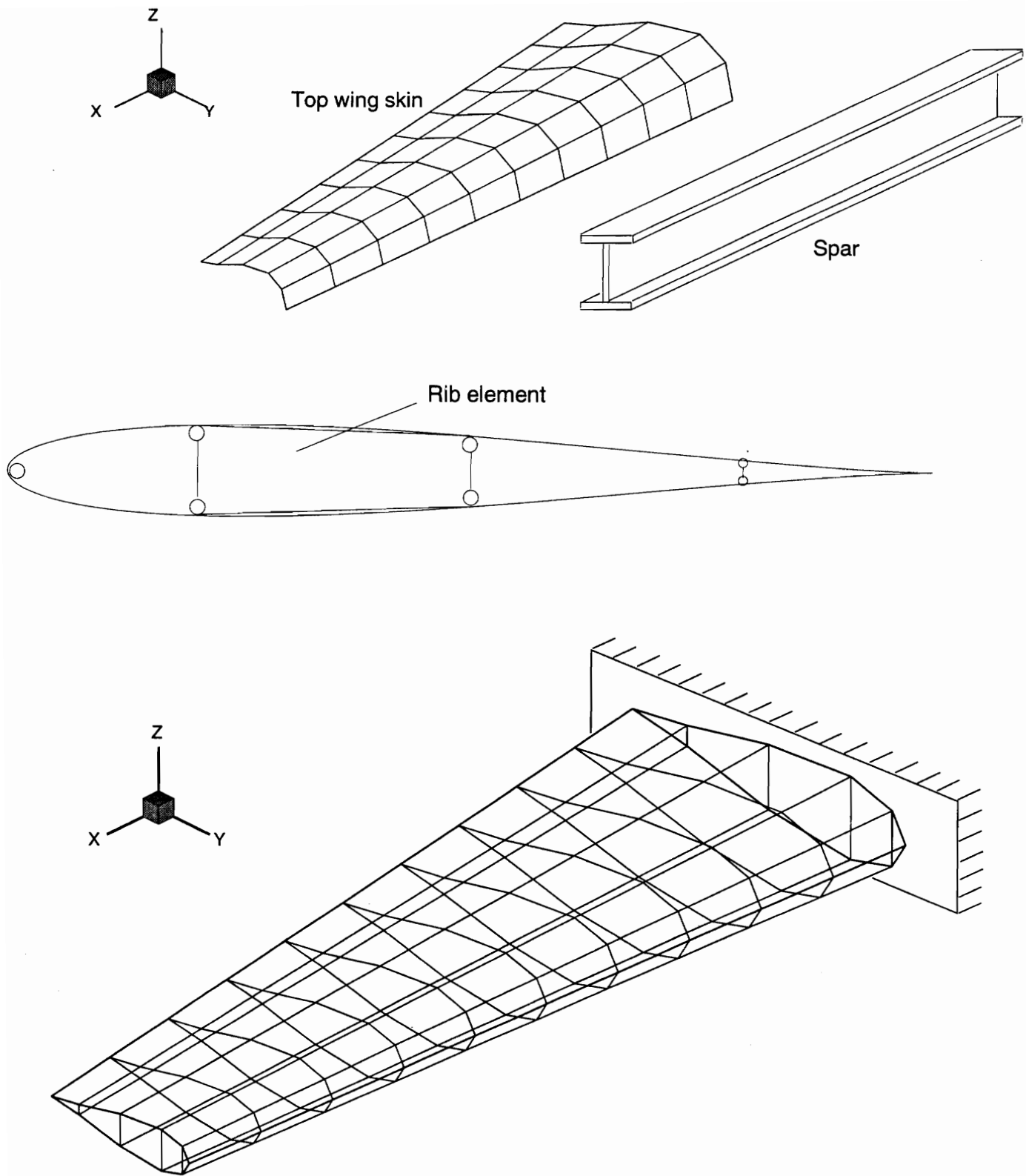
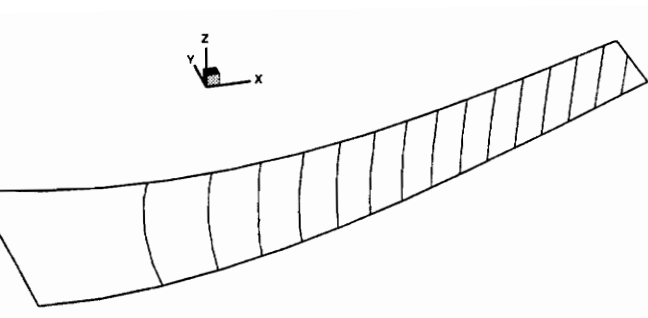
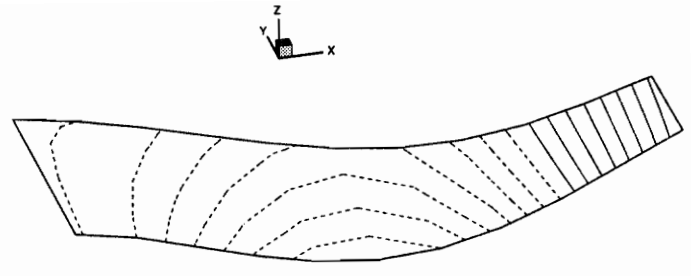


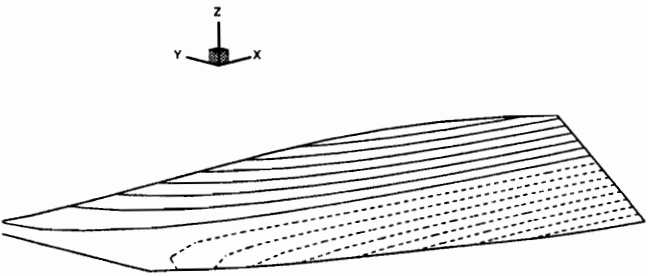
Fig. 5.11 Finite element discretization of the wing



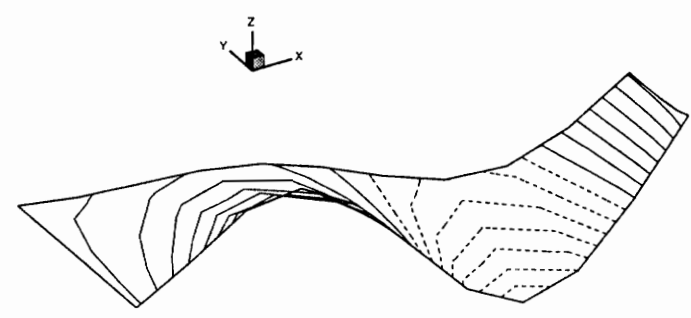
Frequency = 43.25 rad/s



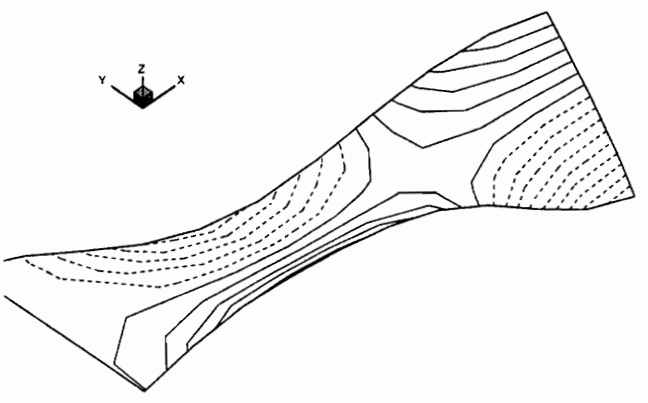
Frequency = 194.79 rad/s



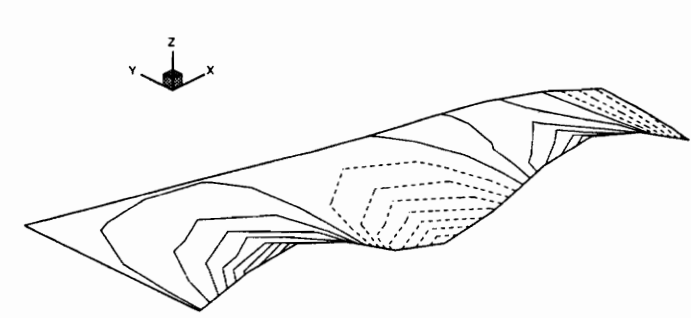
Frequency = 259.73 rad/s



Frequency = 449.38 rad/s



Frequency = 585.82 rad/s



Frequency = 714.82 rad/s

Fig. 5.12 Mode shapes of the wing

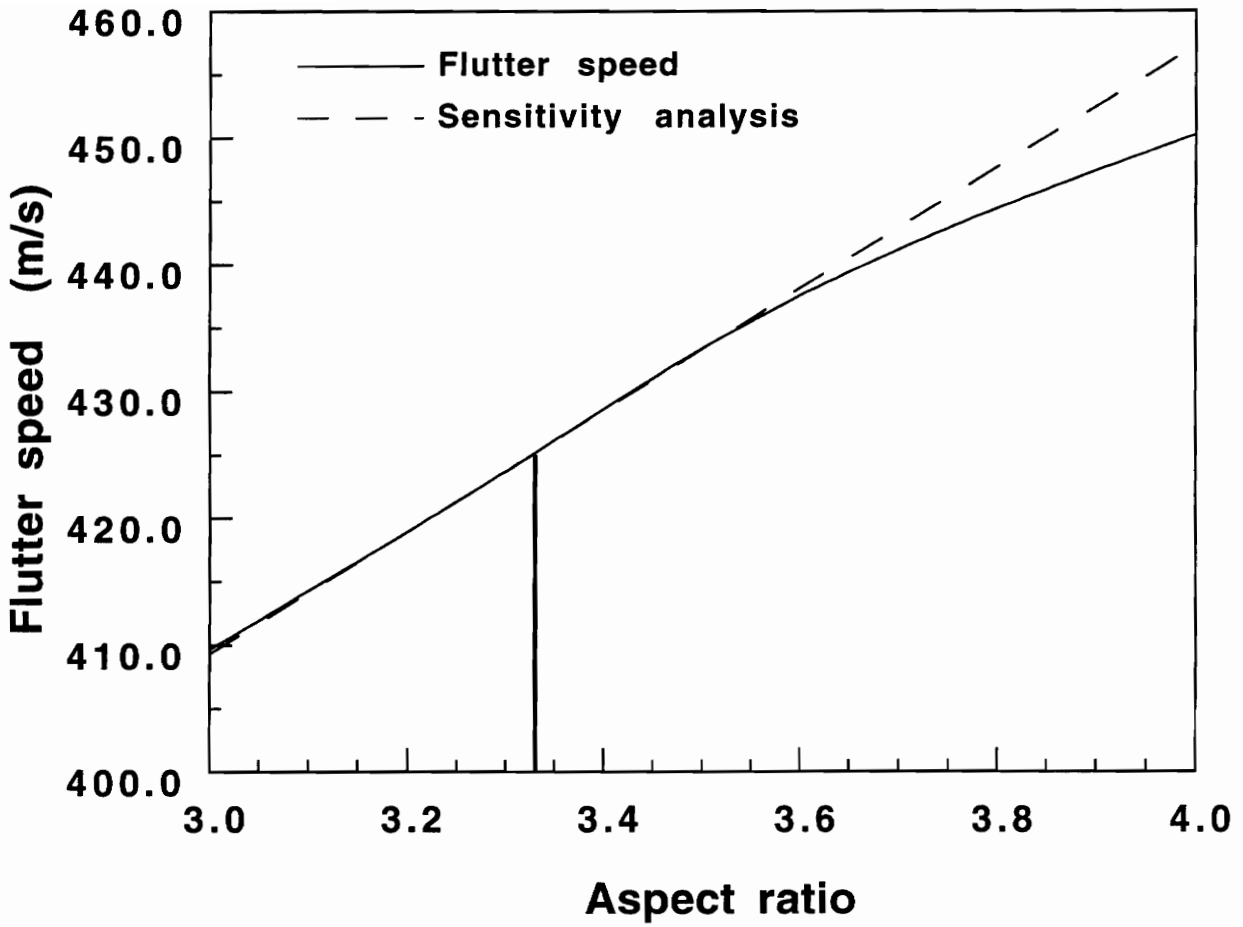


Fig. 5.13 Flutter speed vs Aspect ratio (M=0.6)
(AR=3.33, Area=7.5m², TR=0.5, Sweep=15°)

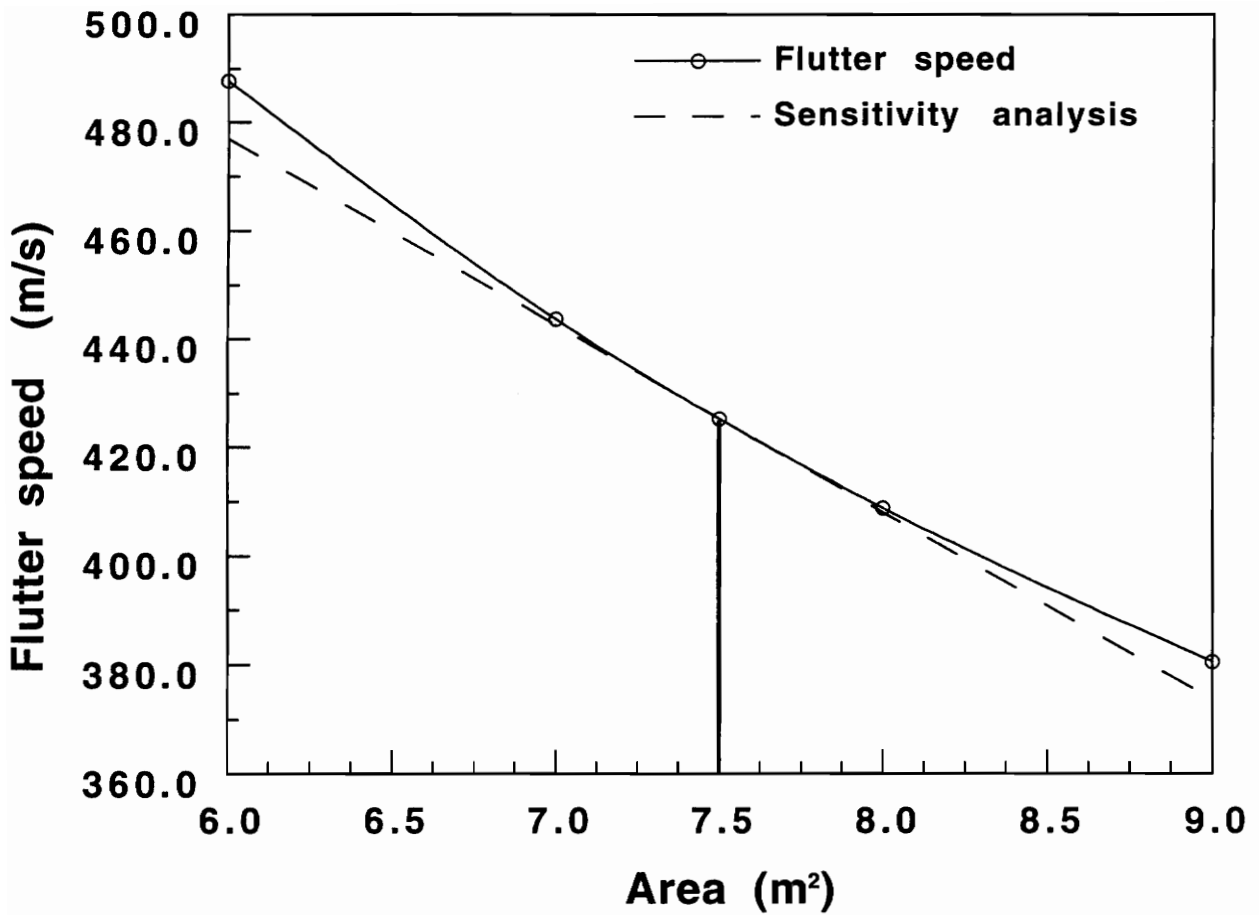


Fig. 5.14 Flutter speed vs Area (M=0.6)
(AR=3.33, Area=7.5m², TR=0.5, Sweep=15°)

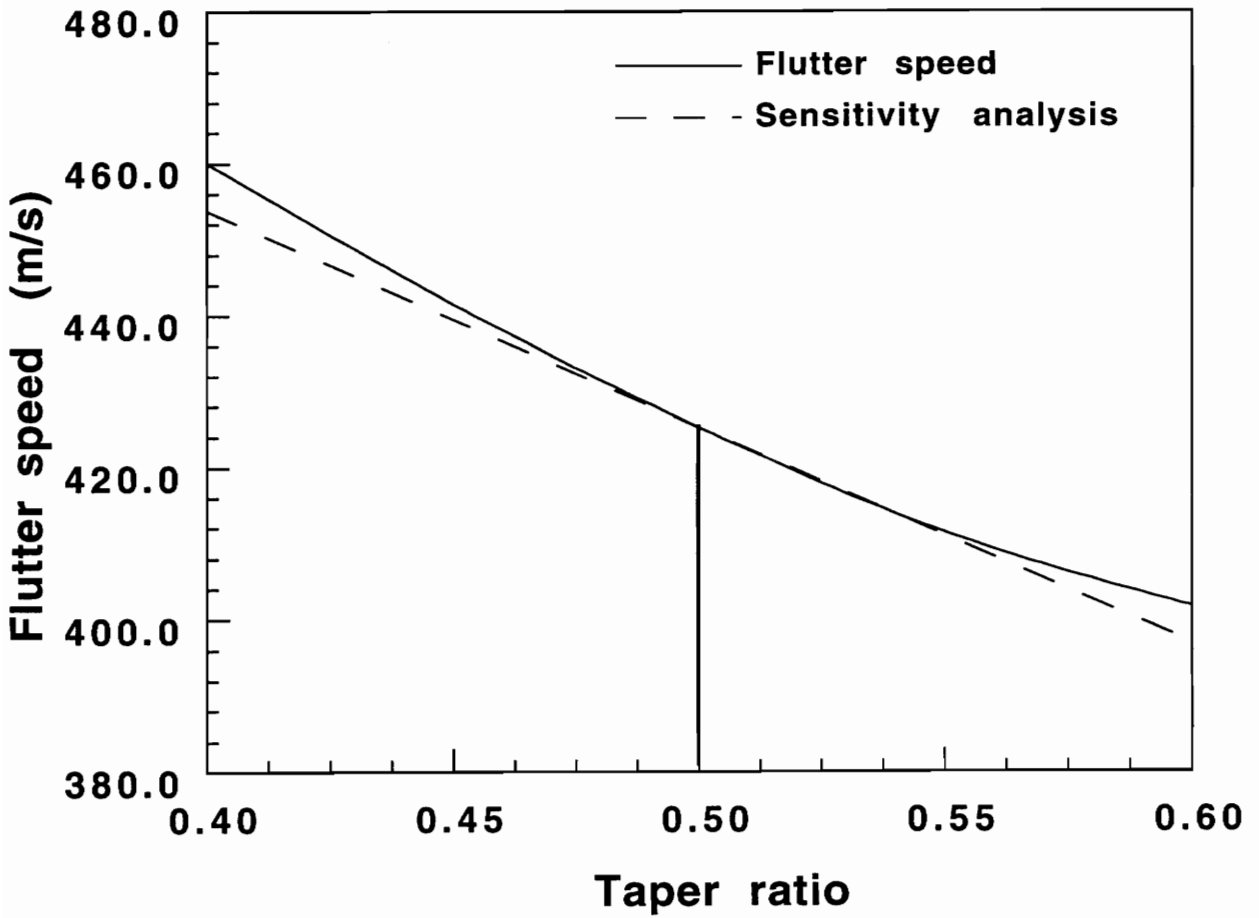


Fig. 5.15 Flutter speed vs Taper ratio (M=0.6)
(AR=3.33, Area=7.5m², TR=0.5, Sweep=15°)

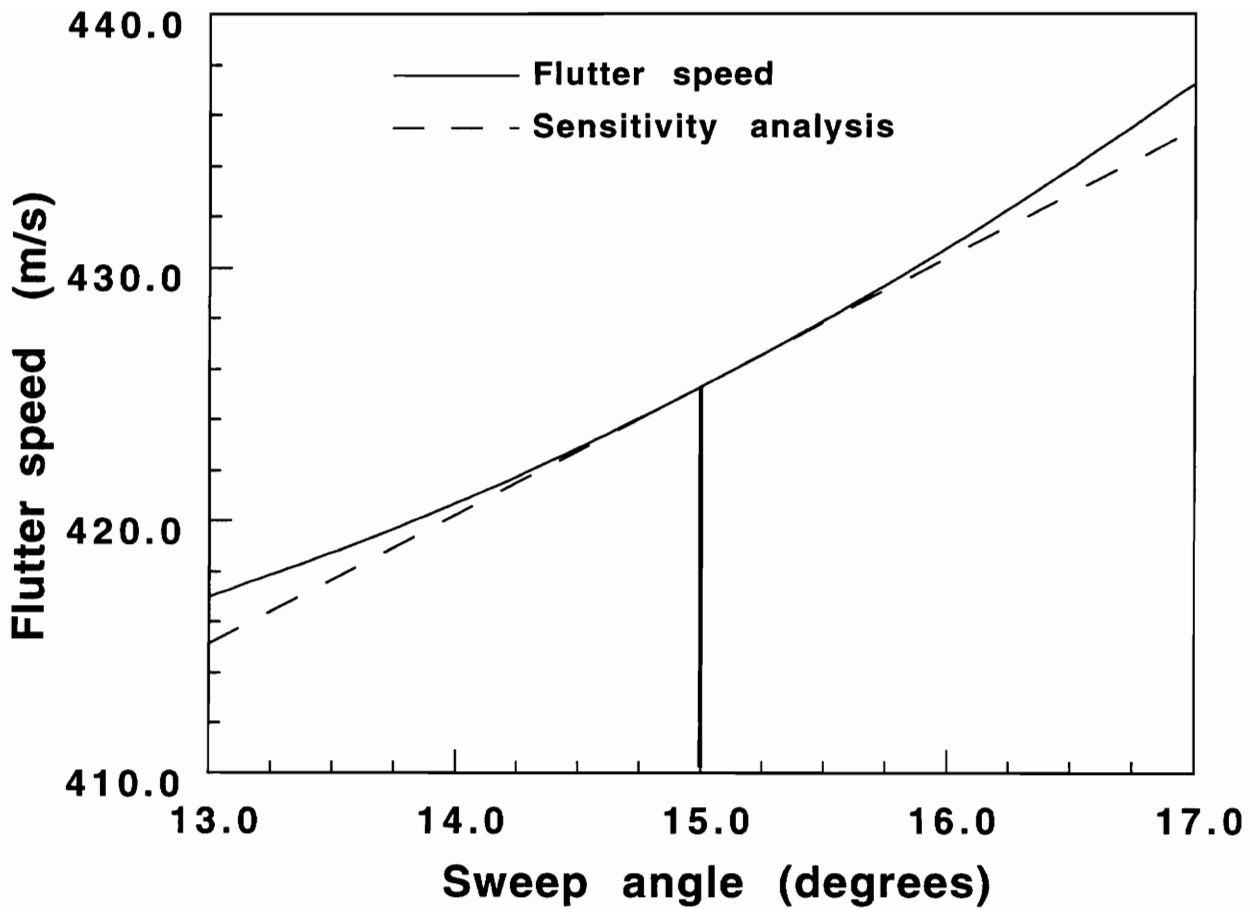


Fig. 5.16 Flutter speed vs Sweep angle (M=0.6)
(AR=3.33, Area=7.5m², TR=0.5, Sweep=15°)

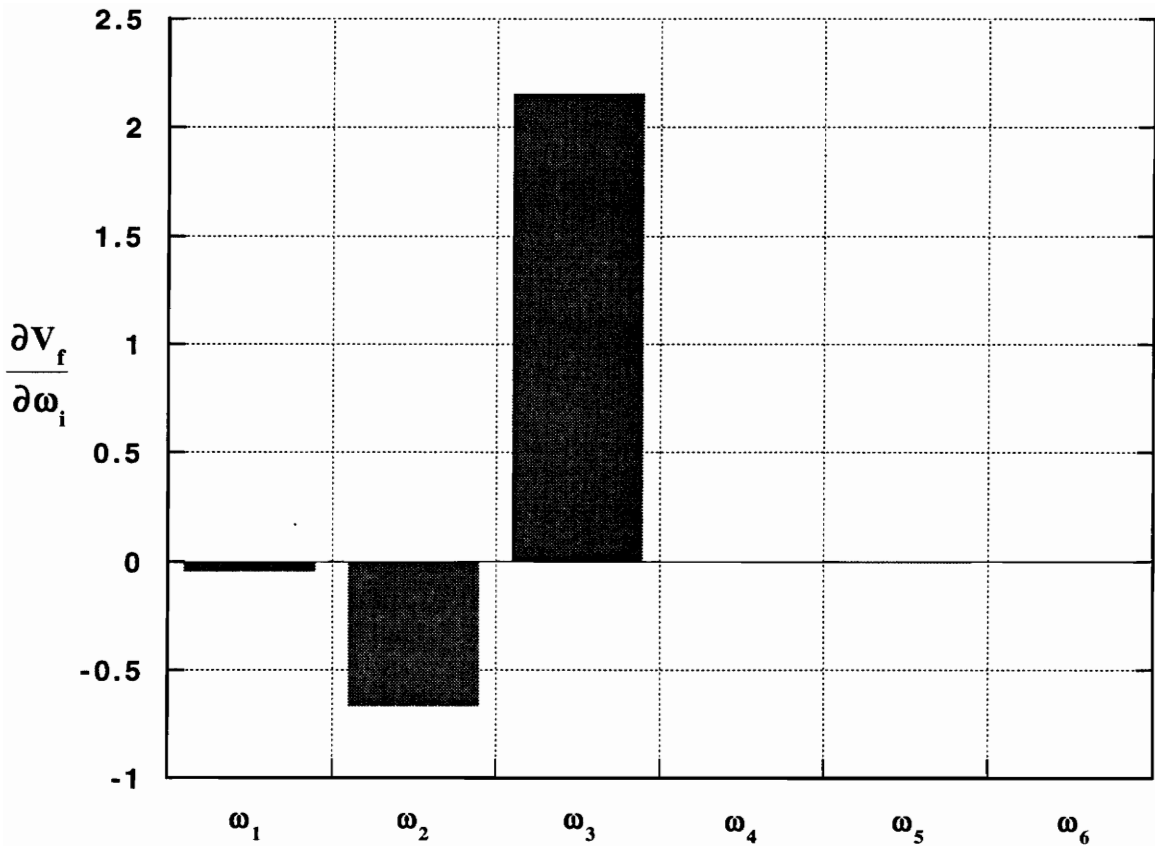
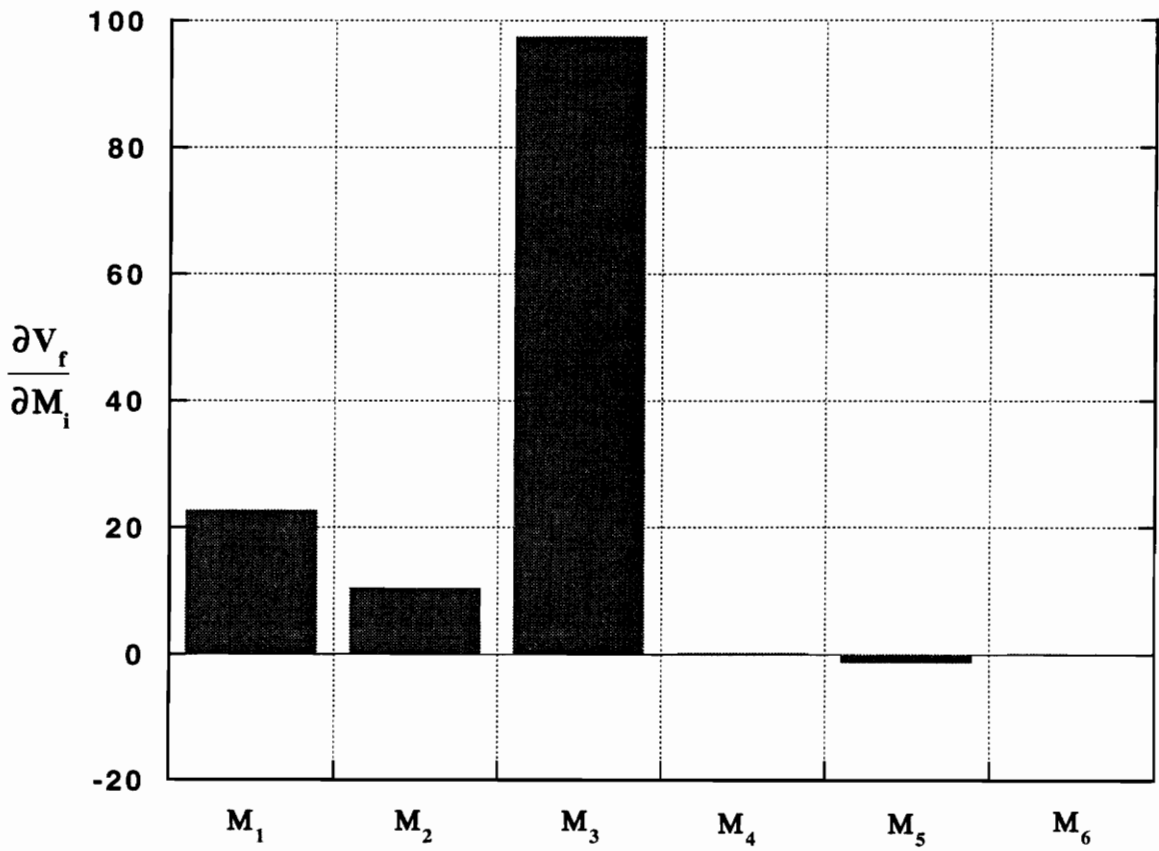


Fig. 5.17 Flutter speed sensitivity to natural frequency (M=0.6)
in (m/s)/(rad/s)
(AR=3.33, Area=7.5m², TR=0.5, Sweep=15°)



**Fig. 5.18 Flutter speed sensitivity to generalized mass (M=0.6)
in (m/s)/(kg)**
(AR=3.33, Area=7.5m², TR=0.5, Sweep=15°)

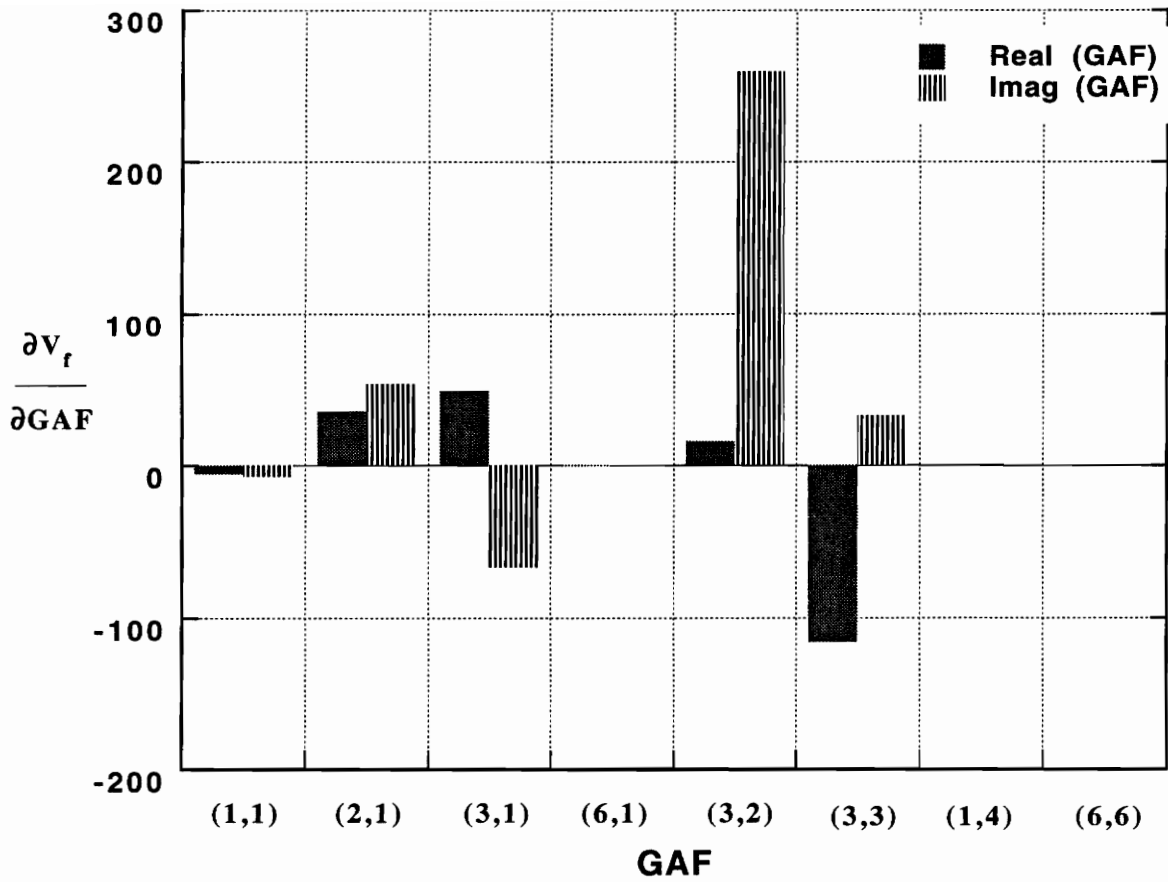


Fig. 5.19 Flutter speed sensitivity to nondimensional generalized aerodynamic forces (GAF) ($M=0.6$) in (m/s)
($AR=3.33$, $Area=7.5m^2$, $TR=0.5$, $Sweep=15^\circ$)

Table 5.1 Natural frequencies of the AGARD Swept Wing Model

Mode Number	Frequencies (Hz.)		
	Present (CSHEAR)	Livne[96]	Present (CQUAD4)
1 (1st Bending)	116.8	115.6	120.8
2 (Inplane)	318.0	317.6	353.0
3 (1st Torsion)	415.4	418.4	416.9
4 (2nd Bending)	579.5	576.4	593.1
5 (2nd Torsion)	1082.3	1086.0	1094.3

CHAPTER 6

SHAPE SENSITIVITY FOR OPTIMIZATION WITH AEROELASTIC CONSTRAINTS

6.1 OVERVIEW

An equivalent plate model which incorporates first-order shear deformation theory is examined so it can be used to model thick wings, where shear deformations are important. The natural frequencies of a thick laminated composite plate obtained using first-order shear deformation theory are compared to those obtained using classical plate theory. The sensitivity of natural frequencies to changes in shape parameters is obtained using ADIFOR.

The use of shape sensitivity derivatives in a gradient-based design optimization subjected to aeroelastic constraints is demonstrated. A simple optimization effort is made towards obtaining a minimum weight design of the wing, subject to flutter constraints, lift requirement constraints for level flight and side constraints on the planform parameters of the wing. The IMSL subroutine NCONG, which is an implementation of successive quadratic programming is used for this purpose.

6.2 STRUCTURAL MODEL

In the previous chapters, equivalent plate models based on classical plate theory and finite element models were used for structural modeling. The first-order shear deformation theory which incorporates transverse shear developed by Kapania and Lovejoy [97] is used for structural modeling in this chapter.

The plate displacements u , v and w are given by

$$\begin{aligned}
 u &= u^o(x, y, t) + z\phi_x(x, y, t) \\
 v &= v^o(x, y, t) + z\phi_y(x, y, t) \\
 w &= w^o(x, y, t)
 \end{aligned} \tag{6.1}$$

where u^o , v^o and w^o are midplane displacements and ϕ_x and ϕ_y are rotations about the y and x axes, respectively.

The original (x, y) coordinate system is transformed to the (η, ξ) coordinate system, and a Rayleigh-Ritz formulation using Chebyshev polynomials to represent the plate displacements is adopted. The mid-plane displacements and rotations are represented in a series as

$$\begin{aligned}
 u^o &= \sum_{i=0}^I \sum_{j=0}^J R_{ij}(t) T_i(\eta) T_j(\xi) \\
 v^o &= \sum_{k=0}^K \sum_{l=0}^L S_{kl}(t) T_k(\eta) T_l(\xi) \\
 w^o &= \sum_{m=0}^M \sum_{n=0}^N P_{mn}(t) T_m(\eta) T_n(\xi) \\
 \phi_x &= \sum_{p=0}^P \sum_{q=0}^Q X_{pq}(t) T_p(\eta) T_q(\xi) \\
 \phi_y &= \sum_{r=0}^R \sum_{s=0}^S Y_{rs}(t) T_r(\eta) T_s(\xi) \quad -1 \leq \eta, \xi \leq 1
 \end{aligned} \tag{6.2}$$

and the Chebyshev polynomials T_i are given in equations(3.1).

It has been shown by Kapania and Lovejoy [97] that for free vibration of the plate, the eigenvalue problem can be obtained as

$$[K - \lambda M]\{x\} = 0 \tag{6.3}$$

where $[K]$ and $[M]$ are the stiffness and mass matrices and the eigenvector $\{x\}$ contains coefficients of the polynomial representing the displacement functions, i.e.,

$$\{x\} = (R_{00}, R_{01}, \dots, R_{ij}; S_{00}, \dots, S_{kl}; P_{00}, \dots, P_{mn}; X_{00}, \dots, X_{pq}; Y_{00}, \dots, Y_{rs})^T \quad (6.4)$$

The plate boundary conditions are handled by using springs of appropriate magnitude at the boundaries. For modeling cantilever wings, linear and rotational springs of large magnitude are placed at the root to satisfy the clamped wing boundary condition. Details of the formulation are given in [97].

Both inplane modes of vibration and rotary inertia terms are included in [97]. However, in this study, considering only transverse vibrations and neglecting the rotary inertia, the coefficients corresponding to the u^o , v^o , ϕ_x and ϕ_y displacements are condensed out using a static condensation.

6.3 EFFECT OF TRANSVERSE SHEAR ON VIBRATION AND AEROELASTIC CHARACTERISTICS

The natural frequencies of a laminated composite plate clamped at one end and free at the other three edges, are computed using this structural model incorporating transverse shear and compared with the classical plate model used in the earlier studies. The sensitivity of natural frequencies to changes in shape parameters of the plate is studied. The influence of transverse shear on the flutter characteristics of a wing is also examined.

6.3.1 EFFECT OF TRANSVERSE SHEAR ON NATURAL FREQUENCY

In order to get an estimate of the effect of transverse shear on the free vibration characteristics, the plate vibrations are analyzed using both the classical plate theory and the first-order shear deformation theory. The results for symmetrically laminated, skew, cantilever plates made of Glass/Epoxy are presented in Tables 6.1 and 6.2. The properties for Glass/Epoxy are $E_1 = 38.61 \text{ GPa}$, $E_2 = E_3 = 8.27 \text{ GPa}$, $G_{12} = G_{13} = 4.14 \text{ GPa}$, $G_{23} = 3.35 \text{ GPa}$, $\nu_{12} = \nu_{13} = 0.26$, $\nu_{23} = 0.49$ and $\rho = 2546.54 \text{ kg/m}^3$. The results are given for a plate with a sweep angle of $\Lambda = 15^\circ$, aspect ratio of 3.111, taper ratio of 0.5 and area of 63 in^2 (406.45 cm^2). The thickness of the plate is varied from 0.14 in. (3.556 mm.) for the thin $[30_2/0]_s$ laminate to 0.84 in. (21.336 mm.) for the thick $[30_2/0]_{6s}$ laminate. It is seen from Tables 6.1 and 6.2 that the frequencies predicted by including shear deformations are lower than those predicted by classical plate theory. As the thickness of the plate is increased, notable differences can be seen in frequencies obtained by the two theories.

6.3.2 SHAPE SENSITIVITY RESULTS

The sensitivity of the natural frequencies of the plate to shape parameters, namely aspect ratio, area, taper ratio and sweep angle was computed using automatic differentiation (ADIFOR). The $[30_2/0]_{10s}$ laminated plate with 60 plies, made of Glass/Epoxy is used for the study. The sensitivity of the first three natural frequencies of the plate with respect to shape parameters is shown in Figs. 6.1–6.4. The free vibration frequencies obtained by perturbing one shape parameter at a time from the baseline configuration are shown by the solid line curve. The

dotted line gives the sensitivity prediction at the baseline configuration. The sensitivity derivative obtained forms a tangent to the frequency curve at the baseline configuration.

It is seen that there is a drop in the vibration frequencies of the first three modes as the aspect ratio, area and taper ratio of the plate are increased. The first two natural frequencies decrease with increasing sweep angle as seen from Fig. 6.4, but the third natural frequency first increases with sweep angle and then decreases, about the baseline value of 15° sweep. By performing one sensitivity calculation at the baseline analytically, this method gives a linear approximation to the frequency curve for changes in the wing shape parameters about the baseline. These shape sensitivity derivatives could be very useful for a gradient-based design optimization of thick plates with frequency constraints.

6.3.3 EFFECT OF TRANSVERSE SHEAR ON FLUTTER SPEED

Studies on the effect of transverse shear on flutter speed of a wing is of great interest, especially when dealing with thick composite wings for which shear deformation effects are not negligible (see Karpouzian and Librescu [98]). In this study, the first-order shear deformation theory (FSDT) is used for the structural model and a lifting-surface unsteady aerodynamics (FAST) is used for generating the generalized aerodynamic forces required for the flutter calculation. The flutter characteristics of the wing shown in Figure 3.2 which has previously been analyzed in Chapter 4 using a classical laminated plate theory (CLPT), is studied here by including the effects of transverse shear. Figures 6.5–6.8 show the variation of

the flutter speed with respect to aspect ratio, area, taper ratio and sweep angle of the wing, as predicted by CLPT and FSDT. It is evident that the inclusion of transverse shear in the structural model has an effect of reducing the flutter speed of the wing.

6.4 OPTIMIZATION WITH AEROELASTIC CONSTRAINTS

Multidisciplinary optimization is of great interest in the aerospace industry and efforts are being made towards integrated wing synthesis to produce better designs. The designs have to satisfy a number of constraints of which flutter constraints form an important subset. The changes in shape of the wing affect both its structural and aerodynamic response. This is an effort to obtain a minimum weight design of the wing, subject to flutter constraints, lift requirement constraints and constraints on the planform parameters of the wing. It should be noted that more constraints can be added to this optimization problem if required. The gradients required for the optimization are computed through a sensitivity analysis of the aeroelastic response of the wing using automatic differentiation (using ADIFOR).

6.4.1 FORMULATION OF THE OPTIMIZATION PROBLEM

The optimization problem can be stated as follows:

Minimize

$$W_w = \rho_m S t g$$

subject to the constraints

$$V_{flutter} \geq 1.2 V_{flight}$$

$$L = \frac{1}{2}\rho V_{flight}^2 SC_L = \frac{W_{ac}}{2}$$

$$AR \geq 5.0$$

$$0.5 \leq TR \leq 1.0$$

$$0^\circ \leq \Lambda \leq 30^\circ \quad (6.5)$$

where W_w is the weight of the wing, ρ_m is the density of the material, S is the area of the wing, t is the thickness, g is the acceleration due to gravity, V is the velocity, L is the lift, ρ is the density of air, C_L is the lift coefficient, W_{ac} is the weight of the aircraft, AR is the aspect ratio, TR is the taper ratio and Λ is the quarter-chord sweep angle.

The wing is designed so that the flutter speed is atleast 20% more than the maximum flight speed. Also the wing is capable of producing sufficient lift required for cruise. The constraint on the aspect ratio ensures that wings with short spans and long chords are not an outcome of the optimization. The constraints on taper ratio and sweep angle ensure that wings that conform to practical designs are generated.

6.4.2 METHOD OF SOLUTION

There are several methods to perform this nonlinear constrained optimization [99]. The gradient projection method is based on projecting the search direction into the subspace tangent to the active constraints. In the method of feasible directions, the concept is to stay in the feasible domain, move in a direction which reduces the objective function and stay away from the constraint boundaries. The

program by Vanderplaats, CONMIN [100] is an implementation of the method of feasible directions. Another method which uses successive quadratic programming is implemented in the IMSL subroutine, NCONG [101]. The method, based on the iterative formulation and solution of quadratic programming subproblems, uses a quadratic approximation of the Lagrangian and linearization of the constraints. Though the solution of the quadratic programming direction seeking problem is cumbersome, it often leads to faster convergence.

The optimization problem can be written as

$$\begin{aligned}
 & \text{Min } f(\mathbf{x}) \\
 & \text{subject to } \quad g_j(\mathbf{x}) = 0, \quad \text{for } j = 1, \dots, m_e \\
 & \quad \quad \quad g_j(\mathbf{x}) \geq 0, \quad \text{for } j = m_e + 1, \dots, m
 \end{aligned} \tag{6.6}$$

We seek the direction \mathbf{d} as the solution of the following quadratic programming problem:

$$\begin{aligned}
 & \text{Min } \frac{1}{2} \mathbf{d}^T \mathbf{B}_k \mathbf{d} + \nabla f(\mathbf{x}_k)^T \mathbf{d} \\
 & \text{subject to } \quad \nabla g_j(\mathbf{x}_k)^T \mathbf{d} + g_j(\mathbf{x}_k) = 0, \quad j = 1, \dots, m_e \\
 & \quad \quad \quad \nabla g_j(\mathbf{x}_k)^T \mathbf{d} + g_j(\mathbf{x}_k) \geq 0, \quad j = m_e + 1, \dots, m
 \end{aligned} \tag{6.7}$$

where \mathbf{B}_k is a positive definite approximation of the Hessian, and \mathbf{x}_k is the current iterate. If \mathbf{d}_k is the solution to the subproblem, a line search is used to find the new point \mathbf{x}_{k+1} ,

$$\mathbf{x}_{k+1} = \mathbf{x}_k + \lambda \mathbf{d}_k, \quad \lambda \in (0, 1] \tag{6.8}$$

\mathbf{B}_k is updated according to the modified BFGS formula [102]. It should be noted that this algorithm can have infeasible points during the solution process.

6.4.3 OPTIMIZATION RESULTS

The optimization problem described in equations(6.5) was solved using the IMSL routine NCONG. The wing is shown in Fig. 3.2. The wing skins are made of 0 deg. laminated Graphite/Epoxy (*T300/N5208*) with the following material properties: $E_1 = 181 \times 10^9 \text{ Pa}$, $E_2 = 10.3 \times 10^9 \text{ Pa}$, $E_3 = 10.3 \times 10^9 \text{ Pa}$, $\nu_{12} = 0.28$, $\nu_{13} = 0.28$, $\nu_{23} = 0.49$, $G_{12} = 7.17 \times 10^9 \text{ Pa}$, $G_{13} = 7.17 \times 10^9 \text{ Pa}$, $G_{23} = 5.82 \times 10^9 \text{ Pa}$ and $\rho_m = 1600 \text{ kg/m}^3$. The analysis is carried out at a Mach number of 0.6. The problem was further simplified by fixing the taper ratio and sweep angle of the wing at 0.5 and 30° , respectively, so the design variables are the aspect ratio and the area of the wing. The following values were chosen:

$$\begin{aligned} V_{flight} &= 100 \text{ m/s} \\ \rho &= 0.8 \text{ kg/m}^3 \\ C_L &= 0.7 \\ W_{ac} &= 100000 \text{ N} \end{aligned} \tag{6.9}$$

The gradients of the aeroelastic constraints are obtained by performing sensitivity analysis of the aeroelastic response with respect to the planform parameters using the automatic differentiation package, ADIFOR. The results of the optimization for each iteration are given in Table 6.3. Since the material and thickness of the wing are not changing, the wing weight is proportional to the area of the wing. It can be seen that at the 3rd iteration, $AR = 5.3913$ and $Area = 17.857 \text{ m}^2$, corresponding to $V_{flutter} = 134.19 \text{ m/s}$. This value of the wing area satisfies the equality constraint, which means it is not possible to obtain a reduction in the value of the objective function by reducing the area since the equality constraint

will then be violated. The minimum weight of the wing, subject to the applied constraints is $W_w = [17.857\rho_m t g] N$.

In this optimization, the equality constraint appears to be the driving constraint and the inequality constraint on the flutter speed is not active. Even though both the constraints are satisfied and the minimum weight as desired by the objective function is achieved, there is a big margin on the flutter speed constraint ($134.19 - 120.00 = 14.19 \text{ m/s}$), which suggests that we could have other designs with higher aspect ratio which will have the same optimum weight value and make both the constraints active. Since the objective function is only a function of area, once its minimum is attained by the satisfaction of the equality constraint, the optimization algorithm does not find a direction in which further minimization of the objective function can be accomplished. This either results in the inequality constraint being satisfied with a wider margin as in this case, or in the case of a violated constraint, it becomes necessary to optimize on the single design variable namely the aspect ratio to meet the inequality constraint. This is avoided by defining a composite objective function by adding to the area of the wing the reciprocal of the difference between the aspect ratio and its lower bound, weighed with a parameter p as shown.

$$f = S + p \frac{1}{(AR - AR_{lb})} \quad (6.10)$$

where f is the new objective function, S is the wing area, AR is the aspect ratio and AR_{lb} is its lower bound. With this newly defined objective function, the results from the optimization are given in Table 6.4 for a value of $p = 10.0$. It

can be seen from Table 6.4 that from the 3rd iteration on, the $Area = 17.857 \text{ m}^2$, which is driven by the equality constraint. However, the optimization algorithm is successful in its search for a direction which minimizes the objective function and proceeds until both the constraints are active, giving a final value of $AR = 6.5994$ and $Area = 17.857 \text{ m}^2$ with $V_{flutter} = 120.00 \text{ m/s}$. The minimum weight of the wing is $W_w = [17.857\rho_m t g] N$.

This is a simple two constraint optimization problem with two design variables. It should be noted that the material properties and skin thicknesses of the wing could also be used as design variables for a full-scale optimization with aeroelastic constraints; however a much simpler problem was chosen here to demonstrate the use of shape sensitivity derivatives in optimization.

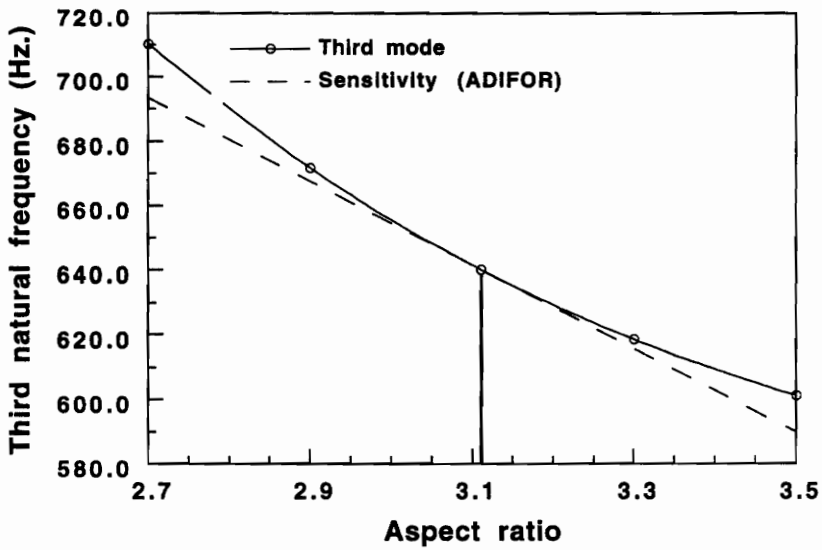
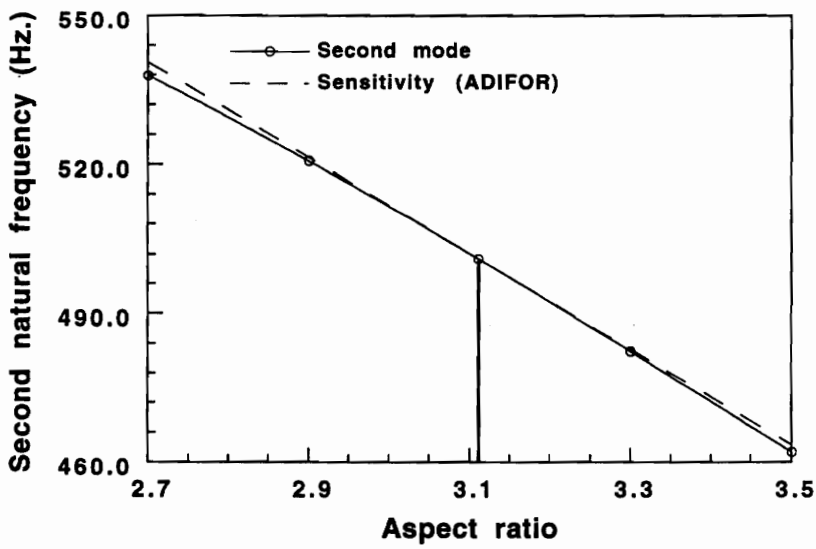
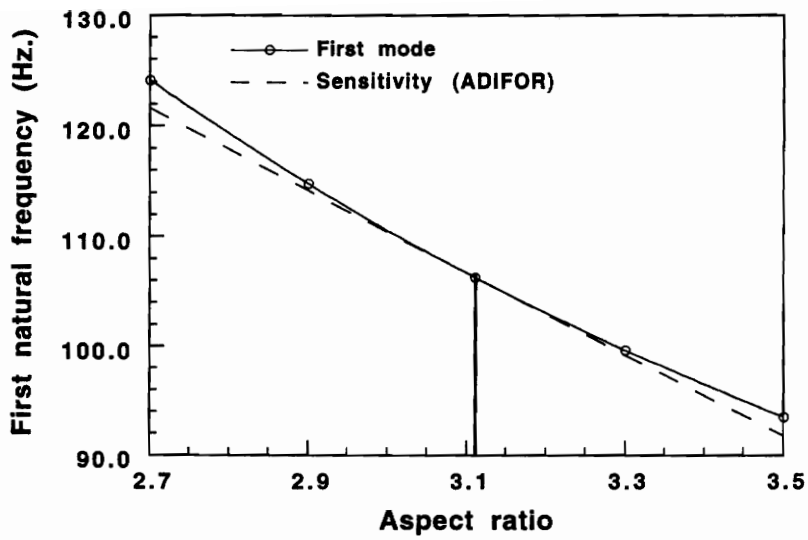


Fig. 6.1 First three natural frequencies vs Aspect ratio for a thick plate

(AR=3.111, Area=0.040645m², TR=0.5, Sweep=15°)

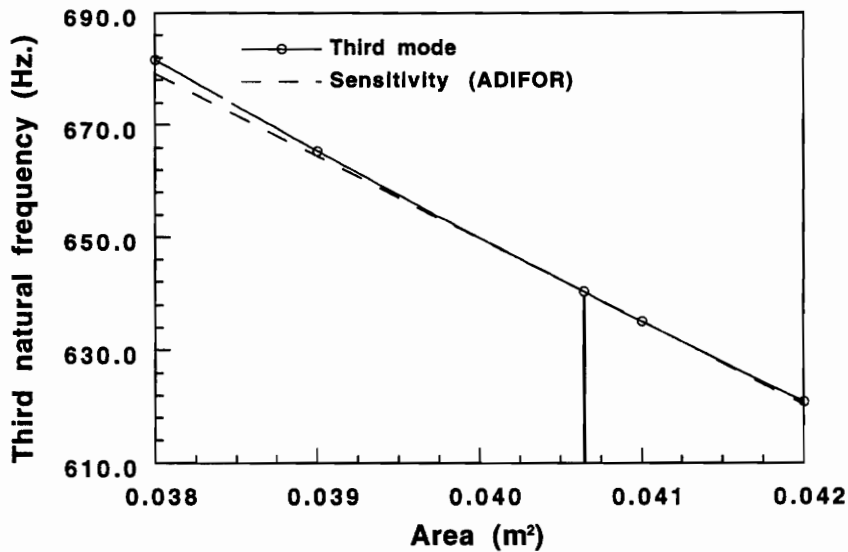
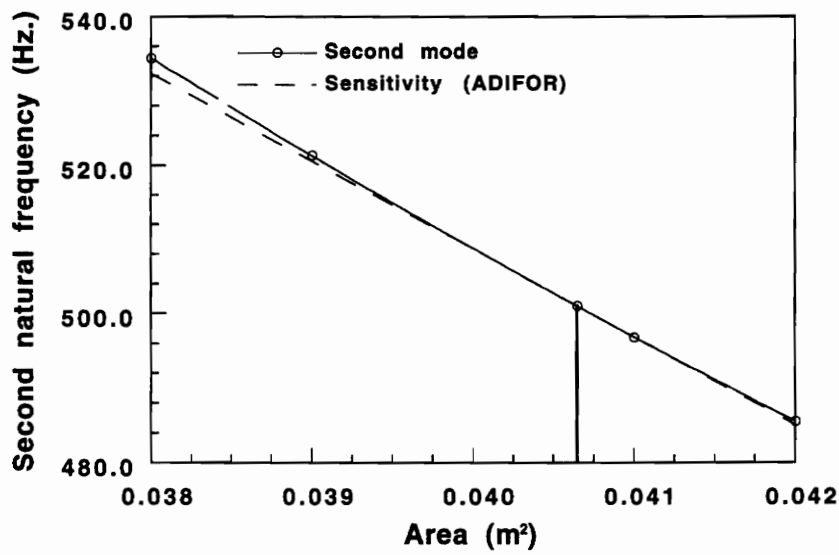
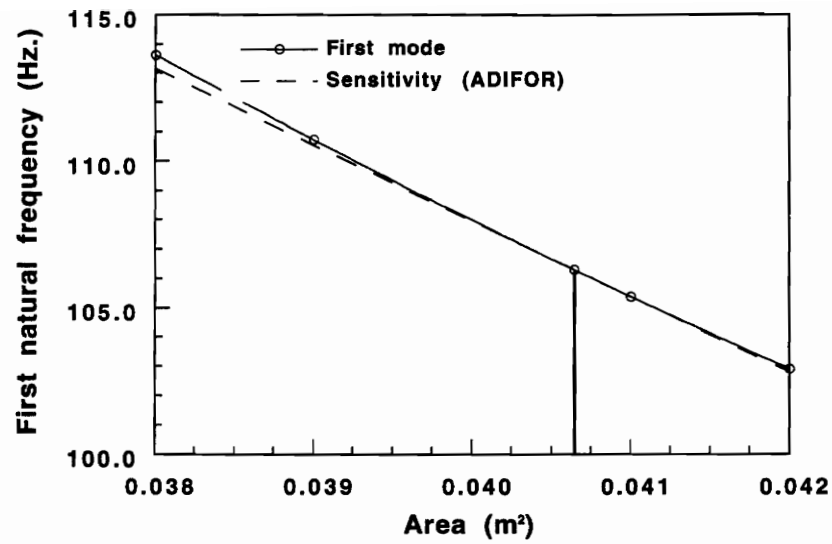


Fig. 6.2 First three natural frequencies vs Area for a thick plate

($AR=3.111$, $Area=0.040645m^2$, $TR=0.5$, $Sweep=15^\circ$)

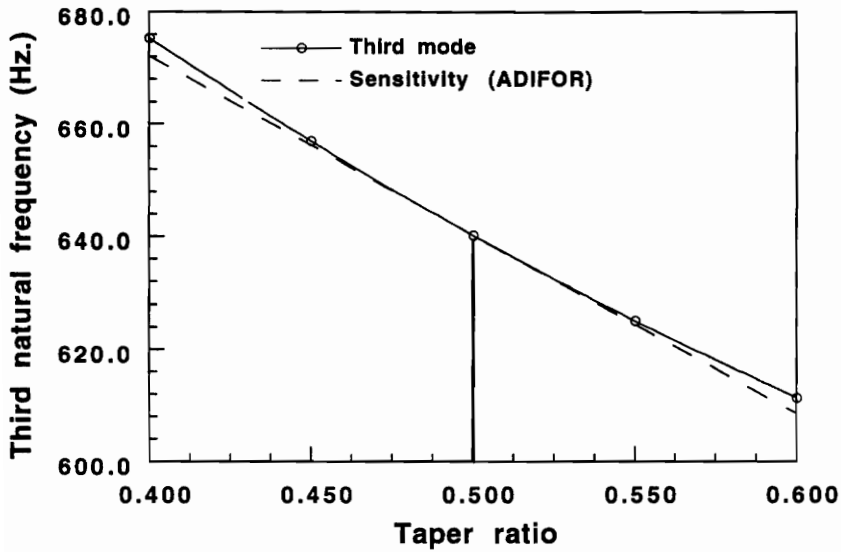
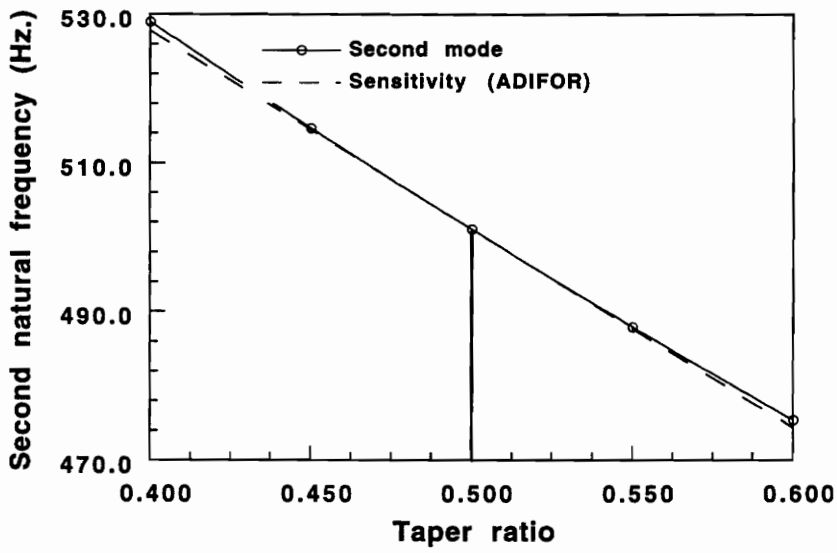
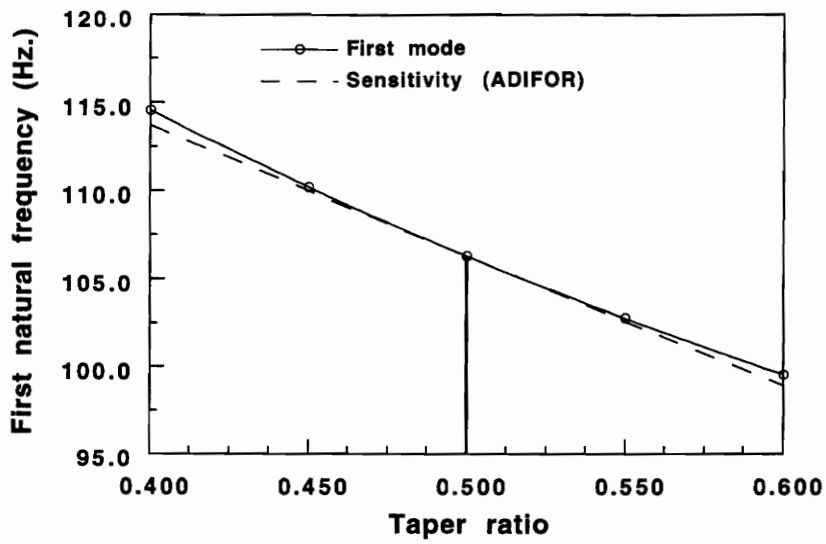


Fig. 6.3 First three natural frequencies vs Taper ratio for a thick plate

($AR=3.111$, $Area=0.040645m^2$, $TR=0.5$, $Sweep=15^\circ$)

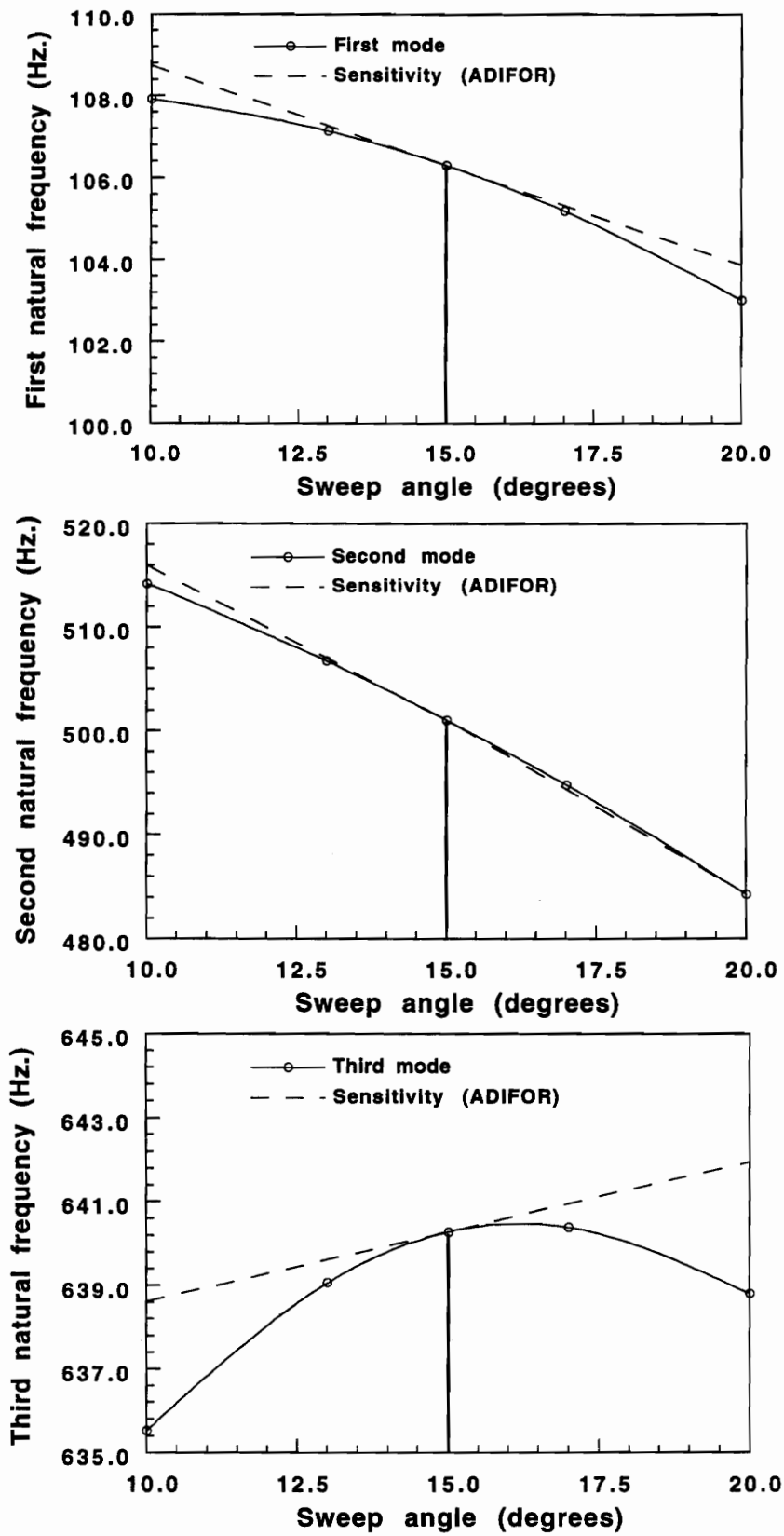


Fig. 6.4 First three natural frequencies vs Sweep angle for a thick plate

(AR=3.111, Area=0.040645m², TR=0.5, Sweep=15°)

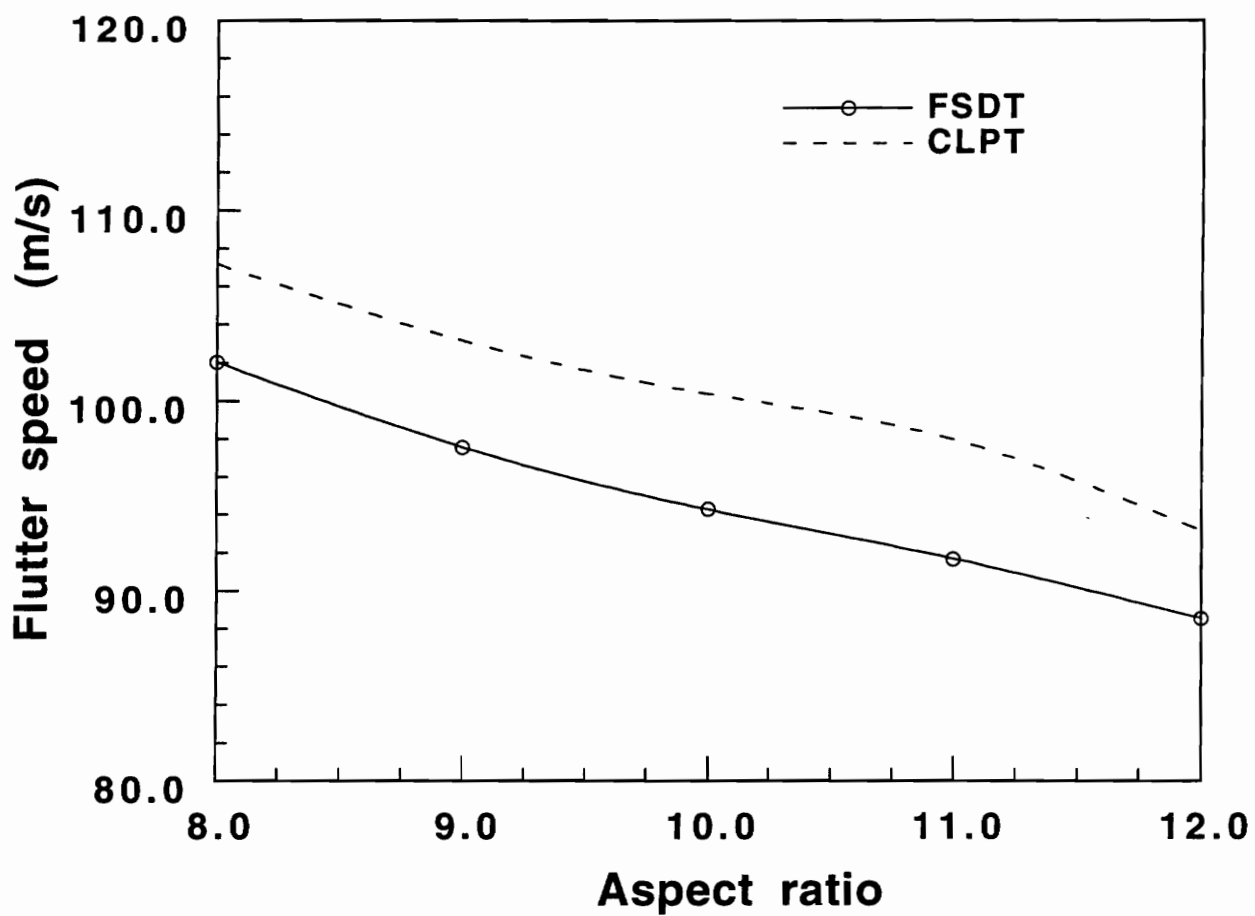
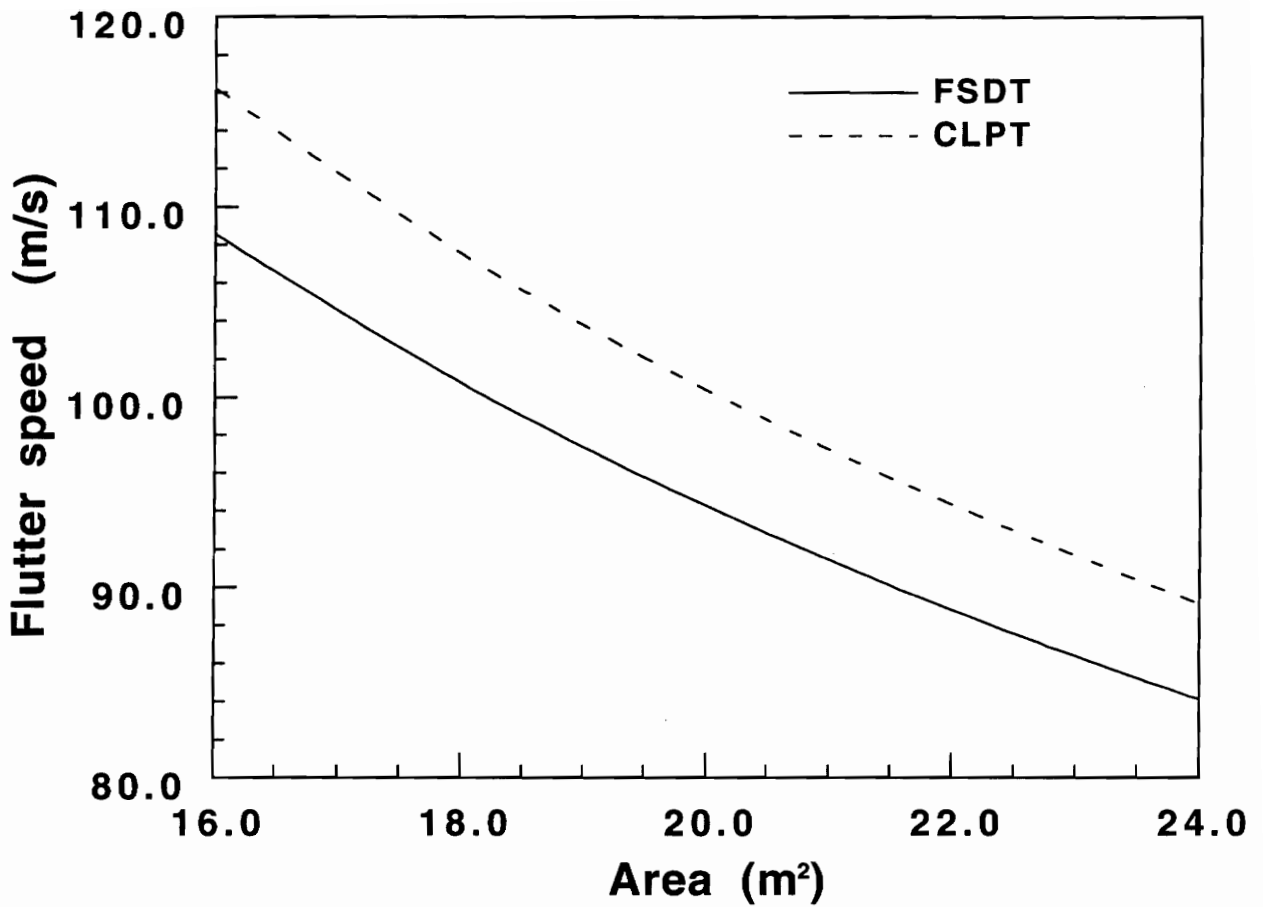


Fig. 6.5 Effect of transverse shear on flutter
[Flutter speed vs Aspect ratio (M=0.6)]

(Area=20m², TR=0.5, Sweep=30°)



**Fig. 6.6 Effect of transverse shear on flutter
[Flutter speed Vs Area (M=0.6)]**

(AR=10, TR=0.5, Sweep=30°)

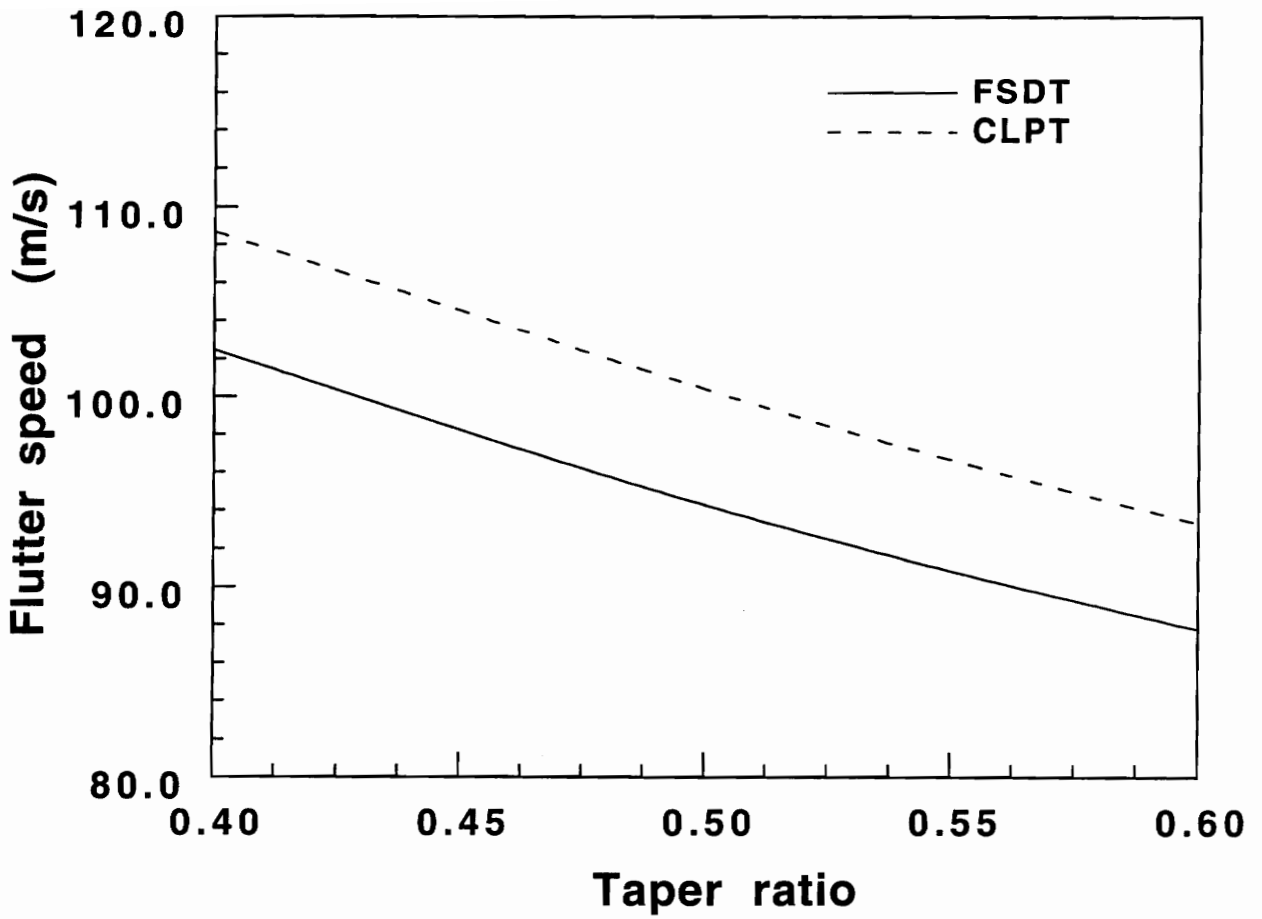


Fig. 6.7 Effect of transverse shear on flutter
[Flutter speed vs Taper ratio (M=0.6)]

(AR=10, Area=20m², Sweep=30°)

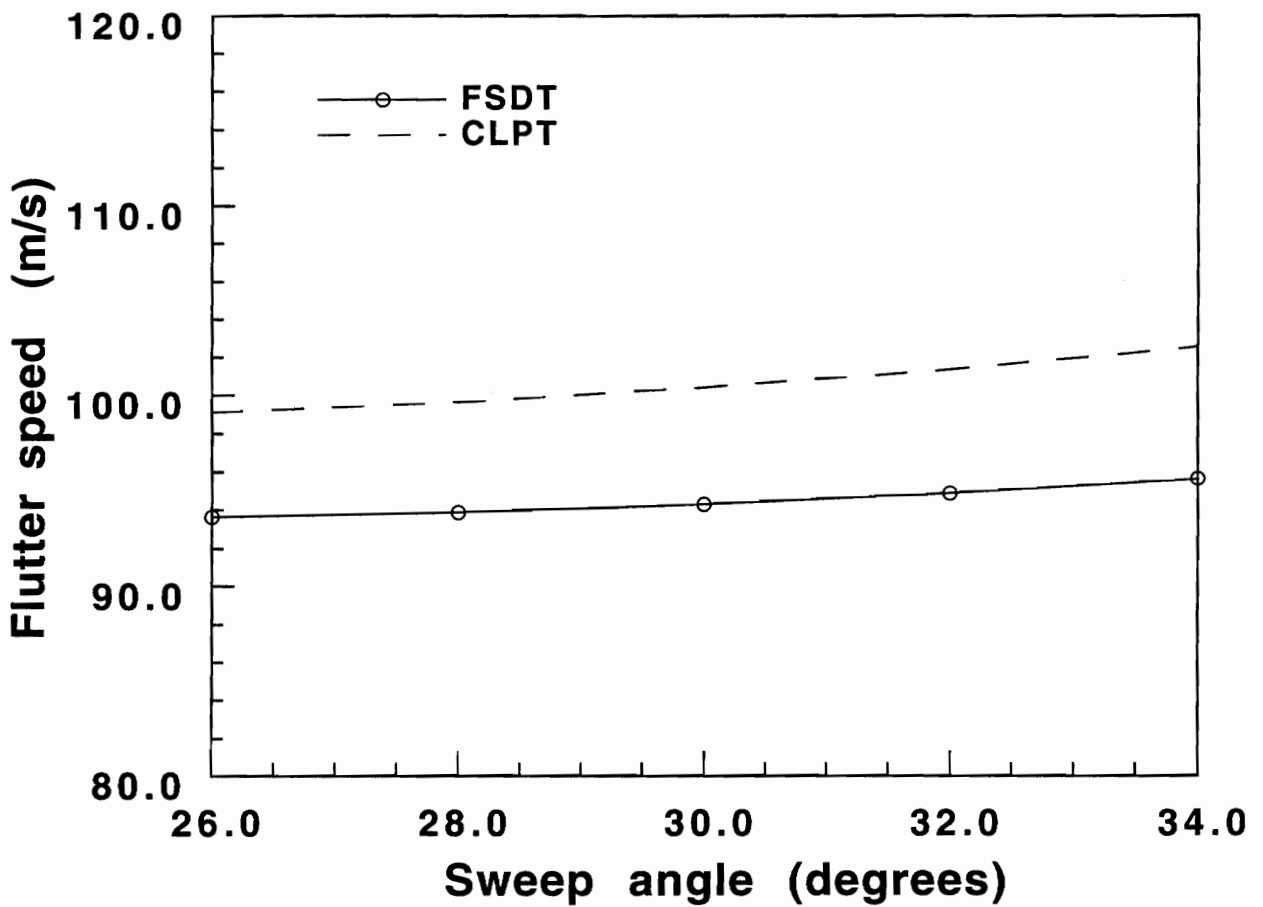


Fig. 6.8 Effect of transverse shear on flutter
[Flutter speed vs Sweep angle (M=0.6)]
(AR=10, Area=20m², TR=0.5)

Table 6.1 Comparison of natural frequencies predicted by the two theories for the 6-ply, 12-ply and 18-ply laminates

Mode Number	Natural frequencies (Hz.)					
	[30 ₂ /0] _s (6-ply)		[30 ₂ /0] _{2s} (12-ply)		[30 ₂ /0] _{3s} (18-ply)	
	CLPT ^a	FSDT ^b	CLPT	FSDT	CLPT	FSDT
1	16.16	16.14	34.49	34.42	52.76	52.57
2	80.19	79.95	170.23	168.58	259.90	255.22
3	118.30	117.30	235.47	230.45	351.96	339.61
4	209.92	208.80	445.04	437.82	679.59	658.99
5	316.95	313.86	636.14	619.30	952.52	908.13

^a CLPT (Classical laminated plate theory)

^b FSDT (First-order shear deformation theory)

Table 6.2 Comparison of natural frequencies predicted by the two theories for the 24-ply and 36-ply laminates

Mode Number	Natural frequencies (Hz.)			
	[30 ₂ /0] _{4s} (24-ply)		[30 ₂ /0] _{6s} (36-ply)	
	CLPT	FSDT	CLPT	FSDT
1	71.08	70.61	107.57	106.30
2	349.77	339.71	528.86	501.06
3	468.91	444.58	701.67	640.29
4	914.84	870.50	1383.71	1259.17
5	1270.76	1178.56	1902.68	1658.03

Table 6.3 Optimization results for the minimum weight wing design

Iteration	Aspect ratio	Area (m^2)	Flutter speed (m/s)
1	10.000	20.000	94.30
2	5.3913	18.551	130.90
3	5.3913	17.857	134.19

**Table 6.4 Optimization results for the minimum weight wing design
(Composite objective function)**

Iteration	Aspect ratio	Area (m^2)	Flutter speed (m/s)
1	10.000	20.000	94.30
2	7.7882	19.304	105.56
3	6.1784	17.857	124.21
4	6.5694	17.857	120.28
5	6.5994	17.857	120.00

CHAPTER 7

CONCLUDING REMARKS

This study has examined the flutter characteristic of a typical section in subsonic compressible flow. Indicial response functions are used for the normal force and pitching moment coefficients of the two degree of freedom airfoil and the unsteady aerodynamics is represented by a state-space model. The aeroelastic equations are solved as an eigenvalue problem to determine the onset of aeroelastic instability. The sensitivity of the flutter speed of the typical section with respect to its mass and stiffness parameters, namely, mass ratio, static unbalance, radius of gyration, bending frequency and torsional frequency are calculated analytically. The sensitivity derivatives show good agreement with finite difference derivatives. The aeroelastic equations are also integrated with respect to time at different values of freestream speed, to observe the aeroelastic phenomena in real time. The stable, neutrally stable and unstable nature of the aeroelastic response can be seen at speeds below, at and above the flutter speeds, respectively, for the typical section.

The above aerodynamics for a typical section was extended to develop a strip-theory formulation representing the unsteady aerodynamic forces on a wing. The structural modeling is done using classical plate theory and is based on a Rayleigh-Ritz formulation using Chebyshev polynomials for the wing displacements. The structural equations are coupled with the time-domain aerodynamic equations to formulate the aeroelastic equations as a set of first-order ordinary differential equations. These equations are solved as an eigenvalue problem to determine the critical

speed of the wing. The natural frequencies and flutter speeds are compared with previously published experimental values obtained from wind tunnel tests and the results agree fairly well. The sensitivity of divergence and flutter speeds to shape parameters, namely, aspect ratio, area, taper ratio and sweep angle are computed analytically. These derivatives have been accurately evaluated and they form a tangent to the critical speed curve at the baseline configuration. These shape sensitivity derivatives give a linear approximation to the critical speed curve about the baseline configuration and will be useful for preliminary design or an optimization with aeroelastic constraints. The time integration of the aeroelastic equations shows the real-time aeroelastic response (tip deflection as a function of time) of the wing when operating at speeds at the verge of instability. Particularly notable is the response of the wing configuration where the divergence speed and the flutter speed are close to each other.

Flutter analysis of the wing is also carried out using a lifting-surface subsonic kernel function aerodynamic theory (FAST) and an equivalent plate structural model. The generalized aerodynamic forces are obtained for a fixed number of free vibration modes of the wing, for the specified Mach number and spanning the range of reduced frequencies. The flutter speed is obtained using a $V-g$ type of solution. The novel method of automatic differentiation using ADIFOR was successfully implemented to generate exact derivatives of the flutter speed as obtained from the discrete system, with respect to shape parameters of the wing. A good sensitivity prediction is obtained using ADIFOR. Also, based on the sensitivity of flutter speed to modal parameters, namely, natural frequency, generalized mass

and generalized aerodynamic forces, computed using ADIFOR, one could make a judicious choice of the number of modes to be used in the aeroelastic analysis for reasonably estimating the flutter speed. These derivatives give a qualitative estimate of the modes that actively participate in flutter. In order to obtain a quantitative estimate of the contribution of a particular mode to flutter, a parameter was formed by constructing a logarithmic derivative of the sensitivity to modal parameters and summing up the absolute values of these derivatives for each mode. The finitely vanishing value of the parameter for higher modes indicates that even if these modes are not used for the flutter calculation, the results would be affected only to an insignificant amount.

Finite element modeling of the wing is done using NASTRAN so that wing structures made of spars and ribs and top and bottom wing skins could be analyzed. The modeling is validated for static and dynamic analysis using a box-beam and an AGARD swept-back wing model. A good agreement with previously published results is obtained. The airfoil shape for the wing cross-section was generated by transformation from a circle using the Joukowski transformation, so it could be parameterized. The free vibration modes of the wing obtained from NASTRAN are input into FAST to compute the flutter speed. The derivatives of flutter speed with respect to shape parameters are computed using a combination of central difference scheme and ADIFOR and the sensitivity to modal parameters are calculated using ADIFOR. A fairly good sensitivity prediction is obtained. It is seen that the higher vibration modes of the wing do not actively participate in flutter.

An equivalent plate model which incorporates first-order shear deformation theory is then examined so it can be used to model thick wings, where shear de-

formations are important. The sensitivity of natural frequencies to changes in shape parameters is obtained using ADIFOR which would be useful in optimization with frequency constraints. The natural frequencies and the flutter speeds calculated using the first-order shear deformation theory are compared with those obtained using a classical laminated plate theory. It is seen that the frequencies and the flutter speeds drop as the transverse shear effects come into play. The shape sensitivity derivatives of the flutter speed are indispensable in a gradient-based optimization with aeroelastic constraints. A simple optimization effort is made towards obtaining a minimum weight design of the wing, subject to flutter constraints, lift requirement constraints for level flight and side constraints on the planform parameters of the wing. The nonlinear constrained optimization problem is solved using the IMSL subroutine NCONG, which uses successive quadratic programming. An optimum design which satisfies all the constraints is obtained. It should be noted that more constraints can be added to this optimization problem as desired.

Further research in this area could be to incorporate a control model so it can be coupled with the structural and aerodynamic model already in the time-domain to perform aeroservoelastic studies. Supersonic kernel function aerodynamics could be implemented to perform sensitivity analysis in the supersonic regime. So far, wings with a general trapezoidal skewed planform have been analyzed. However, some wings have discontinuities along the leading and trailing edges and can be considered to be made up of multiple trapezoidal segments. Shape sensitivities of flutter speed of wings made up of multiple trapezoidal segments, a good example of which is the High Speed Civil Transport (HSCT) wing, can be analyzed.

REFERENCES

- (1.) Bisplinghoff, R.L., and Ashley, H., *Principles of Aeroelasticity*, John Wiley & Sons, New York, N.Y., 1969.
- (2.) Dowell, E.H., *A Modern Course in Aeroelasticity*, Sijthoff & Noordhoff, Alphen aan den Rijn, The Netherland, 1980.
- (3.) Fung, Y.C., *Introduction to the Theory of Aeroelasticity*, Dover Publications, New York, N.Y., 1969.
- (4.) Tolson, R.H., and Sobieszczanski-Sobieski, J., "Multidisciplinary Analysis and Synthesis: Needs and Opportunities," AIAA Paper 85-0584.
- (5.) Sobieszczanski-Sobieski, J., and Haftka, R.T., "Interdisciplinary and Multilevel Optimum Design," *Computer Aided Optimal Design: Structural and Mechanical Systems*, Edited by C.A Mota Soares, Springer-Verlag, Berlin, 1987.
- (6.) Weisshaar, T.A., Newsom, J.R., Zeiler, T.A., and Gilbert, M.G., "Integrated Structure/Control Design - Present Methodology and Future Opportunities," 1986 Conference of the International Council of the Aeronautical Sciences, London, England, 1986, ICAS Paper 86-4.8.1.
- (7.) Sobieszczanski-Sobieski, J., "Sensitivity Analysis and Multidisciplinary Optimization for Aircraft Design: Recent Advances and Results," *Journal of Aircraft*, Vol. 27, No. 12, Dec. 1990, pp. 993-1001.
- (8.) Hassig, H.J., "An Approximate True Damping Solution of the Flutter Equation by Determinant Iteration," *Journal of Aircraft*, Vol. 8, No. 11, Nov. 1971, pp. 885-889.
- (9.) Richardson, J.R., "A More Realistic Method for Routine Flutter Calculation," *AIAA Symposium on Structural Dynamics and Aeroelasticity*, Boston, Mass., Aug. 1965.
- (10.) Landahl, M.T., "Graphical Technique for Analyzing Marginally Stable Dynamic Systems," *Journal of Aircraft*, Vol. 1, No. 5, Sep. 1964, pp. 293-299.
- (11.) Frueh, F.J., and Miller, J.M., "Prediction of Dynamic Response from Flutter Analysis Solutions," Rept. 65-0952, Air Force Office of Scientific Research, Arlington, Va., Jun. 1965.
- (12.) Erickson, A.L., and Stephenson, J.D., "A Suggested Method of Analyzing for Transonic Flutter of Control Surface Based on Available Experimental Evidence," NACA A7E30, Dec. 1947.

- (13.) Theodorsen, T., "General Theory of Aerodynamic Instability and the Mechanism of Flutter," NACA Rept. 496, 1935.
- (14.) Ballhaus, W.F., and Bridgeman, J.O., "Numerical Solution Techniques for Unsteady Transonic Problems," AGARD Rept. 679, June 1980, pp. 16-1-16-24.
- (15.) Ballhaus, W.F., and Goorjian, P.M., "Computation of Unsteady Transonic Flows by the Indicial Method," *AIAA Journal*, Vol. 16, No. 2, 1978, pp. 117-124.
- (16.) Yang, T.Y., Guruswamy, P., Stritz, A.G., and Olsen, J.J., "Flutter Analysis of a NACA 64A006 Airfoil in Small Disturbance Transonic Flow," *Journal of Aircraft*, Vol. 17, No. 4, 1980, pp. 225-232.
- (17.) Guruswamy, P., and Yang, T.Y., "Aeroelastic Time Response Analysis of Thin Airfoils by Transonic Code LTRAN2," *Journal for Computers and Fluids*, Vol. 9, No. 4, Dec. 1981, pp. 409-425.
- (18.) Livne, E., Schmit, L.A., and Friedmann, P.P., "Towards Integrated Multidisciplinary Synthesis of Actively Controlled Fiber Composite Wings," *Journal of Aircraft*, Vol. 27, No. 12, 1990, pp. 979-992.
- (19.) Leishman, J.G., "Indicial Lift Approximations for Two-Dimensional Subsonic Flow as Obtained from Oscillatory Measurements," *Journal of Aircraft*, Vol. 30, No. 3, 1993, pp. 340-351.
- (20.) Wagner, H., "Über die Entstehung des Dynamischen Auftriebes von Tragflügeln," *Zeitschrift für Angewandte Mathematik und Mechanik*, Vol. 5, No. 1, Feb. 1925.
- (21.) Jones, R.T., "The Unsteady Lift of a Wing of Finite Aspect Ratio," NACA Rept. 681, 1940.
- (22.) Venkatesan, C., and Friedmann, P.P., "New Approach to Finite State Modelling of Unsteady Aerodynamics," *AIAA Journal*, Vol. 24, Dec. 1986, pp. 1889-1897.
- (23.) Leishman, J.G., and Nguyen, K.Q., "State-Space Representation of Unsteady Airfoil Behavior," *AIAA Journal*, Vol. 28, No. 5, May 1990, pp. 836-844.
- (24.) Leishman, J.G., and Crouse, G.L., "A State-Space Model of Unsteady Aerodynamics for Flutter Analysis in a Compressible Flow," AIAA Paper 89-0022, Jan. 1989.
- (25.) Leishman, J.G., "Validation of Approximate Indicial Aerodynamic Functions for Two-Dimensional Subsonic Flow," *Journal of Aircraft*, Vol. 25, No. 10, 1988, pp. 914-922.

- (26.) Goman, M., and Khrabrov, A., "State-Space Representation of Aerodynamic Characteristics of an Aircraft at High Angles of Attack," *Journal of Aircraft*, Vol. 31, No. 5, 1994, pp. 1109-1115.
- (27.) Librescu, L., and Simovich, J., "General Formulation for the Aeroelastic Divergence of Composite Swept-Forward Wing Structures", *Journal of Aircraft*, Vol. 25, No. 4, 1988, pp. 364-371.
- (28.) Kapania, R.K., Bergen, F.D., and Barthelemy, J.-F.M., "Shape Sensitivity Analysis of Flutter Response of a Laminated Wing," *AIAA Journal*, Vol. 29, No. 4, 1991, pp. 611-612. Also presented at 30th AIAA/ASME/ASCE/AHS/ASC Structures, Structural Dynamics and Materials Conference, Mobile, Alabama, 1989 and NASA-CR-181725.
- (29.) Borland, C.J., and Rizzetta, D.P., "Transonic Unsteady Aerodynamics for Aeroelastic Application, Vol. 1 - Technical Development Summary for XTRAN3S," AFWAL-TR-80-3107, June 1982.
- (30.) Batina, J.T., Seidel, D.A., Bland, S.R., and Bennett, R.M., "Unsteady Transonic Flow Calculations for Realistic Aircraft Configurations," AIAA Paper 87-0850, April 1987.
- (31.) Albano, E., and Rodden, W.P., "A Doublet-Lattice Method for Calculating Lift Distribution on Oscillating Surfaces in Subsonic Flows," *AIAA Journal*, Vol. 7, No. 2, 1969, pp. 279-285
- (32.) Rodden, W.P., Giesing, J.P., and Kalman, T.P., "New Method for Nonplanar Configurations," *AGARD Conference Proceedings*, CP-80-71, Pt. II, No. 4, 1971.
- (33.) Cunningham, A.M. Jr., "Unsteady Subsonic Collocation Method for Wing With and Without Control Surface," *Journal of Aircraft*, Vol. 9, No. 6, 1972.
- (34.) Watkins, C.E., Woolston, D.S., and Cunningham, H.J., "A Systematic Kernel Function Procedure for Determining Aerodynamic Forces on Oscillating or Steady Finite Wings at Subsonic Speeds," NASA Rept. R-48, 1959.
- (35.) Brayton, R.K., *Sensitivity and Optimization*, Elsevier, New York, 1980.
- (36.) Adelman, H.M., and Haftka, R.T., "Sensitivity Analysis of Discrete Structural Systems," *AIAA Journal*, Vol. 24, No. 5, May 1986, pp. 823-831.
- (37.) Sobieszczanski-Sobieski, J., "A System Approach to Aircraft Optimization," AGARD Rept. 784, Feb. 1992, pp. 2-1-2-15.

- (38.) Rudisill, C.S., and Bhatia, K.G., "Optimization of Complex Structures to Satisfy Flutter Requirements," *AIAA Journal*, Vol. 9, No. 8, August 1971, pp. 1486-1491.
- (39.) Murthy, D.V., and Haftka, R.T., "Survey of Methods for Calculating Sensitivity of General Eigenproblems," Presented at the Symposium on Sensitivity Analysis in Engineering, Hampton, Virginia, Sept. 1986.
- (40.) Murthy, D.V., "Sensitivity Analysis and Approximation Methods for General Eigenvalue Problems," Ph.D Dissertation, Aerospace and Ocean Engineering, Virginia Polytechnic Institute and State University, Blacksburg, Virginia, 1986.
- (41.) Pedersen, P., and Seyranian, A.P., "Sensitivity Analysis for Problems of Dynamic Stability," *International Journal of Solids and Structures*, Vol. 19, No. 4, 1983, pp. 315-335.
- (42.) Hawk, D.J., and Bristow, D.R., "Development of MCAERO Wing Design Panel Method with Interactive Graphics Module," NASA CR-3775, 1984.
- (43.) Yates, E.C., "Aerodynamic Sensitivity from Subsonic, Sonic and Supersonic Unsteady, Nonplanar Lifting Surface Theory," NASA TM-100502, 1987.
- (44.) Livne, E., Sels, R.A., and Bhatia, K.G., "Lessons from Application of Equivalent Plate Structural Modeling to an HSCT Wing," Presented at 34th AIAA/ASME/ASCE/AHS/ASC Structures, Structural Dynamics and Materials Conference, La Jolla, California, 1993, AIAA-93-1413.
- (45.) Livne, E., "Analytic Sensitivities for Shape Optimization in Equivalent Plate Structural Wing Models," *Journal of Aircraft*, Vol. 31, No. 4, 1994, pp. 961-969.
- (46.) Barthelemy, J.-F.M., and Bergen, F.D., "Shape Sensitivity Analysis of Wing Static Aeroelastic Characteristics," NASA TP-2808, May 1988.
- (47.) Kapania, R.K., "Sensitivity Analysis of Dynamic Aeroelastic Responses," AGARD Rept. 784, Feb. 1992, pp. 3-1-3-12.
- (48.) Yates, E.C., "Calculation of Flutter Characteristics for Finite-Span Swept or Unswept Wings at Subsonic and Supersonic Speeds by a Modified Strip Analysis," NACA RM L57110, March 1958.
- (49.) Giles, G.L., "Equivalent Plate Analysis of Aircraft Wing Box Structures with General Planform Geometry," *Journal of Aircraft*, Vol. 23, No. 11, Nov. 1986, pp. 859-864.
- (50.) Giles, G.L., "Further Generalization of an Equivalent Plate Representation for Aircraft Structural Analysis", NASA TM 89105, Feb. 1987.

- (51.) Schmit, L.A., "Structural Analysis – Precursor and Catalyst," *Recent Experiences in Multidisciplinary Analysis and Optimization*, NASA CP-2327, Pt. 1, 1984, pp. 1-17.
- (52.) Schmit, L.A., "Structural Optimization—Some Key Ideas and Insights," *New Directions in Optimum Structural Design*, edited by E. Atrek, R.H. Gallagher, K.M. Ragsdell, O.C. Zienkiewicz, John Wiley & Sons, 1984.
- (53.) Wilkinson, K., Markowitz, J., Lerner, E., George, D., and Batill, S.M., "FASTOP—A Flutter and Strength Optimization Program for Lifting Surface Structures," *Journal of Aircraft*, Vol. 14, No. 6, 1977.
- (54.) Markowitz, J., and Isakson, G., "FASTOP3—A Strength, Deflection and Flutter Optimization Program for Metallic and Composite Structures," Air Force Flight Dynamic Lab, Wright Aeronautical Laboratories, Dayton, OH, AFFDL-TR-78-50, May 1978.
- (55.) Isakson, G., Pardo, H., Lerner, E., and Venkayya, V.B., "ASOP3—A Program for Optimum Structural Design to Satisfy Strength and Deflection Constraints," *Journal of Aircraft*, Vol. 15, No. 7, 1978, pp. 422-428.
- (56.) Hornlein, H.R.E.M., "Takeoff in Optimum Structural Design," *Computer Aided Optimal Design: Structural and Mechanical Systems*, edited by C.A. Mota Soares, Springer-Verlag, Berlin, 1987.
- (57.) Love, M., and Bohlman, J., "Aeroelastic Tailoring and Integrated Wing Design," *Recent Advances in Multidisciplinary Analysis and Optimization*, NASA CP-3031, Pt. 1, 1989, pp. 431-444.
- (58.) Triplett, W.E., "Aeroelastic Tailoring Studies in Fighter Aircraft Design," *Journal of Aircraft*, Vol. 17, No. 7, 1980, pp. 508-513.
- (59.) Triplett, W.E., "Flutter Optimization in Fighter Aircraft Design," *Recent Experiences in Multidisciplinary Analysis and Optimization*, NASA CP-2327, 1984, pp. 47-63.
- (60.) Haftka, R.T., "Automated Procedure for Design of Wing Structures to Satisfy Strength and Flutter Requirements," NASA TN D-7264, 1973.
- (61.) Haftka, R.T., "Optimization of Flexible Wing Structures Subject to Strength and Induced Drag Constraints," *AIAA Journal*, Vol. 15, No. 8, 1977, pp. 1101-1106.
- (62.) Starnes, J.H., Jr., and Haftka, R.T., "Preliminary Design of Composite Wings for Buckling, Strength and Displacement Constraints," *Journal of Aircraft*, Vol 16, No. 2, 1979, pp. 564-570.

- (63.) Lecina, G., and Petiau, C., "Advances in Optimal Design with Composite Materials," *Computer Aided Optimal Design: Structural and Mechanical Systems*, edited by C.A. Mota Soares, Springer-Verlag, 1987.
- (64.) Neill, D.J., Johnson, E.H., and Canfield, R., "ASTROS—A Multidisciplinary Automated Structural Design Tool," AIAA Paper 87-0713, April 1987.
- (65.) Venkayya, V.B., "Recent Developments in Large Scale Structural Optimization," *Recent Advances in Multidisciplinary Analysis and Optimization*, NASA CP-3031, 1989, pp. 1521–1540.
- (66.) Rudisill, C.S., and Bhatia, K.G., "Second Derivatives of the Flutter Velocity and the Optimization of Aircraft Structures," *AIAA Journal*, Vol. 10, No. 12, 1972, pp. 1569–1572.
- (67.) Haftka, R.T., "Structural Optimization with Aeroelastic Constraints: A Survey of US Applications," *International Journal of Vehicle Design*, Vol. 7, No. 3-4, 1986, pp. 381–392.
- (68.) Haftka, R.T., and Yates, E.C., Jr., "Repetitive Flutter Calculations in Structural Design," *Journal of Aircraft*, Vol. 13, 1976, pp. 454–461.
- (69.) Haftka, R.T., and Prasad, B., "Programs for Analysis and Resizing of Complex Structures," *Computers and Structures*, Vol. 10, 1979, pp. 323–330.
- (70.) Unger, E.R., Hutchison, M.G., Haftka, R.T., and Grossman, B., "Variable-Complexity Design of a Transport Wing", *International Journal of Systems Automation: Research and Applications (SARA)*, Vol. 2, No. 2, 1992, pp. 87–113.
- (71.) Hutchison, M.G., Unger, E.R., Mason, W.H., Grossman, B. and Haftka, R.T., "Variable-Complexity Aerodynamic Optimization of a High-Speed Civil Transport Wing", *Journal of Aircraft*, Vol. 31, No.1, 1994, pp. 110–116.
- (72.) Huang, X., Dudley, J., Haftka, R.T., Grossman, B. and Mason, W.H., "Structural Weight Estimation for Multidisciplinary Optimization of a High-Speed Civil Transport", To appear *Journal of Aircraft*, Vol. 33, No. 3, May–June 1996.
- (73.) Karpel, M., "Multidisciplinary Optimization of Aeroservoelastic Systems Using Reduced-Size Models," *Journal of Aircraft*, Vol. 29, No. 5, 1992, pp. 939–946.
- (74.) Hajela, P., Bloebaum, C.L., and Sobieszczanski-Sobieski, J., "Application of Global Sensitivity Equations in Multidisciplinary Aircraft Synthesis," *Journal of Aircraft*, Vol. 27, No. 12, 1990, pp. 1002–1010.

- (75.) Barthelemy, J.-F.M., Coen, P.G., Wrenn, G.A., Riley, M.F., and Dovi, A.R., "Application of Multidisciplinary Optimization Methods to the Design of a Supersonic Transport," AGARD Rept. 784, Feb. 1992, pp. 4-1-4-5.
- (76.) Bathe, K.J., and Wilson, E.L., "Solution Methods for Eigenvalue Problem in Structural Mechanics," *International Journal of Numerical Methods in Engineering*, Vol. 6, 1973, pp. 213-226.
- (77.) Borri, M. and Mantegazza, P., "Efficient Solution of Quadratic Eigenproblems Arising in Dynamic Analysis of Structures," *Computer Methods in Applied Mechanics and Engineering*, Vol. 12, 1977, pp. 1-19.
- (78.) Fox, R.L., and Kapoor, M.P., "Rates of Change of Eigenvalues and Eigenvectors," *AIAA Journal*, Vol. 6, 1968, pp. 2426-2429.
- (79.) Murthy, D.V., and Haftka, R.T., "Derivatives of Eigenvalues and Eigenvectors of a General Complex Matrix," *International Journal for Numerical Methods in Engineering*, Vol. 26, 1988, pp. 293-311
- (80.) Rudisill, C.S., "Derivatives of Eigenvalues and Eigenvectors for a General Matrix," *AIAA Journal*, Vol. 12, 1974, pp. 721-722.
- (81.) Cardani, C., and Mantegazza, P., "Calculation of Eigenvalue and Eigenvector Derivatives for Algebraic Flutter and Divergence Eigenproblems," *AIAA Journal*, Vol. 17, No. 4, 1979, pp. 408-412.
- (82.) Leishman, J.G., and Crouse, G.L., "Transonic Aeroelasticity Analysis Using State-Space Unsteady Aerodynamic Modeling," *Journal of Aircraft*, Vol. 29, No. 1, 1992, pp. 153-160.
- (83.) Newmark, N.M., "A Method of Computation for Structural Dynamics," *Trans. ASCE*, Vol. 127, Pt. 1, 1962, pp. 1406-1435.
- (84.) Wilson, E.L., Farhoomand, I., and Bathe, K.-J., "Nonlinear Dynamic Analysis of Complex Structures," *Earthquake Engr. and Str. Dyn.*, Vol. 1, 1973, pp. 241-252.
- (85.) Burden, R.L., and Faires, J.D., *Numerical Methods*, PWS-KENT Publishing Co., 1989.
- (86.) Kapania, R.K., and Singhvi, S., "Free Vibration Analysis of Generally Laminated Tapered Skew Plates," *Composites Engineering*, Vol. 2, No. 3, 1992, pp. 197-212.
- (87.) Singhvi, S., and Kapania, R.K., "Analysis, Shape Sensitivities and Approximations of Modal Response of Generally Laminated Tapered Skew Plates," CCMS

Rept., Virginia Polytechnic Institute and State University, Blacksburg, VA, September 1991.

- (88.) Dugundji, J., and Landsberger, B.J., "Experimental Aeroelastic Behavior of Unswept and Forward Swept Cantilever Graphite Epoxy Wings," *Journal of Aircraft*, Vol. 22, No. 8, Aug. 1985, pp. 679-686.
- (89.) Desmarais, R.N., and Bennett, R.M., "User's Guide for a Modular Flutter Analysis Software System," NASA TM 78720, May 1978.
- (90.) Bischof, C., "Principles of Automatic Differentiation," ADIFOR Workshop, NASA Langley Research Center, Hampton, VA, Sept. 1993.
- (91.) Zienkiewicz, O.C., *The Finite Element Method*, McGraw-Hill, London, 1977.
- (92.) Cook, R.D., *Concepts and Applications of Finite Element Analysis*, John Wiley, New York, 1981.
- (93.) Reddy, J.N., *An Introduction to the Finite Element Method*, McGraw-Hill, 1984.
- (94.) MSC/NASTRAN Version 67, User's Manual, 1991.
- (95.) Turner, M.J., Martin, H.C., and Weikel, R.C., "Further Development and Applications of the Stiffness Method," *Matrix Methods of Structural Analysis*, AGARDograph 72, edited by F.B. de Veubeker, Pergamon, Oxford, England, UK, 1964, pp. 203-266.
- (96.) Livne, E., "Equivalent Plate Structural Modeling for Wing Shape Optimization Including Transverse Shear," *AIAA Journal*, Vol. 32, No. 6, 1994, pp. 1278-1288.
- (97.) Kapania, R.K., and Lovejoy, A.E., "Natural Frequencies and an Atlas of Mode Shapes for Generally-Laminated, Thick, Skew, Trapezoidal Plates," Center for Composite Materials and Structures Report, Virginia Polytechnic Institute and State University, Blacksburg, VA, August 1994.
- (98.) Karpouzian, G., and Librescu, L., "Exact Flutter Solution of Advanced Composite Swept Wings in Various Flight Speed Regimes," *AIAA Journal*, Vol. 34, No. 4, 1996, pp. 786-794.
- (99.) Haftka, R.T., and Gurdal, Z., *Elements of Structural Optimization*, Kluwer Academic Publishers, 1992.
- (100.) Vanderplaats, G.N., "CONMIN-A Fortran Program for Constrained Function Minimization," NASA TM X-62282, 1973.
- (101.) IMSL MATH/LIBRARY User's Manual, FORTRAN Subroutines for Mathematical Applications, Jan. 1989.
- (102.) Powell, M.J.D., "A Fast Algorithm for Nonlinearly Constrained Optimization Calculations," Proceedings of the 1977 Dundee Conference on Numerical Analysis, Lecture Notes in Mathematics, Vol. 630, 1978, pp. 144-157.

APPENDIX A

The a_{ij} 's are given by

$$\begin{aligned}
 a_{11} &= -\left(\frac{2V}{c}\right)\beta^2 b_1 \\
 a_{22} &= -\left(\frac{2V}{c}\right)\beta^2 b_2 \\
 a_{33} &= -\frac{1}{K_\alpha T_I} \\
 a_{44} &= -\frac{1}{K_q T_I} \\
 a_{55} &= -(b_3 K_{\alpha M} T_I)^{-1} \\
 a_{66} &= -(b_4 K_{\alpha M} T_I)^{-1} \\
 a_{77} &= -b_5 \beta^2 \left(\frac{2V}{c}\right) \\
 a_{88} &= -\frac{1}{K_{qM} T_I}
 \end{aligned} \tag{1}$$

where

$$\begin{aligned}
 K_\alpha(M) &= [(1 - M) + \pi\beta M^2 (A_1 b_1 + A_2 b_2)]^{-1} \\
 K_q(M) &= [(1 - M) + 2\pi\beta M^2 (A_1 b_1 + A_2 b_2)]^{-1} \\
 K_{\alpha M}(M) &= \left[\frac{A_3 b_4 + A_4 b_3}{b_3 b_4 (1 - M)} \right] \\
 K_{qM}(M) &= \left[\frac{7}{15(1 - M) + 3\pi\beta M^2 b_5} \right]
 \end{aligned} \tag{2}$$

The c_{ij} 's are given by

$$\begin{aligned}
 c_{11} &= C_{N_\alpha} \left(\frac{2V}{c} \right) \beta^2 A_1 b_1 \\
 c_{12} &= C_{N_\alpha} \left(\frac{2V}{c} \right) \beta^2 A_2 b_2 \\
 c_{13} &= \frac{4}{M} \left(-\frac{1}{K_\alpha T_I} \right) \\
 c_{14} &= \frac{1}{M} \left(-\frac{1}{K_q T_I} \right) \\
 c_{21} &= C_{N_\alpha} \left(\frac{2V}{c} \right) \beta^2 A_1 b_1 (0.25 - x_{ac}) \\
 c_{22} &= C_{N_\alpha} \left(\frac{2V}{c} \right) \beta^2 A_2 b_2 (0.25 - x_{ac}) \\
 c_{25} &= -\frac{A_3 a_{55}}{M} \\
 c_{26} &= -\frac{A_4 a_{66}}{M} \\
 c_{27} &= -\frac{C_{N_\alpha}}{16} b_5 \beta^2 \left(\frac{2V}{c} \right) \\
 c_{28} &= \frac{7}{12M} \left(\frac{1}{K_{qM} T_I} \right)
 \end{aligned} \tag{3}$$

The constants are given by $A_1 = 0.3$, $A_2 = 0.7$, $A_3 = 1.5$, $A_4 = -0.5$, $b_1 = 0.14$, $b_2 = 0.53$, $b_3 = 0.25$, $b_4 = 0.1$, $b_5 = 0.5$.

Analytical derivatives

Aspect ratio (AR), Area (S), Taper ratio (tr), Sweep (Λ)

The wing coordinates are (x_1, y_1) , (x_2, y_2) , (x_3, y_3) and (x_4, y_4) .

$$span = \sqrt{AR S}$$

$$cr = \frac{2S}{span(1 + tr)}$$

$$ct = tr cr$$

$$x_1 = 0.75 cr$$

$$x_2 = span \tan \Lambda + 0.75 ct$$

$$x_3 = span \tan \Lambda - 0.25 ct$$

$$x_4 = -0.25 cr$$

$$y_1 = y_4 = 0.0 y_2 = y_3 = span p = (x_1 + x_2 + x_3 + x_4)$$

$$pp = (x_2 + x_3) - (x_1 + x_4)$$

$$crct = cr + ct$$

$$rt = cr - ct$$

For any point ψ on the quarter chord line ($-1 \leq \psi \leq 1$)

$$y = 0.5 span (1 + \psi)$$

$$x = y \tan \Lambda$$

$$\xi = \frac{2y}{span} - 1$$

$$\eta = \frac{(\xi pp - 4x + p)}{(\xi rt - crct)}$$

$$c = [cr + (ct - cr)(1 + \psi) 0.5] \cos \Lambda$$

Local chord (c)

$$\frac{\partial c}{\partial AR} = -\frac{S^{0.5}[1 - (1 - tr)(1 + \psi) 0.5] \cos \Lambda}{AR^{1.5}(1 + tr)}$$

$$\frac{\partial c}{\partial S} = \frac{[1 - (1 - tr)(1 + \psi) 0.5] \cos \Lambda}{\sqrt{AR} S(1 + tr)}$$

$$\frac{\partial c}{\partial tr} = \frac{cr \psi \cos \Lambda}{(1 + tr)}$$

$$\frac{\partial c}{\partial \Lambda} = -c \tan \Lambda$$

p = (x₁ + x₂ + x₃ + x₄)

$$\frac{\partial p}{\partial AR} = \frac{0.5 S^{0.5}}{AR^{0.5}} \left[2 \tan \Lambda - \frac{1}{AR} \right]$$

$$\frac{\partial p}{\partial S} = \frac{0.5 p}{S}$$

$$\frac{\partial p}{\partial tr} = 0.0$$

$$\frac{\partial p}{\partial \Lambda} = \frac{2 \text{ span}}{\cos^2 \Lambda}$$

pp = (x₂ + x₃) - (x₁ + x₄)

$$\frac{\partial pp}{\partial AR} = 0.5 S^{0.5} \left[\frac{2 \tan \Lambda}{AR^{0.5}} + \frac{(1 - tr)}{(1 + tr) AR^{1.5}} \right]$$

$$\frac{\partial pp}{\partial S} = \frac{0.5 pp}{S}$$

$$\frac{\partial pp}{\partial tr} = \frac{cr}{(1 + tr)}$$

$$\frac{\partial pp}{\partial \Lambda} = \frac{2 \text{ span}}{\cos^2 \Lambda}$$

crct = cr + ct

$$\frac{\partial crct}{\partial AR} = -\frac{S^{0.5}}{AR^{1.5}}$$

$$\frac{\partial crct}{\partial S} = \frac{0.5 crct}{S}$$

$$\frac{\partial crct}{\partial tr} = 0.0$$

$$\frac{\partial crct}{\partial \Lambda} = 0.0$$

$$\underline{rt = cr - ct}$$

$$\frac{\partial rt}{\partial AR} = -\frac{S^{0.5} (1 - tr)}{AR^{1.5} (1 + tr)}$$

$$\frac{\partial rt}{\partial S} = \frac{0.5 rt}{S}$$

$$\frac{\partial rt}{\partial tr} = -\frac{2 cr}{(1 + tr)}$$

$$\frac{\partial rt}{\partial \Lambda} = 0.0$$

$$\underline{x = y \tan \Lambda}$$

$$\frac{\partial x}{\partial AR} = \frac{S^{0.5} \tan \Lambda (1 + \psi)}{4 AR^{0.5}}$$

$$\frac{\partial x}{\partial S} = 0.5 (1 + \psi) \text{span} \tan \Lambda$$

$$\frac{\partial x}{\partial tr} = 0.0$$

$$\frac{\partial x}{\partial \Lambda} = \frac{0.5 \text{span} (1 + \psi)}{\cos^2 \Lambda}$$

$$\underline{\eta = (\xi pp - 4x + p) / (\xi rt - crct)}$$

For any parameter v ,

$$\frac{\partial \eta}{\partial v} = \frac{(\xi rt - crct) \left(\xi \frac{\partial pp}{\partial v} - 4 \frac{\partial x}{\partial v} + \frac{\partial p}{\partial v} \right) - (\xi pp - 4x + p) \left(\xi \frac{\partial rt}{\partial v} - \frac{\partial crct}{\partial v} \right)}{(\xi rt - crct)^2}$$

$$\frac{\partial \xi}{\partial v} = 0.0$$

APPENDIX B

Main program: main.f

```
program main
c
  real x(3),y
  x(1)=1.0
  x(2)=2.0
  x(3)=3.0
  call func(x,y)
  write(*,*)x(1),x(2),x(3),y
end
```

Subroutine: func.f

```
subroutine func(x,y)
  real x(3),y
  y=x(1)+2.*x(2)**2+3.*x(3)**3
  return
end
```

ADIFOR generated code: g_func.f

```
subroutine g_func(g_p_, x, g_x, ldg_x, y, g_y, ldg_y)
  real x(3), y
  integer g_pmax_
  parameter (g_pmax_ = 3)
  integer g_i_, g_p_, ldg_y, ldg_x
  real r2_p, r1_p, r9_b, r5_b, r3_v, r7_v, g_y(ldg_y), g_x(ldg_x,
*3)
  if (g_p_ .gt. g_pmax_) then
    print *, 'Parameter g_p_ is greater than g_pmax_'
    stop
  endif
  r3_v = x(2) * x(2)
  r2_p = 2.0e0 * x(2)
  r7_v = x(3) ** ( 3 - 2)
  r7_v = r7_v * x(3)
  r1_p = 3 * r7_v
  r7_v = r7_v * x(3)
  r5_b = 3. * r1_p
  r9_b = 2. * r2_p
  do g_i_ = 1, g_p_
    g_y(g_i_) = g_x(g_i_, 1) + r9_b * g_x(g_i_, 2) + r5_b * g_x(g_
*i_, 3)
  enddo
  y = x(1) + 2. * r3_v + 3. * r7_v
C-----
  return
end
```


VITA

The author was born in Kerala, India on March 20, 1966. He obtained his B.Tech degree (First Class with Honors) in Mechanical Engineering in 1988 from Regional Engineering College, Calicut, India. He received his M.E degree (First Class with Distinction) in Aerospace Engineering in 1990 from Indian Institute of Science, Bangalore, India. He continued at Indian Institute of Science for a year and a half as a Research Assistant after which he joined the Ph.D program at Virginia Polytechnic Institute and State University (VPI&SU) in 1992. His research was supported by a NASA Grant and also worked as a Research Associate at NASA Langley Research Center from June-September, 1994. After graduation, he plans to have an active career in engineering.